INVESTIGATION OF FATIGUE BEHAVIOUR OF EXTERNAL STORES UNDER FIXED WING AIRCRAFT PLATFORMS DURING RANDOM VIBRATION

A THESIS SUBMITTED TO
THE GRADUATE SCHOOL OF NATURAL AND APPLIED SCIENCES
OF
MIDDLE EAST TECHNICAL UNIVERSITY

BY

EMRE OKUR

IN PARTIAL FULFILLMENT OF THE REQUIREMENTS
FOR
THE DEGREE OF MASTER OF SCIENCE
IN
MECHANICAL ENGINEERING

SEPTEMBER 2015

Approval of the thesis:

INVESTIGATION OF FATIGUE BEHAVIOUR OF EXTERNAL STORES UNDER FIXED WING AIRCRAFT PLATFORMS DURING RANDOM VIBRATION

submitted by **EMRE OKUR** in partial fulfillment of the requirements for the degree of **Master of Science in Mechanical Engineering Department, Middle East Technical University** by,

Prof. Dr. Gülbin Dural Ünver _____
Dean, Graduate School of **Natural and Applied Sciences**

Prof. Dr. R. Tuna Balkan _____
Head of Department, **Mechanical Engineering**

Prof. Dr. Serkan Dağ _____
Supervisor, **Mechanical Engineering Dept., METU**

Examining Committee Members:

Prof. Dr. Suat Kadıoğlu _____
Mechanical Engineering Dept., METU

Prof. Dr. Serkan Dağ _____
Mechanical Engineering Dept., METU

Asst. Prof. Dr. Gökhan Özgen _____
Mechanical Engineering Dept., METU

Asst. Prof. Dr. Hüsnü Dal _____
Mechanical Engineering Dept., METU

Asst. Prof. Dr. Emir Kutluay _____
Mechanical Engineering Dept., Hacettepe University

Date: 10.09.2015

I hereby declare that all information in this document has been obtained and presented in accordance with academic rules and ethical conduct. I also declare that, as required by these rules and conduct, I have fully cited and referenced all material and results that are not original to this work.

Name, Last name: Emre OKUR

Signature :

ABSTRACT

INVESTIGATION OF FATIGUE BEHAVIOUR OF EXTERNAL STORES UNDER FIXED WING AIRCRAFT PLATFORMS DURING RANDOM VIBRATION

Okur, Emre
M.S., Department of Mechanical Engineering
Supervisor : Prof. Dr. Serkan Dağ

September 2015, 98 pages

In this study, fatigue behaviour of an external store during captive carriage at the underwing and wingtip of a fixed wing aircraft platform is investigated. The F-16C jet aircraft was determined as a fixed wing aircraft platform in this thesis which is commonly used by Turkish Army. As the external store, a data measurement store (DMS) was designed to measure loads during captive carrage. While the DMS was being attached to the F-16C jet aircraft, it flew in 5 different sorties. Acceleration and strain data were collected during these sorties. Accelerometers were used to generate power specral densities (PSD) for the vibration tests and fatigue analyses. Strain gages were placed to the most critical locations for fatigue calculations. For fatigue calculations, annual flight of F-16C jet aircraft was taken into consideration. From this annual flight data, an ideal average sortie for F-16C jet aircraft (IASF-16JA) was generated. Acceleration and strain data collected from 5 different sorties were separated and picked according to this ideal average F-16C jet aircraft sortie. For data processing and analyses Matlab, MS Excel, Ncode, MSC – Patran ve MSC – Nastran were used. Strain data were used for fatigue calculations and acceleration

data were used to generate captive carriage vibration profiles. Also, using these vibration profiles a sample fatigue analysis was done. Moreover, reduction and determination of the vibration test duration was explanied.

Keywords: Multiaxial Fatigue, Vibration Fatigue, Random Vibration, Fatigue Damage Spectrum, Extreme Response Spectrum, Shock Response Spectrum.

ÖZ

RASTGELE TİTREŞİM ALTINDA SABİT KANATLI HAVA PLATFORMLARINA BAĞLI HARİCİ YÜKLERİN YORULMA DAVRANIŞLARININ İNCELENMESİ

Okur, Emre
Yüksek Lisans, Makine Mühendisliği Bölümü
Tez yöneticisi : Prof. Dr. Serkan Dağ

Eylül 2015, 98 sayfa

Bu çalışmada, sabit kanatlı hava platformlarında kanat altına ve kanat ucuna takılan bir harici yükün esir taşıma sırasındaki gelen yüklere göre yorulma davranışı incelenmiştir. Bu tezde sabit kanatlı hava platformu olarak belirlenen uçak Türk Ordusu tarafından da kullanılan F-16 jet uçağıdır. Esir taşıma ömrü boyunca gelen yükleri bulabilmek için harici yük olarak, bir veri ölçüm podu tasarlanmıştır. Bu pod F-16 jet uçağına takılıp toplam 5 farklı sorti yapmıştır. Bu sortilerde ivme ve gerinim verileri toplanmıştır. İvmeölçerlerden, titreşim testleri ve yorulma analizlerinde kullanabilmek için ivme tayf yoğunlukları (İTY) çıkarılmıştır. Gerinim ölçerler ise yorulma hesapları için en kritik yerlere yerleştirilmiştir. Yorulma hesapları için, F-16 jet uçağının yıllık uçuşları göz önünde bulundurulmuştur. Bu yıllık uçuş verilerinden, ortalama bir F-16 jet uçağı uçuş sortisi çıkarılmıştır. Füzenin yaptığı 5 farklı sortiden alınan ivme ve gerinim verileri ise oluşturulan bu ortalama F-16 sortisine göre ayıklanmıştır. Veri işleme ve analizlerde Matlab, MS Excel, nCode, MSC – Patran ve MSC – Nastran yazılımlarından yararlanılmıştır. Gerinim verileri yorulma hesaplarında, ivme verileri ise esir taşıma titreşim profili oluşturma da kullanıldı.

Buna ek olarak titreşim profilleri kullanılarak örnek bir yorulma analizi yapıldı. Ayrıca, titreşim test süresinin kısaltılması ve belirlenmesi açıklandı.

Anahtar kelimeler: Çok Eksenli Yorulma, Titreşim Kaynaklı Yorulma, Yorulma Hasarı Spektrumu, Ekstrem Cevap Spektrumu, Şok Cevap Spektrumu.

To My Family

ACKNOWLEDGEMENTS

The author wishes to express his gratitude to his supervisor Prof. Dr. Serkan Dağ for his helpful criticism, guidance and patience in the progress and preparation of this thesis.

The author would like to thank to his parents Harika Okur and Mehmet Okur, his sister Yıldız Okur and his brothers Selçuk Okur and Kemal Okur for their help, support and patience not only during the author's thesis preparation, but also throughout his life.

The work in this thesis was performed for the practical research objectives of TÜBİTAK-SAGE (The Scientific and Technological Research Council of Turkey-Defense Industries Research and Development Institute). The author wishes to thank to TÜBİTAK-SAGE administration for allowing him to make this investigation and for unfolding the computational and testing capabilities. The author would like to extend his special thanks to Structural and Mechanical Design Division in TÜBİTAK-SAGE especially Mr. Burak Durak, Dr. Ümit Ceyhan, Mrs. Özlem Sümer, Mr. Yaşar Paça, Mrs. Özlem Deniz Oygür, Mr. Muhammed Emin Cerit, Mr. Ahmet Ünal, Mr. Mevlüt Burak Dalmış and Mr. Ethem Bozkurt for their cooperation in testing, consulting and supervising.

TABLE OF CONTENTS

LIST OF TABLES

TABLES

LIST OF FIGURES

FIGURES

LIST OF ABBREVIATIONS

AISI	:	American Iron and Steel Institute
AMRAAM	:	Advanced Medium Range Air-to-Air Missile
CATM	:	Captive Air Training Missile
CDF	:	Cumulative Distribution Function
DMS	:	Data Measurement Store
ε-N	:	Strain vs. Number of Cycles to Failure
erf	:	error function
ERS	:	Extreme Response Spectrum
F/T	:	Fuel Tank
FDS	:	Fatigue Damage Spectrum
FRF	:	Frequency Response Function
HRC	:	Rockwell Hardness C
IASF-16JA	:	Ideal Average Sortie for F-16C Jet Aircraft
LEFM	:	Linear-Elastic Fracture Mechanicns
MPC	:	Multi Point Constraint
MuxBus	:	Multiplex Bus
PSD	:	Power Spectral Density
RBE	:	Rigid Body Element
RMS	:	Root Mean Square
S-N	:	Stress vs. Number of Cycles to Failure
SAGE	:	Defense Industries Research and Development Institute
SDOF	:	Single Degree of Freedom
SRS	:	Shock Response Spectrum
S-W-T	:	Smith Watson Topper
TET10	:	10-Node Tetrahedron Mesh
TÜBİTAK	:	The Scientific and Technological Research Council of Turkey

LIST OF SYMBOLS

da/dN	:	Fatigue crack propagation rate per stress cycle
ΔK	:	Stress intensity factor range
N	:	Number of cycles to failure
S_e	:	Fully reversed endurance limit
$\sigma_a \; or \; S$	:	Alternating stress amplitude
$\sigma_f{}'$	:	Fatigue strength coefficient
b	:	Fatigue strength exponent
N_f	:	Number of half cycles to failure
$\varepsilon_p/2$	:	Plastic strain amplitude
$\varepsilon_f{}'$	:	Fatigue ductility coefficient
c	:	Fatigue ductility exponent
ε_a	:	Total strain amplitude
$\varepsilon_e/2$	:	Elastic strain amplitude
E	:	Elastic modulus
S_n	:	Nominal stress
a	:	Crack or half of the crack length
K	:	Stress intensity factor
w	:	Width dimension
$f(a/w)$	:	Dimensionless geometry parameter
K_c	:	Fracture toughness
K_{Ic}	:	Plane strain fracture toughness
ΔK_{th}	:	Stress intensity factor range threshold
C	:	Material constant which equals to the da/dN when $\Delta K = 1$
n	:	Material constant which equals to the slope of the fatigue crack growth curve at 2nd region.
a_i	:	Initial crack length
a_f	:	Critical crack length

R	:	Stress ratio
σ_m	:	Mean stress
S_{ut}	:	Ultimate tensile strength
S_y	:	Yield strength
σ_f	:	Fracture strength
C'	:	Material crack growth rate constant for Forman correction
n'	:	Material crack growth rate constant for Forman correction
λ	:	Material crack growth rate constant for Walker correction
D	:	Damage
N_i	:	Number of cycles to failure at stress level σ_i
D_t	:	Total damage
n_i	:	Number of cycles at stress level σ_i
$\Delta\tau_{oct}$	:	Octahedral shear stress range
σ_h^{mean}	:	Hydrostatic mean stress
α	:	Mean stress influence parameter (Sine method)
β	:	Equivalent octahedral shear stress (Sine method)
${\tau_f}'$	:	Shear fatigue strength coefficient
$\Delta\tau$	:	Shear stress range
σ_n	:	Normal stress on the plane
k	:	Normal stress influence parameter (Findley method)
f	:	Findley damage parameter (Findley method)
θ	:	Plane angle
τ	:	Shear stress
σ_h	:	Hydrostatic stress
a	:	Hydrostatic stress influence parameter (Dang Van method)
b	:	Fatigue strength determined from a torsion test (Dang Van method)
n	:	Safety factor (Dang Van method)
$\Delta\gamma_{max}$	:	Maximum shear strain range
$\Delta\varepsilon_n$	:	Normal strain range
S	:	Normal strain influence parameter (Brown-Miller method)

ν	:	Poisson's ratio
β_1	:	material constant (Brown-Miller method)
β_2	:	material constant (Brown-Miller method)
$\sigma_{n,max}$	:	Maximum normal stress
k	:	Normal stress influence parameter (Fatemi-Socie method)
G	:	Shear modulus
${\gamma_f}'$	:	Shear fatigue ductility coefficient
b_0	:	Shear fatigue strength exponent
c_0	:	Shear fatigue ductility exponent
$\sigma_{n,a}$	:	Alternating normal stress
$\sigma_{n,m}$	:	Mean normal stress
$\Delta\varepsilon_1$	:	Principal strain range
${\varepsilon_f}'$	:	Fatigue ductility coefficient
ΔK_q	:	Equivalent stress intensity factor
ΔK_I	:	Mode I stress intensity factor
ΔK_{II}	:	Mode II stress intensity factor
ΔK_{III}	:	Mode III stress intensity factor
K	:	Constant (relation between stress and displacement)
σ	:	Stress
$z(t)$	:	Relative displacement response of the SDOF system
z_p	:	Peak value of $z(t)$

CHAPTER 1

INTRODUCTION

1.1 General Introduction

Fixed wing aircraft platforms have great importance and are very commonly used vehicles in militaries. However without mounting external stores like missiles, bombs etc. on these aircrafts as shown in Figure 1, usage of these aircrafts will be pointless. Therefore, external stores are indispensable necessities for these aircrafts. Consequently, design and production of external stores is very crucial for military applications.

Figure 1. A fixed wing aircraft with external stores [1]

During the design of an external store, one must know the loads which the external store will encounter during its lifespan. During this lifespan, external stores encounter several types of loading like inertial loads, shock loads etc.

Among these loads, random vibration loads are one of the most important ones. By definiton, random vibration is the excitation of all frequencies while value of this random vibration is not predictable at any time. For an external stores, there are five main sources for these random vibrations during captive carriage. These sources are:

- Aerodynamic flow along the external stores
- Aircraft engine noise which is produced by turbulence in the boundary of the jet exhaust plume
- Airframe structural motions due to maneuvers, aerodynamic buffet, landing, taxi, etc.
- Gunfire
- Vibration generated by internal material and local aerodynamic effects

Moreover, some external stores can be exposed to these random vibration loads for a long time. For instance, some missiles must be attached to the aircrafts continuously for emergency situations; thus, random vibration exposure duration of these missiles can be very long such as several hundreds or thousand hours. As a result, these loads cause structural failure of the external stores especially due to fatigue. By definiton, fatigue is one of the reasons of structural failure which can occur in a metallic material due to the repeated application of stresses and strains which never reach a level sufficient to cause failure in a single application. Therefore, it is important to know the loads on the external stores to avoid fatigue. Aloha Accident one of the most famous result of fatigue is shown in Figure 2. The accident was caused by fatigue failure which took place in lap splice at one of the stringers that was a cold bonded and riveted joint. Fatigue failure occured because of knife edge effect due to deep countersunk.

Figure 2. Aloha Accident, 1988 [2]

There are several ways to guess these random vibration loads on the external stores.

One of them is using related military standards like MIL-STD-810 [3]. This is an easy way to calculate the random vibration loads. However, obtaining the random vibration load data from these standards causes a conservative design because it is not interested in a specific system. These standards usually do not take account of a lot of situation which is special for a specific case such as type of the aircraft, mounting station of the external store, air properties for the flight etc. These standards generally choose the most critical situations and this makes the loads calculated from those standards more conservative. Therefore, even these standards recommend to take measurements as a first option for the loads used in the calculations.

Another way to guess random vibration loads is using measurements which has been obtained from the similar systems. This is more accurate approach to guess loads. However, in this option, differences between structural properties of the designed system and the similar system may cause some problems. Natural frequencies and mode shapes etc. of the designed system and the similar system will be different and overcoming these problems is a very complicated and difficult task.

The best way to guess random vibration loads is to take measurement from the actual system. To take measurement one should decide sensor types, locations, directions,

data acquisition properties, etc. before the flight of the store. Installation of the sensors and data acquisition system is also a time consuming process. After data acquisition, processing the data and extracting meaningful and useful results for fatigue analysis and tests should be done. In spite of the fact that this is the most challenging method to obtain random vibration loads, it gives the most accurate results.

After finding random vibration loads, these loads must be prepared for fatigue analyses and fatigue tests. Thus, with these analyses and tests, design of the store can be verified and optimized.

1.2 Objective of the thesis

The objective of this thesis is to investigate the fatigue behavior of an external store. For this purpose a data measurement store (DMS) shown in Figure 3 was used to measure random vibration loads. After getting data from sorties, fatigue behavior of the store was investigated. Steps of investigation of fatigue behavior of the store are briefly described below:

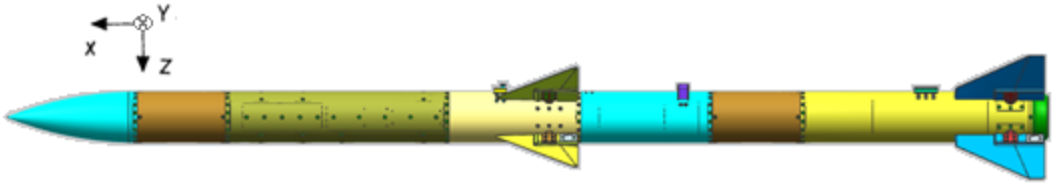

Figure 3. The DMS

1. Mounting measurement sensors to necessary locations on the DMS, determining data acquisition properties
2. Data acquisition and pprocessing
3. Generating PSDs for duration reduced vibration tests
4. Fatigue calculation and analysis

1.3 Historical Overview

The word “fatigue” comes from the Latin verb fatigare - "to tire". There has been research about fatigue since the first half of the nineteenth century. The study of fatigue begins with W. Albert [4], a German mining engineer who carried out repeated loading tests on welded chains in 1829. In 1839, S.P. Poncelet [5] was the first to use the term “fatigue” in connection with metal failure. In 1840s, W. J. M. Rankine [6], a Scottish mechanical engineer, examined the locomotive axles, especially after the Versailles train crash of 1842 and noticed the fatigue failures of railway axles by growth of a crack from stress concentration locations. Between 1852 and 1869, the first fatigue tests were carried by Wöhler [7]. His work led to the characterization of stress – life [S-N] curves. In 1910, Basquin [8] stated that the lifetime of the system has a power-law dependence on the external load amplitude and proposed a log-log relationship for S-N curves. In 1913, Inglis [9] provided the mathematical tools for quantitative treatments of fracture in brittle solids. By his work on the importance of cracks, Griffith [10] in 1925 developed the basis for fracture mechanics. In 1924, Palmgren [11] and in 1945, Miner [12] suggested a linear cumulative damage model for variable amplitude loading. In 1939, Westergaard [13] developed a method to determine the stress and displacement field ahead of the crack tip. In 1957, Irwin [14] introduced the stress intensity factor. In 1963, Paris and Erdogan [15] proposed a relation between fatigue crack propagation rate per stress cycle (da/dN) and the range of the stress intensity factor (ΔK). In 1971, Elber [16] showed the importance of crack closure on fatigue crack growth. During the 1980s and 1990s many researchers investigated the complex problem of multiaxial fatigue. Interests in the fatigue of the electronic materials also increased along with the significant research in thermo-mechanical fatigue.

1.4 Literature Review

Dreher [17] worked on the development of random vibration test criteria for aircraft equipments. He collected acceleration data from 4 different aircrafts, two of them were fighter bomber types and two of them were cargo types. He showed variance of the vibration level by speed of the aircraft, aerodynamic pressure, surface geometry for different parts of aircraft. Findings of this study was generalized to pertinent,

adaptable random vibration test criteria for aircraft equipment and this criteria is included in MIL-STD-810.

Eldred et al. [18] presented the various sources of vibrations in space vehicles and equipments with formulation and experimental data. They also investigated the response of the parts with both empirical and analytical approaches. Moreover, they discussed combining of various dynamic responses during the service life of the vehicle for vibration tests.

Lyon [19] also presented dynamic environment of a flight vehicle, prediction of vehicle response and simulation of expected environment in the test.

Bendat et al. [20] did research on checking data for randomness, stationarity and normality. Some basic inspection methods and tests were recommended in their study.

Padera [21] took out a patent about a control surface for force measurements. In his patent, he designed a control surface and used twelve linear pattern strain gages as shown in Figure 4 to measure the forces. While flow over the control surface creates forces and moments, one can measure these forces and moments on this control surface with this design.

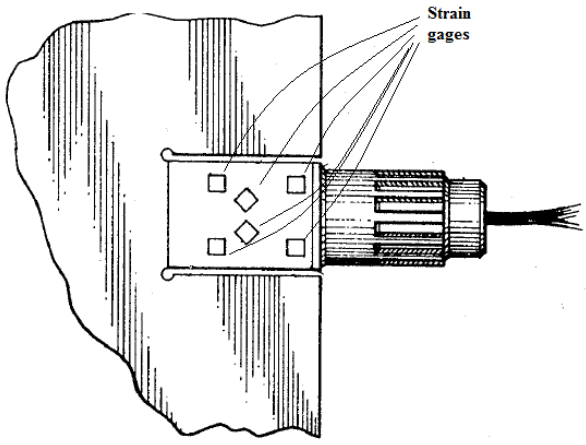

Figure 4. Padera's sensor design for force measurement [21]

Dirlik [22] proposed an empirical closed form solution to the problem following extensive computer simulations using the Monte Carlo technique for performing fatigue analysis from PSDs.

Halfpenny [23] compared fatigue life results of different frequency domain fatigue analyses (Narrow Band, Dirlik, Wirsching, Bishop, Chaudhury and Hancock methods) and time domain analysis. In his research, he found Dirlik method gives the best comparable results with the traditional time domain approaches. Dirlik method gives average discrepancy of only 4% from the fatigue life calculated in the time domain. Bishop, Chaudhury, Hancock, Wirsching and Narrow Band methods give 36%, 208%, 232%, 508% and 698% average discrepancy from the fatigue life calculated in the time domain, respectively.

Lalanne [24] showed that for a sufficiently long period of time the probability density function of rainflow range would tend to the probability density function of the peak. As a result, he proposed that Rice's original formula would also suffice for rainflow ranges.

Lalanne [24] proposed a method to generate vibration test profiles by using fatigue damage spectrum, shock response spectrum and extreme response spectrum. He used fatigue damage spectrums to calculate vibration test profile, extreme response spectrum and shock response spectrum for test profile validity.

Halfpenny and Kihm [25] created an accelerated and realistic test specification for a muffler used on a city bus. They used Dirlik and Lalanne/Rice cycle count methods and found that the Lalanne/Rice method is as robust as Dirlik's. Moreover, they used fatigue damage spectrum to get vibration profile and extreme response spectrum and shock response spectrum for the vibration test profile validity. They also checked the results with tests and got the results within a factor of safety 2.

Topham [26] evaluated and compared the fatigue damage from two different vibration events and an envelope of both events. He used the Advanced Medium Range Air-to-Air Missile (AMRAAM) as the test item and the McDonnell Douglas F-15 Eagle as its platform for his study. Then, he used the same vibration test profile

for the equipment test and the section test and compared fatigue damage from these both tests.

Freitas et al. [47] evaluated multiaxial loading methods for fatigue crack growth path and compared the results with the experimental results. The results were obtained for 6 different cases as in Table 1.

Table 1. Comparison of the observed crack plane

	Case 1	Case 2	Case 3	Case 4	Case 5	Case 6
Experiment	$-16°$	$0°$	$-5°$	$15°$	$0°$	$-28°$
Brown-Miller	$-21°$ /$69°$	$0°/\pm 90°$	$0°/\pm 90°$	$\pm 21°$ /$\pm 69°$	$0°/\pm 30°$	$0°/\pm 30°$
Findley	$-16°$ /$65°$	$0°$	$0°$	$\pm 21°$	$0°$	$\pm 29°$
Wang-Brown	$-14°$ /$63°$	$0°$	$0°$	$\pm 21°$	$\pm 3°$ /$\pm 27°$	$\pm 3°$ /$\pm 27°$
Fatemi-Socie	$-14°$ /$63°$	$0°$	$0°$	$\pm 21°$	$0°$	$\pm 29°$
S-W-T	$25°$	$0°$	$0°$	$\pm 25°$	$\pm 0°$	$\pm 25°$
Liu I	$25°$	$0°$	$0°$	$\pm 25°$	$\pm 15°$	$\pm 15°$
Liu II	$-21°$ /$69°$	$0°/\pm 90°$	$0°/\pm 90°$	$\pm 21°$ /$\pm 69°$	$0°/\pm 30°$	$0°/\pm 30°$

Where loading paths of case 1 to 6 are proportional loading, 90° shift loading, cross loading, square loading, mean stress negative and mean stress positive loading respectively. The results in Table 1 show that specially Findley and Fatemi-Socie methods give very accurate results close to the experiment.

Behrooz et al. [48] compared Findley and McDiarmid multiaxial stress based methods with the test results. They calculated fatigue life for a steel shaft of a high speed microgenerator rotor which was exposed to the torsional and bending stresses at the same time. They did multiaxial fatigue life analysis with Findley and McDiarmid methods and compared the results with fatigue tests. Using Findley and McDiarmid methods they found almost the same order of magnitude of life prediction with the test results.

Gao et al. [49] conducted uniaxial, torsion and axial-torsion fatigue experiments on a pressure vessel steel. Fatemi-Socie multiaxial fatigue criteria was used for fatigue calculations and the results were compared with the tests. In Figure 5, fatigue life comparison is shown for different loading conditions. In Figure 6, cracking orientation comparison is shown for axial-torsion loading.

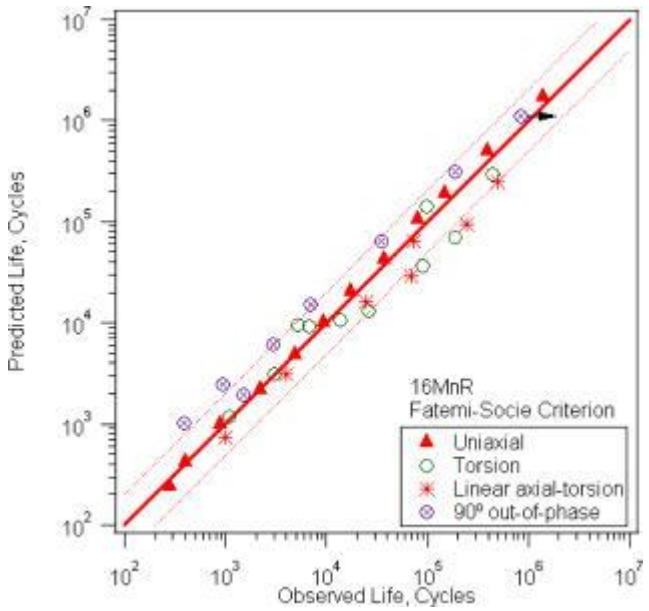

Figure 5. Comparison of experimentally observed fatigue life and prediction obtained by using the Fatemi-Socie method [49]

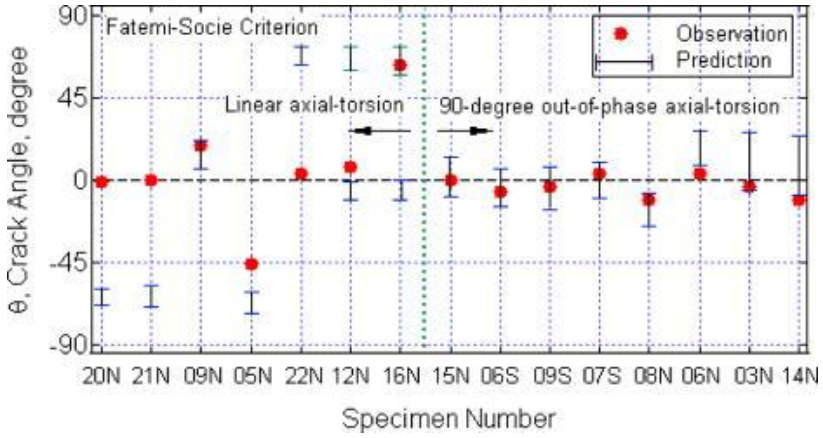

Figure 6. Comparison of the experimentally observed cracking orientation with the predictions based on the Fatemi-Socie method [49]

Figure 5 shows that fatgue life calculated by Fatemi-Socie method are very close to the experiment results. In Figure 6, cracking orientation results are not as good as the life results but still more than half of the results correlates well.

Mršnik et al. [50] conducted fatigue experiments on a Y-shaped aluminum alloy (AlSi7Cu3) sample shown in Figure 7 and compared experiment results with predicted ones.

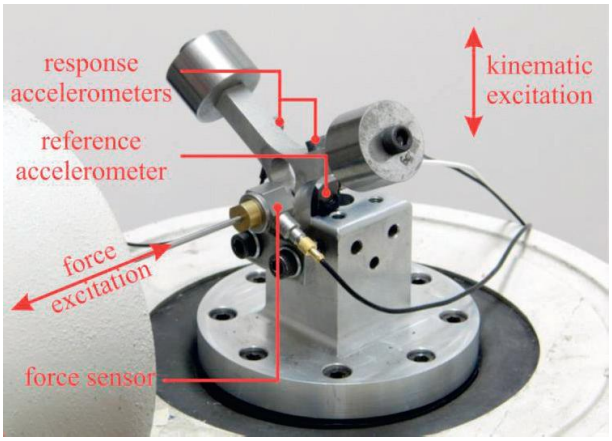

Figure 7. Experimental setup [50]

They used two excitation sources as shown in Figure 7. The sample was excited using kinematical excitation with a controlled acceleration profile in the vertical direction and open-loop force excitation in the horizontal direction. The frequency range and load range for kinematic excitation are between 380 – 480 Hz and 0.7 – 1.7 GRMS, respectively. The frequency range and load range for force excitation are between 290 – 390 Hz and 4 - 20 NRMS respectively. These frequency ranges correspond to the natural frequencies for specified axes. Tovo-Benasciutti method was used for cycle counting during fatigue calculations.

10 specimens were tested in total and Figure 8 shows that the comparison of the numerical and the experimental results are very well within the ±300% band. In general, they found both maximum normal stress criterion and maximum shear stress criterion give quite good prediction of time-to-failure for high cycle fatigue of aluminum alloy samples.

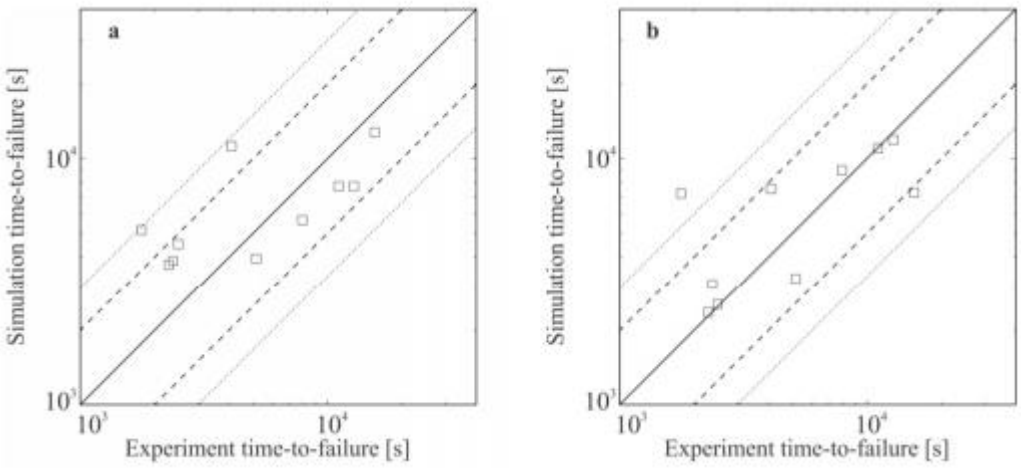

Figure 8. (a) results for the maximum normal stress criterion; (b) results for the maximum shear stress criterion [50]

1.5 Outline of the thesis

The outline of the thesis is as follows:

In Chapter 2, the DMS and properties of sensors used for measurement are mentioned. Flight properties such as type of the aircraft, mounting stations, sortie properties are also presented in this chapter. Besides collected data results are mentioned here.

In Chapter 3, fatigue theory and data processing for fatigue analyses and tests are mentioned. Moreover, fatigue calculation and analysis results are mentioned. Vibration test profiles for reduced duration tests are also generated in this chapter.

In Chapter 4, brief summary of the work done is given with conclusions and discussions. Finally, suggestions for further studies are given.

CHAPTER 2

LOAD MEASUREMENT

2.1 Data Measurement Store (DMS) and Sensor Placement

In this thesis, a data measurement store (DMS) as shown in Figure 9 was used to measure the vibration loads for fatigue calculations. Accelerometers were placed at critical parts and locations considering vibration tests and strain gages were placed to high stress expected locations. Accelerometers were used to generate power specral densities (PSDs) for the vibration tests and fatigue analyses. Strain gages were used for fatigue calculations; therefore, they were placed at the most critical locations on the store. In total, 7 accelerometers and 51 strain gages were placed on the store.

All accelerometers were 3 axial and dynamic accelerometers which measure the data above 1 Hz. However, one of the 7 accelerometers broke down during the flights and no meaningful data were retrieved from this accelerometer. Locations of other 6 accelerometers are shown in Figure 9.

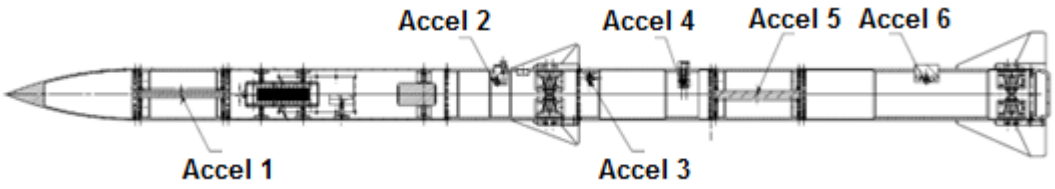

Figure 9. Locations of the accelerometers on the DMS

From 51 strain gages, 3 of them were rectangular rosette pattern, 16 of them were shear pattern and 32 of them were linear pattern stain gages. One of the 3 rectangular rosette strain gages also broke down during the flights and no meaninful data retrieved from this strain gage. Locations of other strain gage are shown in Figure 10.

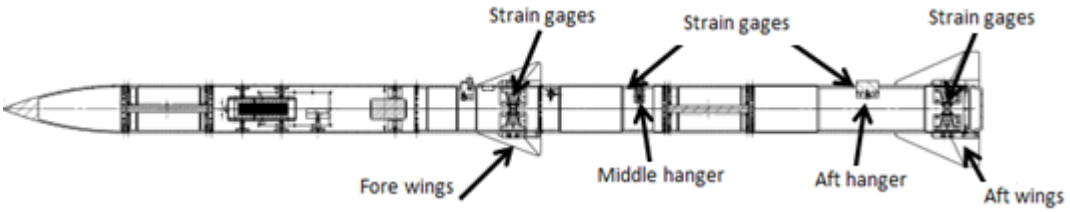

Figure 10. Locations of the strain gages on the DMS

In Figure 10, two of the symbols which point at the wings of the store represents all 48 strain gages on the shafts of the wings. Other two symbols in the middle represents the rectangular rosette strain gages in front of the store hangers. Actually, there are three hangers (front, mid and aft hangers) in the store and there were three rosette strain gages in front of each of them. However, the rosette in front of the front hanger broke down and no meaningful data were retrieved from this rosette strain gage. Figure 11 shows the locations of other two rosette strain gages. All gages in rosettes (3 gages for 1 rosette) were connected to the data acquisition system to form a quarter bridge.

Figure 11. Locations of rosette strain gages on the DMS

Strain gages on the shaft of the one of the wings are shown in Figure 12. The middle strain gage is a shear pattern type strain gage. Other two are linear type strain gages. The same arrangement also exists on the opposite surface of the shaft. Therefore, linear pattern types strain gages are connected to form a half bridge with the pairs on the other surface and shear pattern types strain gages are connected to form a full bridge with the pairs on the other surface. This sensor layout was done for all 8 wings (4 front wings and 4 aft wings).

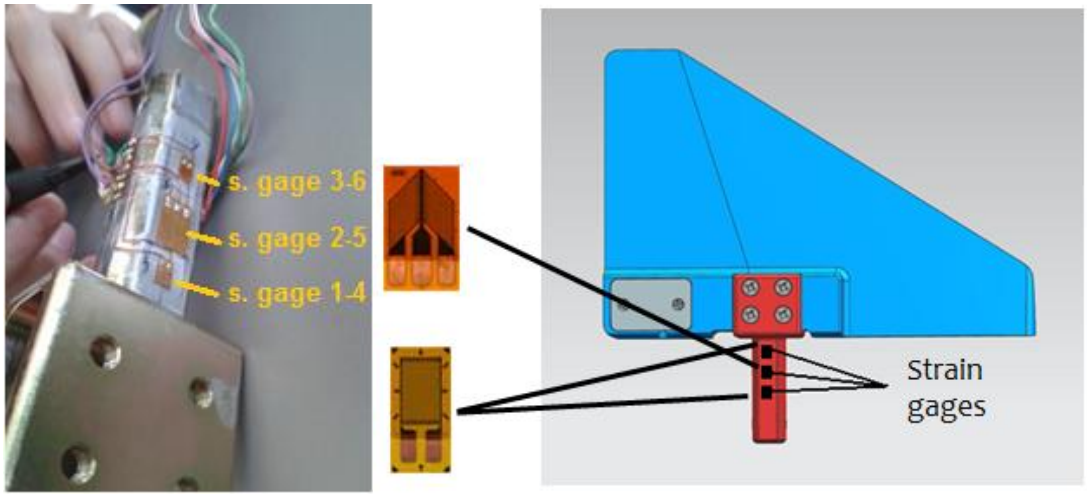

Figure 12. Location of strain gages on the shaft of the one of the wings

During flights, cut off frequencies were adjusted to 3000 Hz.

2.2 Sortie Properties

The DMS was mounted to the F-16C jet aircraft during sorties. In total, the DMS attached to the the aircraft flew 5 sorties. In 2 of these sorties, the DMS was attached to 9th station of the aircraft and during other sorties, it was attached to the 8th station of the aircraft as shown in Table 2 because of mechanical interface convenience.

Table 2. Sortie configuations

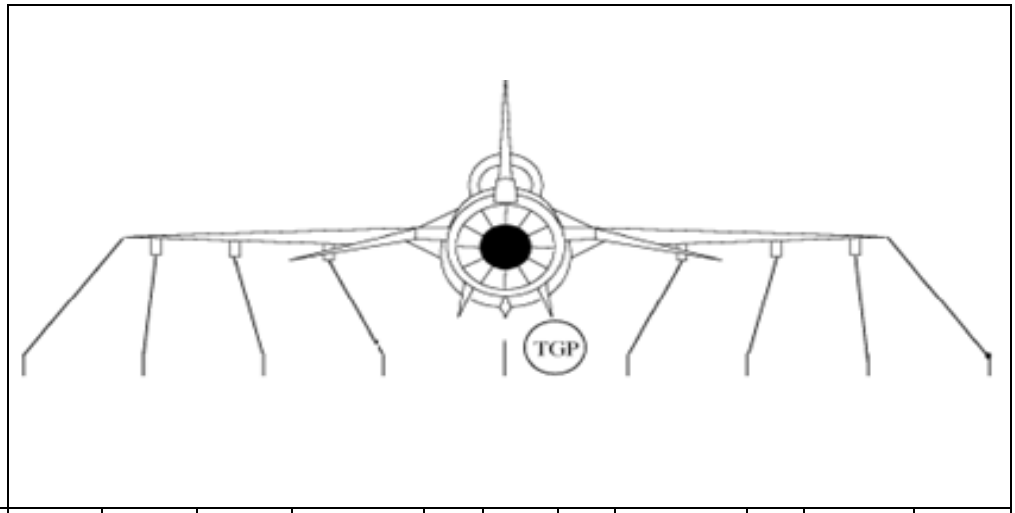

Sortie No	1	2	3	4	5L	5	5R	6	7	8	9
1 and 2	CATM 120	CATM AIM9	-	370 Gallon F/T	-	-	-	370 Gallon F/T	-	CATM AIM9	**DMS**
3, 4 and 5	CATM 120	CATM 120	-	370 Gallon F/T	-	-	-	370 Gallon F/T	-	**DMS**	CATM 120

2.3 Data Results

In general, 3 types of data were obtained from the sorties. One of them is MuxBus data obtained from the aircraft which consists of aircraft dynamic data such as altitude, speed, accelerations of the aircraft. Other two are acceleration and strain data obtained from the DMS.

2.3.1 MuxBus Data

MuxBus data give information about sortie properties. Figures from Figure 14 to Figure 18 show altitude, speed and acceleration of the aircraft for 5 different sorties respectively when the DMS was attached to the aircraft. MuxBus data acquisition sampling frequency was 50 Hz during the sorties. In Figure 13, coordinate axes of the aircraft are shown. All MuxBus acceleration data directions are based on these coordinate axes. During the sorties, aircraft flew to cover as much different combinations of altitude, speed and acceleration as possible.

Figure 13. The coordinate axes of the aircraft

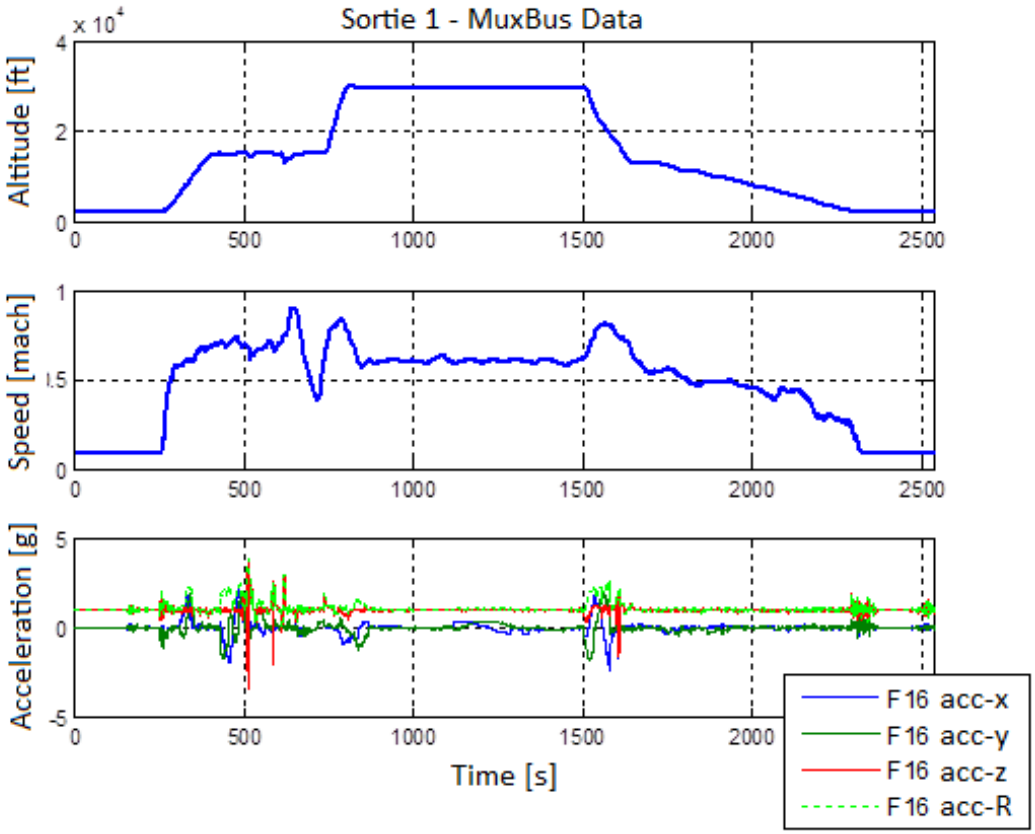

Figure 14. Sortie 1 – MuxBus Data

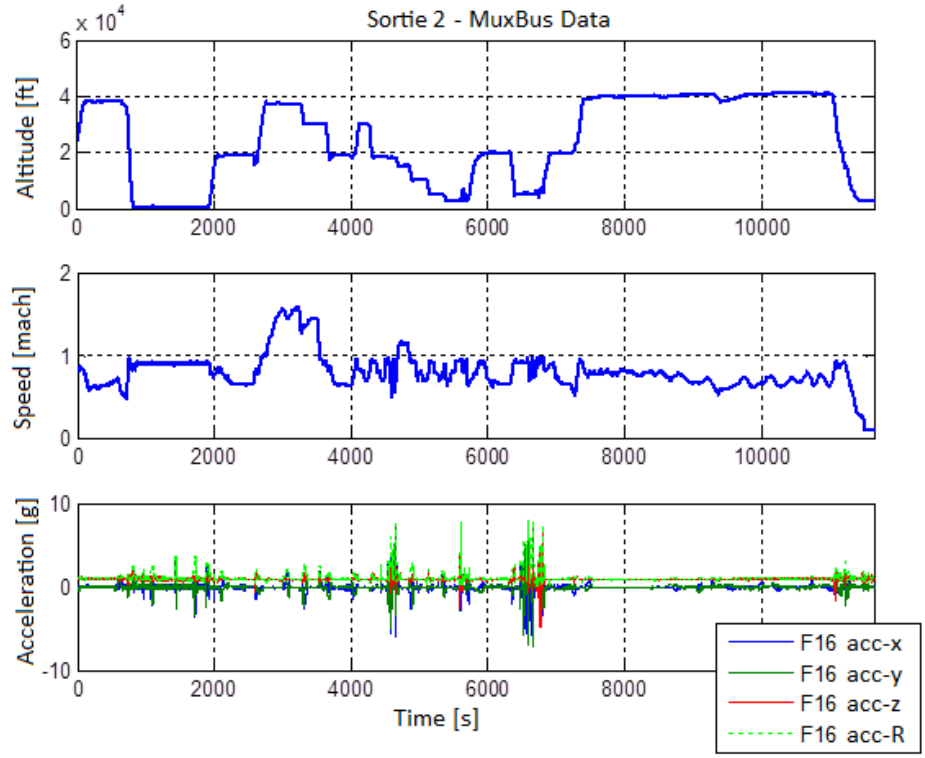

Figure 15. Sortie 2 – MuxBus Data

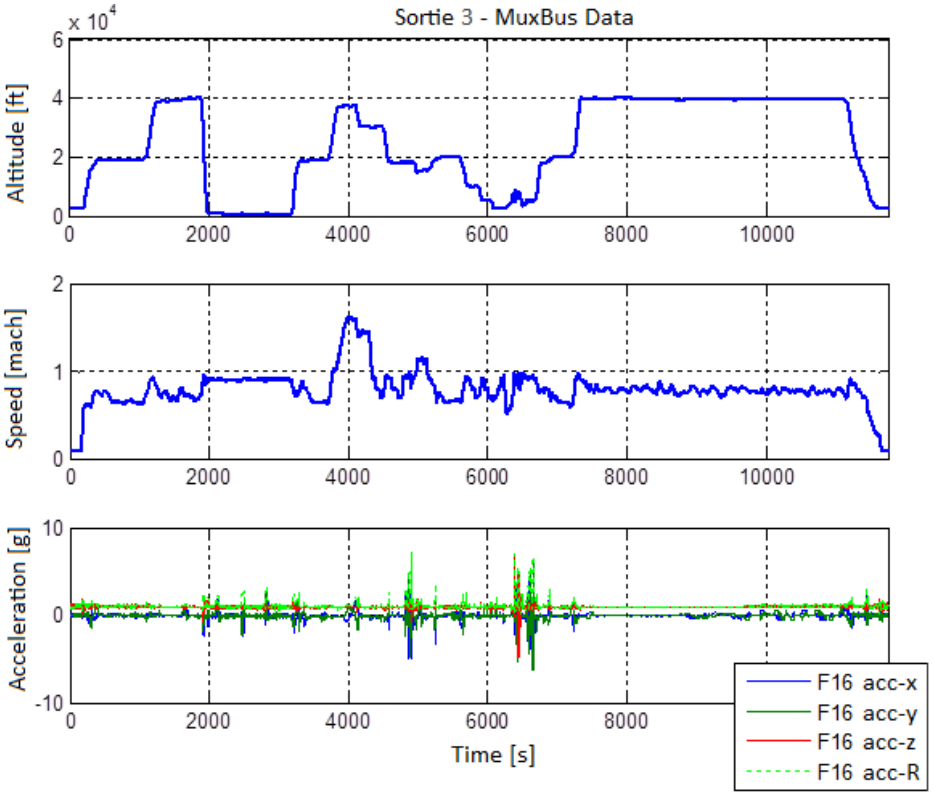

Figure 16. Sortie 3 – MuxBus Data

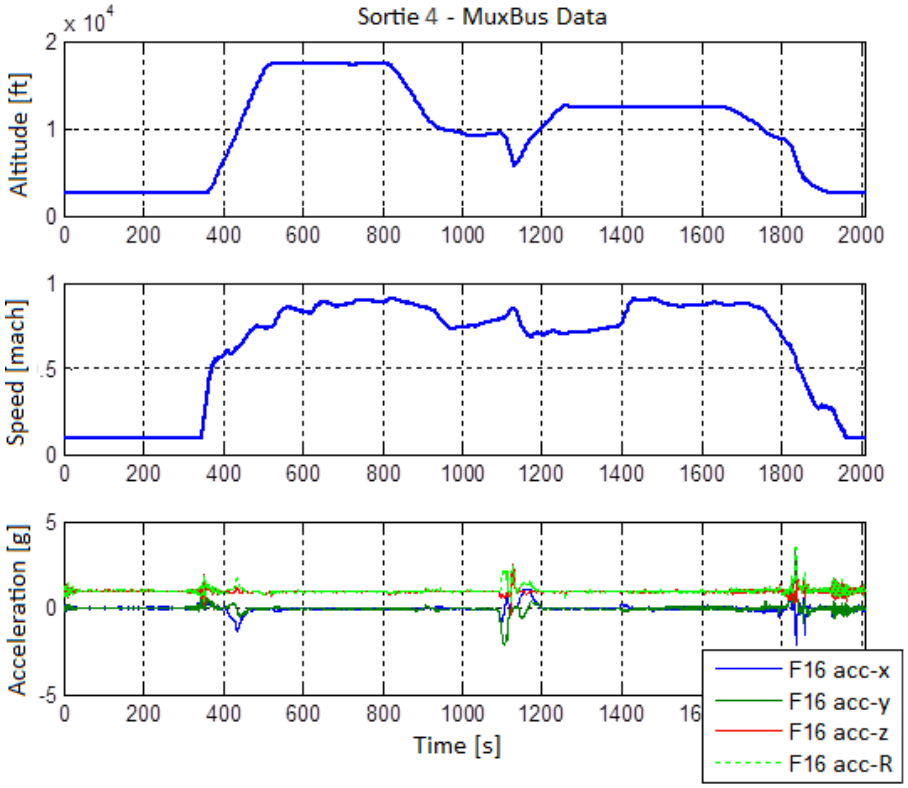

Figure 17. Sortie 4 – MuxBus Data

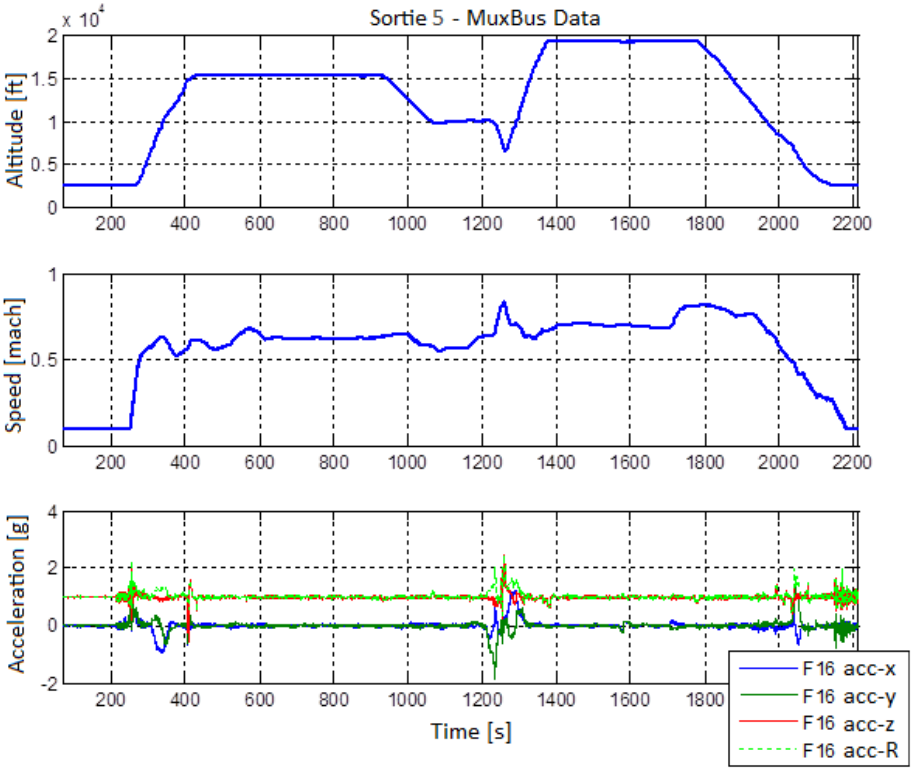

Figure 18. Sortie 5 – MuxBus Data

2.3.2 Acceleration Data

Acceleration data were collected with 3000 Hz cut-off frequency to restrain aliasing. Coordinate axes of the DMS are shown in Figure 3 and acceleration direction of the DMS are based on these coordinate axes. Therefore, acceleration axes are the same with the aircraft axes shown in Figure 13 for sortie 3, 4 and 5 but for sortie 1 and 2, +y direction of the accelerometers corresponds the -z direction of the aircraft and +z direction of the accelerometers corresponds the +y direction of the aircraft.

Accelerometers are numbered from 1 to 6 to describe the data figures in a simple way. The foremost accelerometer of the DMS shown in Figure 9 is numbered as accelerometer 1 and numbers of the accelerometers increases in order from the front to the back of the store. A sample acceleration data collected from the accelerometer 1 is shown in Figure 19. These data were collected during sortie 2 while F-16 was doing level flight at 30000 ft and 0.7 Mach.

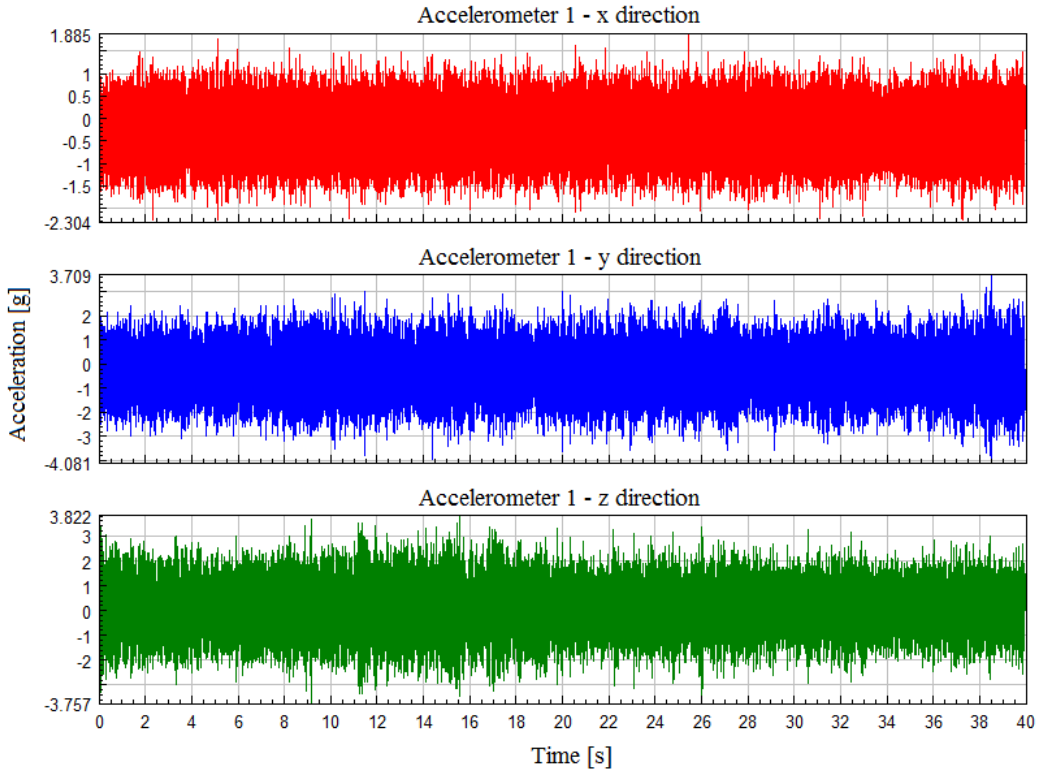

Figure 19. A sample acceleration data from accelerometer 1

2.3.3 Strain Data

Strain data were also collected with 3000 Hz cut-off frequency to restrain aliasing. Naming of the strain gages are shown in Figure 11 and Figure 12. Besides, the numbering of the wings are shown in Figure 20.

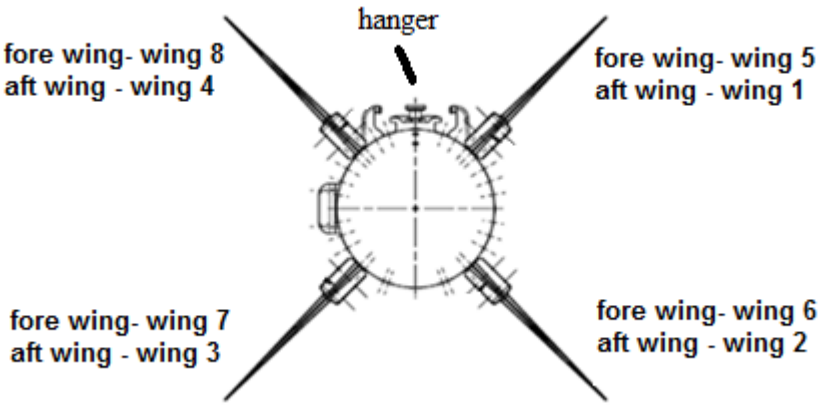

Figure 20. Numbering of the wings

A sample strain data collected from the wing 1 is shown in Figure 21. These data were collected during sortie 2 while F-16 was doing level flight at sea level (~150 ft) and maximum speed (0.9 Mach).

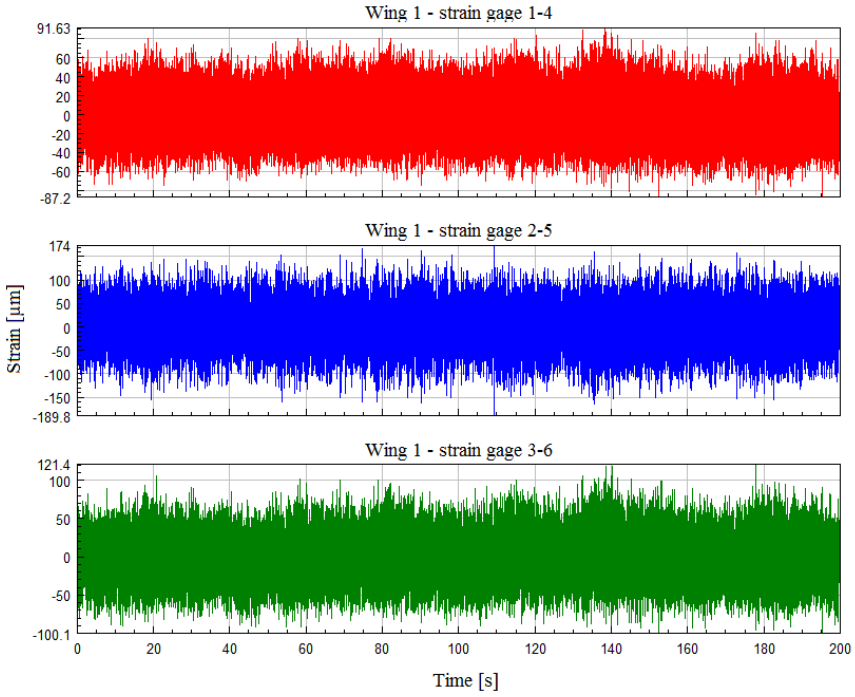

Figure 21. A sample strain data from the wing 1

CHAPTER 3

DATA PREPARATION

3.1 An Ideal Average F-16 Jet Aircraft Sortie

According to the collected data and literature survey, there are three main reasons that change vibration levels on the store. One of them is the altitude of the aircraft. Higher altitude generally means less vibration on the external store. Another reason is the speed of the aircraft. As the speed of the aircraft increases, vibration level increases as well. The relationship between the speed and the vibration is almost linear except transonic region. In transonic region, there is a huge increase in vibration levels. The other reason is the manuevers of the aircraft which especially induce buffet vibration. Knowing these reasons and annual flights of the F-16 jet aircrafts, an ideal average F-16 jet aircraft sortie was generated as shown in Table 3 for this thesis. In this table, “flight duration” column involves level flight and maneuvers at certain altitude and speed.

The aircraft did not sortie according to Table 3 because of some limitations since fatigue was not the only consideration and issue during sorties. Therefore, for fatigue analyes and tests, MuxBus data of 5 sorties and Table 3 were matched. Altitude, speed and maneuvers in Table 3 were found in 5 sorties which aircraft flew. Then, acceleration and strain data collected from the DMS were seperated and picked after matching altitude, speed and accleration of the aircraft of during 5 sorties with the data on Table 3.

Table 3. The ideal average F-16 jet aircraft sortie

Altitude [kft]	Speed [Mach]	Flight Duration [s]	2g Manuever Duration [s]	5g Manuever Duration [s]	7g Manuever Duration [s]	9g Manuever Duration [s]
Taxi & Take off	-	600	0	0	0	0
0 to 10	0.8	853.2	28.48	0	0	0
10	0.65	53.2	5.97	0	0	0
10	0.8	590	0	73.46	46.41	0.73
15	0.7	43.2	0	0	7.20	0
15	0.8	251.4	28.21	0	0	0
18	0.7	2362.8	57.59	204.17	0	0
18	0.8	1007.4	0	75.94	65.41	0
1	0.8	9	0.16	1.21	0	0
25	0.75	659.7	27.26	0	0	0
25	0.9	2277.1	47.4	259.51	0	0
30	0.8	160.2	6.08	17.54	0	0.99
30	0.9	443.2	0	0	8.26	0
30 to 5	0.5	291	43.28	0	0	0
Taxi & Landing	-	300	0	0	0	0
Sum	-	9899.4	244.43	631.83	127.28	1.72

3.2 Strain Data Preparation

3.2.1 Theory

3.2.1.1 Fatigue Life Methods

There are basically three major fatigue life methods used in design and analyses. They are the stress-life method, the strain-life method and the linear elastic frature method. These methods are used to calculate fatigue life in number of cycles, N.

3.2.1.1.1 The Stress – Life Method

The Stress – Life method is the most traditional one because of easiness of implementation. However, it is not very accurate for especially low cycle fatigue where stresses are high and cycles are low ($N<10^3$). The relation between stresses and life cycles are obtained from S-N curves of the material of the component which is exposed to variable stress. In Figure 22, a sample S-N curve is shown. To determine the S-N curve, specimens are subjected to repeating or varying forces of specified magnitudes while cycles are counted to destruction.

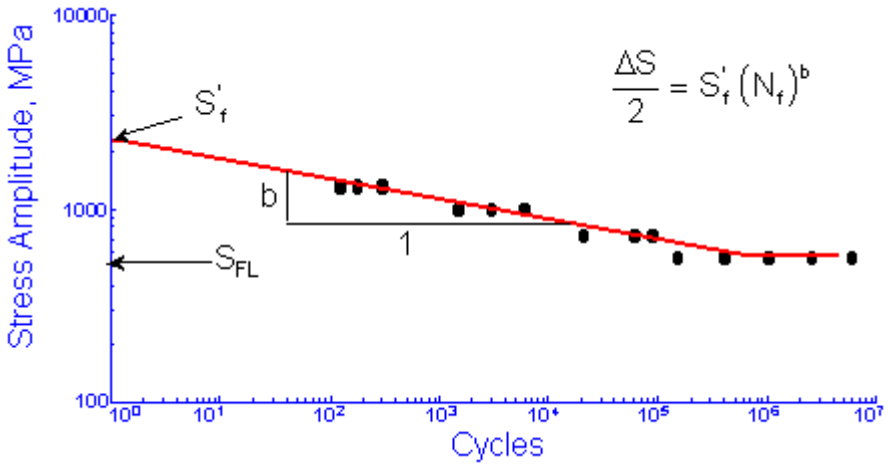

Figure 22. S-N curve [27]

The relation between the stress and cycle is sometimes expressed with Basquin's relation [8]:

$$\sigma_a = \sigma_f'(N)^b \tag{3.1}$$

where $\sigma_a \; or \; S$ is the alternating stress amplitude, σ_f' is the fatigue strength coefficient represents the value of $\sigma_a \; or \; S$ at one cycle, N is the cycle number and b is the fatigue strength exponent which is the slope of the log-log S-N curve.

S-N curve of a material changes according to the surface quality, size, temperature, load type, corrosion, plating type etc.

3.2.1.1.2 The Strain – Life Method

When the load history contains large overloads, the strain-life method is a better method than the stress-life method. When the stress exceeds the elastic limit, plastic strain occurs and the strain-life method are interested in both plastic and elastic strain. Application of the strain-life approach requires the material strain-life curve. In Figure 23, a sample ε-N curve is shown with plastic and elastic parts.

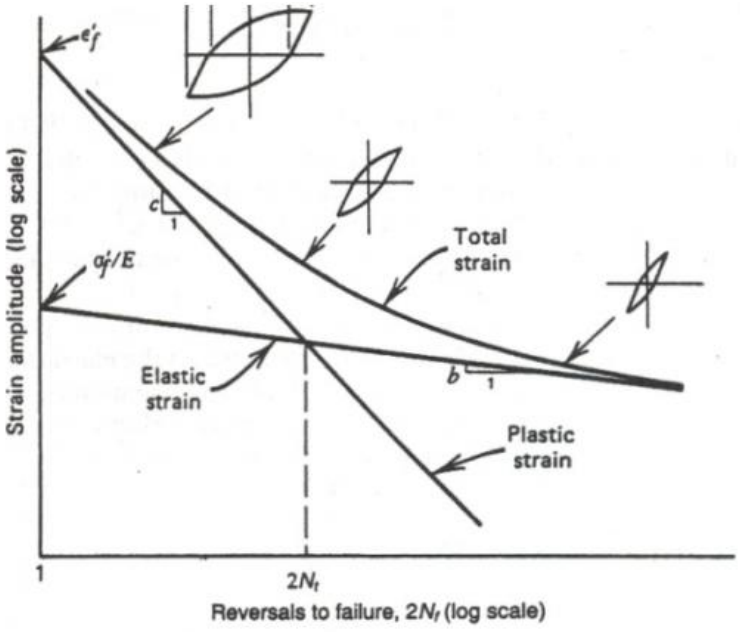

Figure 23. ε-N curve [28]

The relation between the elastic strain and life can be transformed to Basquin's equation:

$$\sigma_a = \sigma_f'(2N_f)^b \tag{3.2}$$

Where N_f is the half cycle number

The relation between the plastic strain and life can be transformed Manson-Coffin relationship [39]:

$$\frac{\varepsilon_p}{2} = \varepsilon_f'(2N_f)^c \tag{3.3}$$

Where $\varepsilon_p/2$ is the plastic strain amplitude, ε_f' is the fatigue ductility coefficient represents the value of ε_p at one cycle and c is fatigue ductility exponent which is the slope of log-log plastic line.

Adding the plastic and the elastic lines give the alternating strain amplitude, the total strain amplitude formula is obtained as follows:

$$\varepsilon_a = \frac{\varepsilon_e}{2} + \frac{\varepsilon_p}{2} = \frac{\sigma_f'}{E}(2N_f)^b + \varepsilon_f'(2N_f)^c \tag{3.4}$$

The above equation shows strain-life take account of low cycle fatigue with plastic line. Moreover, for elastic strains where the plastic strain term is negligible, the total strain-life equation reduces to Basquin's Eq. which is also used for the stress-life (S-N) method.

3.2.1.1.3 The Linear-Elastic Fracture Mechanics Method

This method assumes a discontinuity, flaw, crack etc. exists on the component. A sharp crack causes a high stress concentration at the its tip resulting in slip and plastic deformation in the crack tip vicinity. Variable loading causes the crack to grow until a critical size is reached causing fracture.

Based on energy balance of a cracked body Griffith [10] showed that $S_n\sqrt{a} = const.$ where S_n is the nominal stress and a is the crack length. Then, the stress intensity factor, K is defined which is:

$$K = S_n\sqrt{\pi a} f\left(\frac{a}{w}\right) \tag{3.5}$$

where $f(a/w)$ is the dimensionless geometry parameter and w is the width dimension.

The stress intensity factor which corresponds to the time when a crack extends in an unstable manner is called fracture toughness which is shown with K_c. The fracture toughness depends on the material, thickness, temprature, strain rate, envionment etc. The fracture toughness decreases with thickness and after a certain thickness, it approaches an asymptotic minimum value which is called the plane strain fracture toughness, K_{Ic}. This situation is shown in Figure 24.

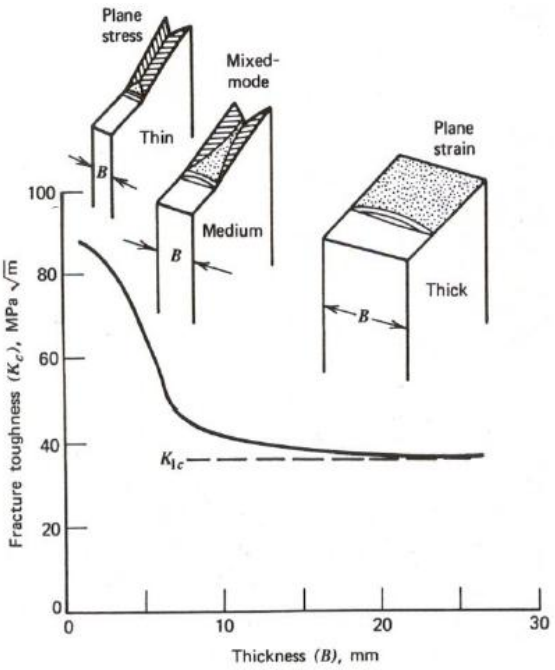

Figure 24. Fracture toughness vs thickness [29]

The tests also showed that for a given initial crack size the life to fracture depends on the stress intensity factor range, ΔK which is shown in Figure 25.

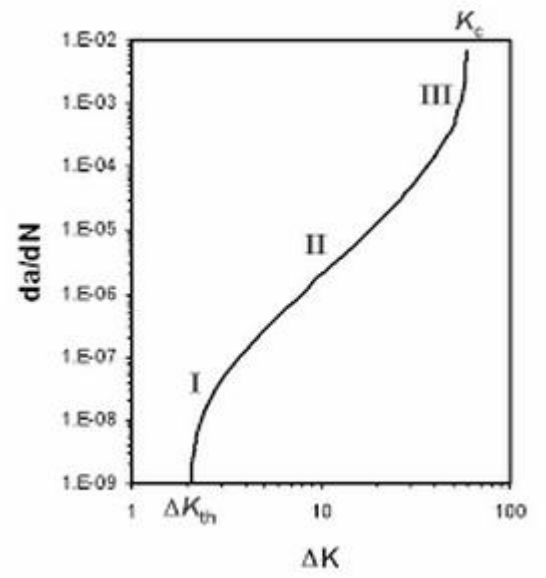

Figure 25. Fatigue Crack Growth Curve [30]

In Figure 25, in the 1st region, ΔK_{th} shows the threshold value below which there is no crack growth. In the 3rd region, fatigue growth rates are very high and in the end it reaches the fracture toughness. In the 2nd region, da/dN and ΔK show an almost linear relationship which is described by Paris-Erdogan as below [15]:

$$\frac{da}{dN} = C(\Delta K)^n \tag{3.6}$$

Where C is a material constant which equals to the da/dN when $\Delta K = 1$ and n is also a material constant which equals to the slope of the curve.

Substituting the equation 3.5 to the above equation 3.6:

$$\frac{da}{dN} = C(\Delta K)^n = C\left(\Delta S\sqrt{\pi a} f\left(\frac{a}{w}\right)\right)^n \tag{3.7}$$

$$N = \frac{{a_f}^{\left(-\frac{n}{2}\right)+1} - {a_i}^{\left(-\frac{n}{2}\right)+1}}{\left(\left(-\frac{n}{2}\right)+1\right) C(\Delta S)^n \pi^{n/2} \left(f\left(\frac{a}{w}\right)\right)^n} \tag{3.8}$$

Where a_i is the initial crack length and a_f is the critical crack length which can be defined as below:

$$a_f = \frac{1}{\pi}\left(\frac{K_c}{S_{max} f\left(\frac{a}{w}\right)}\right)^2 \tag{3.9}$$

3.2.1.2 Mean Stress Correction

Cyclic fatigue properties of a material for stress-life or strain-life fatigue behaviors are often obtained from completely reversed, constant amplitude tests where stress ratio $R = -1$. Stress ratio, R is simply the ratio of the minimum stress experienced during a cycle to the maximum stress experienced during a cycle. However, for LEFM data, R usually equals to 0 since during compression loading the crack is closed and hence no stress intensity factor, K, can exist. However, actual components are not only exposed these types of loading. Therefore, mean stress corrections are used to add the influence of the mean stress.

Mean stress corrections also change according to the fatigue life methods. Gerber, modified Goodman and Soderberg, Morrow theories are used for stress-life fatigue calculation. There is also a Morrow theory commonly used for strain-life fatigue calculation. For the LEFM method, Former and Walker equations can be used for mean stress correction.

Mean stress corrections for stress-life:

Gerber mean stress correction:

$$\frac{\sigma_a}{S_e} + \left(\frac{\sigma_m}{S_{ut}}\right)^2 = 1 \tag{3.10}$$

Modified Goodman correction:

$$\frac{\sigma_a}{S_e} + \frac{\sigma_m}{S_{ut}} = 1 \tag{3.11}$$

Soderberg correction:

$$\frac{\sigma_a}{S_e} + \frac{\sigma_m}{S_y} = 1 \tag{3.12}$$

Morrow correction:

$$\frac{\sigma_a}{S_e} + \frac{\sigma_m}{\sigma_f} = 1 \tag{3.13}$$

Where σ_m is the mean stress, S_e is the fully reversed endurance limit of the fatigue test specimens, S_{ut} and S_y are the ultimate tensile strength and yield strength of the material, respectively and σ_f is equal the fracture strength.

Mean stress corrections for strain-life:

Morrow correction:

$$\varepsilon_a = \frac{\sigma_f{}' - \sigma_m}{E}(2N_f)^b + \varepsilon_f{}'(2N_f)^c \tag{3.14}$$

An alternative version of Morrow's mean correction:

$$\varepsilon_a = \frac{\sigma_f{}' - \sigma_m}{E}(2N_f)^b + \varepsilon_f{}'\left(\frac{\sigma_f{}' - \sigma_m}{\sigma_f{}'}\right)^{c/b}(2N_f)^c \tag{3.15}$$

Mean stress corrections for the LEFM method:

Forman correction:

$$\frac{da}{dN} = \frac{C'(\Delta K)^{n'}}{(1-R)K_c - \Delta K} \tag{3.16}$$

Walker correction:

$$\frac{da}{dN} = \frac{C(\Delta K)^n}{(1-R)^{n(1-\lambda)}} \tag{3.17}$$

Where C', n' and λ are empirical material fatigue crack growth rate constants and R is the stress ratio.

3.2.1.3 Variable Loading

3.2.1.3.1 Cycle Counting Methods

To carry out estimated fatigue life calculations for a part with variable random loading, stress or strain data, cycle numbers of the loading must be known. To overcome this problem, cycle counting methods are generated. There are a lot of cycle counting methods such as peak count, range count, range mean count, level-crossing count, rainflow count etc. Among them the rainflow counting method is one of the most accurate and commonly used one.

In the rainflow counting method which is also referred to as the Pagoda roof method, counting is carried out on the basis of the stress-strain behaviour which is shown in Figure 26.

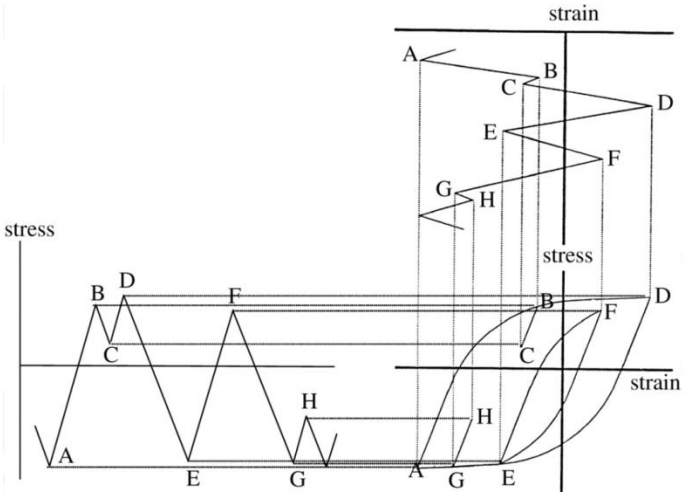

Figure 26. Stress-strain cycles [31]

If the load, stress or strain data is plotted such that the time axis is vertically downward, the rainflow counting method can be visualized better. While the time axis is vertically downward, the load, stress or strain data represents a series of roofs

where rain falls. The rules of the cycle counting while the rain fallls are described in the following:

1. The rain falls and flows form every valleys and peaks in order from top to bottom.
2. A new path cannot start before its predecessor has finished.
3. The flow will stop if it meets an opposing peak or valley larger than the departure.
4. The flow will stop if it meets the path traversed by a previous rainflow
5. Each rainflow corresponds to a half-cycle and the horizontal length of each rainflow defines the range of the half-cycle.

In Figure 27, a rainflow counting method example is shown.

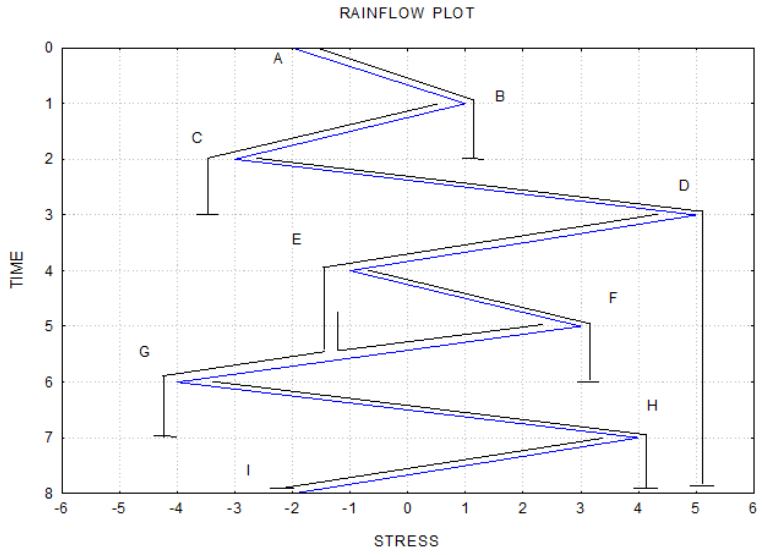

Rainflow Cycles by Path		
Path	Cycles	Stress Range
A-B	0.5	3
B-C	0.5	4
C-D	0.5	8
D-G	0.5	9
E-F	1.0	4
G-H	0.5	8
H-I	0.5	6

Figure 27. The rainflow counting method

3.2.1.3.2 Damage Accumulation Methods

The damage from a stress cycle can be found by the following formula:

$$D = \frac{1}{N_i} \tag{3.18}$$

where D is the damage, N_i is the number of cycles to failure at stress level σ_i.

According to the Palmgren-Miner cycle-ratio summation rule (as known as Miner's rule) the total damage "D_t" is defined as:

$$D_t = \sum \frac{n_i}{N_i} \tag{3.19}$$

where n_i is the the number of cycles at stress level σ_i.

To remedy the deficiencies with the linear damage assumption, many nonlinear cumulative damage rules have been proposed. However, Miner's rule is commonly used because of its simplicity. Moreover other complex methods do not make much improvements in failure prediciton. Therefore, in this thesis, Miner's rule is used for fatigue calculations.

3.2.1.4 Multiaxial Fatigue

Components are commonly exposed to multiaxial strains and stresses. The strain gage locations on the DMS used in this thesis were chosen from the finite element analyses. The strain gages were placed to the maximum stress locations on the DMS and these locations are shown in Figure 10, Figure 11 and Figure 12. From the finite element analyses and the tests' results, it is seen that the strains at these locations are multiaxial.

There are 2 type of loading according to the principle direction of the stress. They are proportional and nonproportional loading. During cyclic loading if the direction of the principal stresses remains fixed whether its magnitude changes or not, this is called proportinal loading. If the direction of the principal stresses changes, this type of loading is called the nonproportinal loading.

There are several multiaxial fatigue prediction approaches similar to the uniaxial methods such as stress-based methods, strain-based methods and fracture mechanic methods.

3.2.1.4.1 Stress-based methods

Multiaxial fatigue is predicted by various stress-based methods such as the Sines, the Findley and the Dang Van methods .

Sines Method [40]

Sines method uses alternating octahedral shear stress and hydrostatic mean stress to find an equivalent shear stress. And to find the life, this equivalent stress can be compared with the material S-N curve where stresses are plotted in terms of the octahedral shear stress.

$$\frac{\Delta\tau_{oct}}{2} + \alpha(3\sigma_h^{mean}) = \beta = \tau_f{}'(N)^b \tag{3.20}$$

Where $\Delta\tau_{oct}$ is the octahedral shear stress range, σ_h^{mean} is the hydrostatic mean stress. α is the mean stress influence constant and β is the equivalent octahedral shear stress which is compared with stress-life curve to estimate the life. $\tau_f{}'$ is the shear fatigue strength coefficient.

Sines method looks the stress acting on one specific plane for fatigue prediction; therefore it is limited to the proportional loading, does not give very accurate results for nonproportional loading.

Findley Method [41]

Findley method uses the influence of the maximum normal stress acting on the shear stress plane.

$$\max_{\theta}\left(\frac{\Delta\tau}{2} + k\sigma_n\right) = f = \sqrt{1+k^2}\,\tau_f{}'(N)^b \tag{3.21}$$

Where $\Delta\tau$ is the shear stress range, σ_n is the normal stress on the plane, k is the material constant which shows the influence of the normal stress to the shear stress.

f is Findley damage parameter which is compared with the right part of the above equation to find the life, N.

Findley method is different from Sine method which looks only one specific plane. Findley method calculates the Findley damage parameters for many planes and finds the fatigue life according to the maximum Findley damage parameter. θ in the formula specifies the plane angle. Therefore; this method can be used for both proportional and nonproportional loading. Moreover, this method find the critical plane angle which crack propagates.

Dang Van Method [42]

Dang Van method is based on the concept of microstresses within a critical volume of the material as follows:

$$\tau + a\sigma_h = b \tag{3.22}$$

Where τ is the shear stress, σ_h is the hydrostatic stress, a is the material constant which shows the influence of the hydrostatic stress to the shear stress and b is the fatigue strength determined from a torsion test. Dang Van method is used to predict the safety factor instead of the life. Material properties a and b are found from the material tests and the failure lines are generated as while τ and σ_h are variables. If the analyses or test results cross these lines, failure occurs. This is shown in Figure 28.

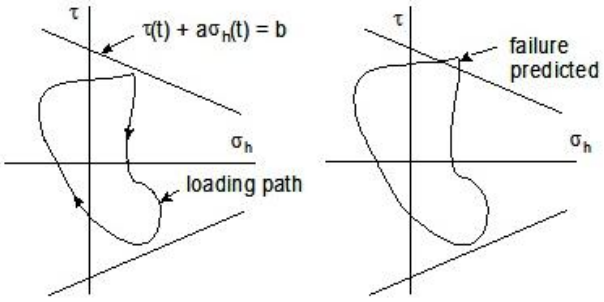

Figure 28. Dang Van method [32]

The safety factor is calculated using analyses or test results as follows:

$$n = \frac{b}{(\tau + a\sigma_h)_{max}} \tag{3.23}$$

Dang Van method is also valid for both proportional and nonproportional loading.

3.2.1.4.2 Strain-based methods

Multiaxial fatigue is predicted by various strain-based methods. Brown-Miller, Fatemi-Socie and Smith-Watson are a few of them.

Brown-Miller Method [43]

According to this method, cyclic shear strain and normal strain must be taken into consideration for fatigue prediction.

$$\max_{\theta}\left(\frac{\Delta\gamma_{max}}{2} + S\Delta\varepsilon_n\right) = \beta_1 \frac{\sigma_f{}'}{E}(2N_f)^b + \beta_2 \varepsilon_f{}'(2N_f)^c \tag{3.24}$$

Where $\Delta\gamma_{max}$ is the maximum shear strain range, $\Delta\varepsilon_n$ is the normal strain range on the plane experiencing the shear strain range $\Delta\gamma_{max}$, S is the material constant which shows the influence of the normal strain on material crackgrowth and E is the elastic modulus of the material. β_1 and β_2 are defined as follows:

$$\beta_1 = 1 + \nu + S(1 - \nu) \tag{3.25}$$

$$\beta_2 = 1.5 + 0.5S \tag{3.26}$$

Fatemi-Socie Method [44]

Fatemi and Socie predict the multiaxial fatigue using cyclic shear strain and normal stress as follows:

$$\max_{\theta}\left(\frac{\Delta\gamma_{max}}{2}\left(1 + k\frac{\sigma_{n,max}}{S_y}\right)\right) = \frac{\tau_f{}'}{G}(2N_f)^{b_0} + \gamma_f{}'(2N_f)^{c_0} \tag{3.27}$$

Where $\Delta\gamma_{max}$ is the maximum shear strain range, $\sigma_{n,max}$ is the maximum normal stress, S_y is the yield strength of the material, k is the material constant which shows the influence of the normal stress on material crackgrowth, G is the shear modulus of

the material, $\tau_f{}'$ and $\gamma_f{}'$ are the shear fatigue strength and shear fatigue ductility coefficient respectively, b_0 and c_0 are the shear fatigue strength and shear fatigue ductility exponent respectively.

Mean or residual stress effects on fatigue life in this model are accounted for by the maximum normal stress term:

$$\sigma_{n,max} = \sigma_{n,a} + \sigma_{n,m} \tag{3.28}$$

Smith-Watson Method [45]

Smith-Watson Method is based on the effect of the normal strain and the normal stress to the fatigue failure as follows:

$$\max_{\theta}\left(\sigma_{n,max}\frac{\Delta\varepsilon_1}{2}\right) = \frac{{\sigma_f}'^2}{G}(2N_f)^{2b} + {\sigma_f}'^2{\varepsilon_f}'(2N_f)^{b+c} \tag{3.29}$$

Where $\Delta\varepsilon_1$ is the principal strain range on the plane. $\varepsilon_f{}'$ is the fatigue ductility coefficient.

This model is suitable for materials that that fail predominantly on planes of maximum tensile strain or stress such as cast iron.

In Figure 29, the parameters used in above strain-based methods are summarized.

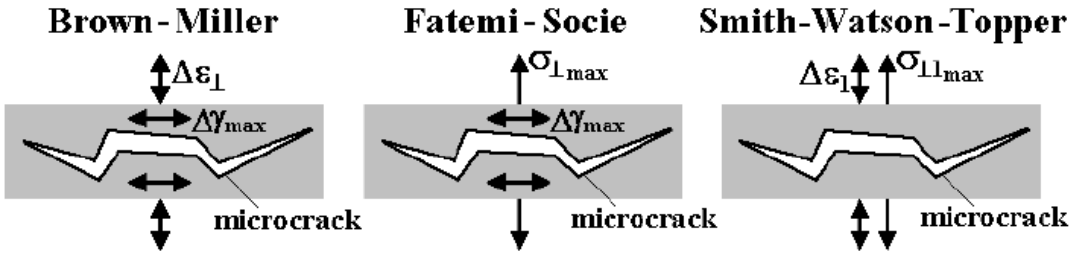

Figure 29. Parameters which affect the strain-based multiaxial methods [33]

All of the strain-based methods mentioned above are also critical plane methods which means planes with different orientation can be investigated by these methods. Therefore, they can be used for nonproportional loading.

3.2.1.4.3 Fracture Mechanics Methods

Mixed mode crack growth can occur on components because of multiaxial stress state. Therefore, crack can change its growth direction. There are several methods based on the calculation of the equivalent stress intensity factor are suggested for fatigue predicition. One of them is Tanaka's suggestion which is as follows [46]:

$$\Delta K_q = \left(\Delta K_I^4 + 8\Delta K_{II}^4 + \frac{8\Delta K_{III}^4}{1^{-\nu}} \right)^{0.25} \tag{3.30}$$

Where ΔK_q is the equivalent stress intensity factor and ΔK_I, ΔK_{II} and ΔK_{III} are the mode I, II and III stress intensity factors respectively. Three mode of loading is shown in Figure 30.

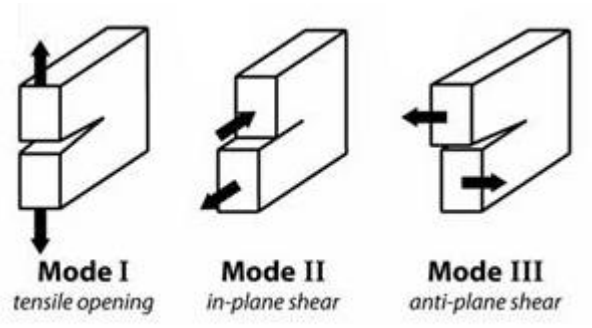

Figure 30. The three modes of loading [34]

After finding the equivalent stress intensity factor, Paris-Erdogan law can be used to predict the life.

3.2.2 Fatigue Calculation

The strain gages were placed to the maximum stress locations on the DMS and these locations are shown in Figure 10, Figure 11 and Figure 12. All the components where strain gages located are made of AISI 4140 36-42 HRC steel. After making strain and stress transformation calculations and comparing the results, it is seen that among all locations, strains and stresses of the aft wings are much higher than the rest. Therefore, in this thesis, fatigue calculations using strain gages were made for the aft wings.

There are 2 critical locations for every shaft of the wings. In Figure 31, these critical locations are shown. These critical locations were verified with finite element analysis. For these critical locations, 1 torsional shear strain and 1 tensile strain along the shaft axis were obtained from strain gages which are more dominant strains than the others [21].

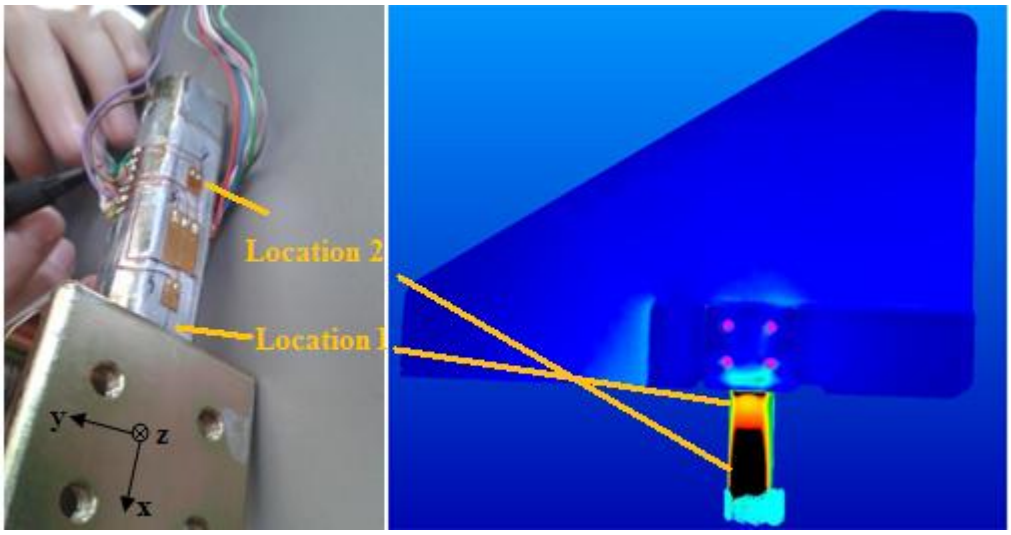

Figure 31. Critical locations for the shaft of the wing

Fatigue calculation methodology for 2 critical locations of 4 aft wings can be summarized as follows:

1. Multiaxial state of stress occurs on the shaft of the wings. Therefore, proportionality of the stress was checked at first. In Figure 32, it is seen that the relation between the shear strain and normal strain is not linear. This shows that the loading is nonproportional.

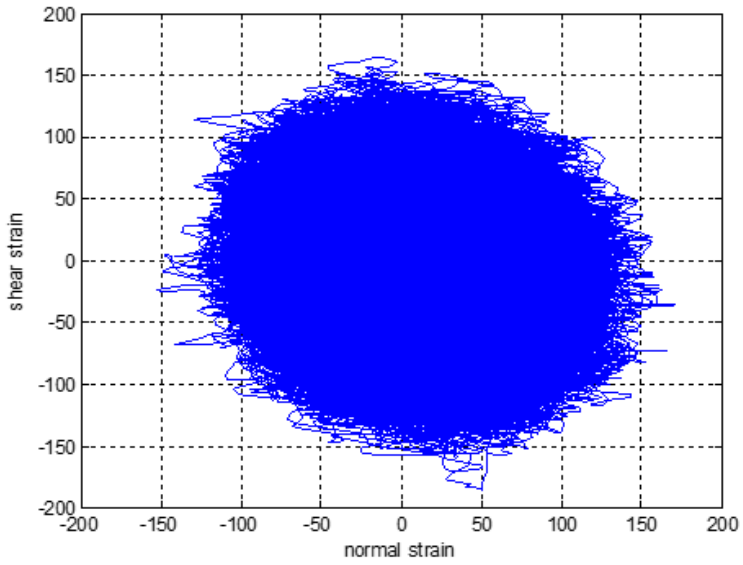

Figure 32. Proportionality of the loading

2. Strains are too small on the shafts of the wings for the formation of plastic deformation. Therefore, tensile and shear stresses for 2 critical locations were found from strain gage data using Hooke's law:

$$\varepsilon_x = \frac{\sigma_x}{E} - \nu\frac{\sigma_y + \sigma_z}{E} \tag{3.31}$$

$$\gamma_{xy} = \frac{\tau_{xy}}{G} \tag{3.32}$$

Where ε_x and γ_{xy} are tensile and shear strain respectively. Coordinate axis is shown in Figure 31. σ_z, γ_{xz} and γ_{yz} equal to 0 because of free surface. $\sigma_y \sim 0$ because the shaft is not thick enough for the formation of this stress. Material constants are as follows:

$$E = 207\ GPa \tag{3.33}$$

$$\nu = 0.29 \tag{3.34}$$

$$G = \frac{E}{2(1+\nu)} \cong 80233\ MPa \tag{3.35}$$

3. After adding stress concentration factors etc., shear and normal stresses were found for every 4° plane angle using stress transformation formula as defined below:

$$(\sigma_n)_\theta = \frac{\sigma_x}{2} + \frac{\sigma_x}{2} cos(2\theta) + \tau_{xy}\, sin(2\theta) \tag{3.36}$$

$$(\tau)_\theta = -\frac{\sigma_x}{2} sin(2\theta) + \tau_{xy}\, cos(2\theta) \tag{3.37}$$

4. Shear strains were found for every plane angle using Hooke's law (eq. 3.31).

5. Cycles were counted by rainflow counting method for every 4° angled plane which is explained in 3.2.1.3.1.

6. Life and damage were calculated for every data blocks in Table 3 for every 4° angled plane.

Among multiaxial fatigue prediction methods, the Fatemi-Socie method was chosen for life calculation because this method can be used for elastic deformation and is suitable for ductile materials and gives quite accurate results [49]. The formulation of the method is stated in equation 3.27 which is as follows:

$$\max_\theta \left(\frac{\Delta\gamma_{max}}{2} \left(1 + k \frac{\sigma_{n,max}}{S_y} \right) \right) = \frac{\tau_f{}'}{G} (2N_f)^{b_0} + \gamma_f{}' (2N_f)^{c_0} \tag{3.27}$$

Mean stress effects on fatigue life in this model are accounted by the influence of the maximum normal stress. Because:

$$\sigma_{n,max} = \sigma_{n,m} + \sigma_{n,a} \tag{3.38}$$

Where $\sigma_{n,m}$ and $\sigma_{n,a}$ are the mean normal and alternating normal stresses, respectively.

AISI 4140 36-42 HRC steel properties used in the Fatemi-Socie method as follows:

$$k = 0.6 \tag{3.39}$$

$$S_y = 929\ MPa \tag{3.40}$$

$$\tau_f' = 968\ MPa \tag{3.41}$$

$$G = 80233\ MPa \tag{3.42}$$

$$\gamma_f' = 1.42 \tag{3.43}$$

$$b_0 = -0.0846 \tag{3.44}$$

$$c_0 = -0.6505 \tag{3.45}$$

Substituting above equations into equation 3.27, $2N_f$ and consequently, subdamages were found for every data blocks in Table 3 by below formula:

$$D = 1/2N_f \tag{3.46}$$

7. The total damage for every 4^o angled plane was found by adding subdamages for that plane. The total life for every 4^o angled plane was found by equation 3.19.

8. The most critical plane, damage and life were found and compared for different plane angles.

Damage of one ideal average sortie for F-16C jet aircraft for different plane angles at 2 different locations for wings 1-4 are shown in Figure 33 - Figure 40. Numerations of the wings are shown in Figure 20.

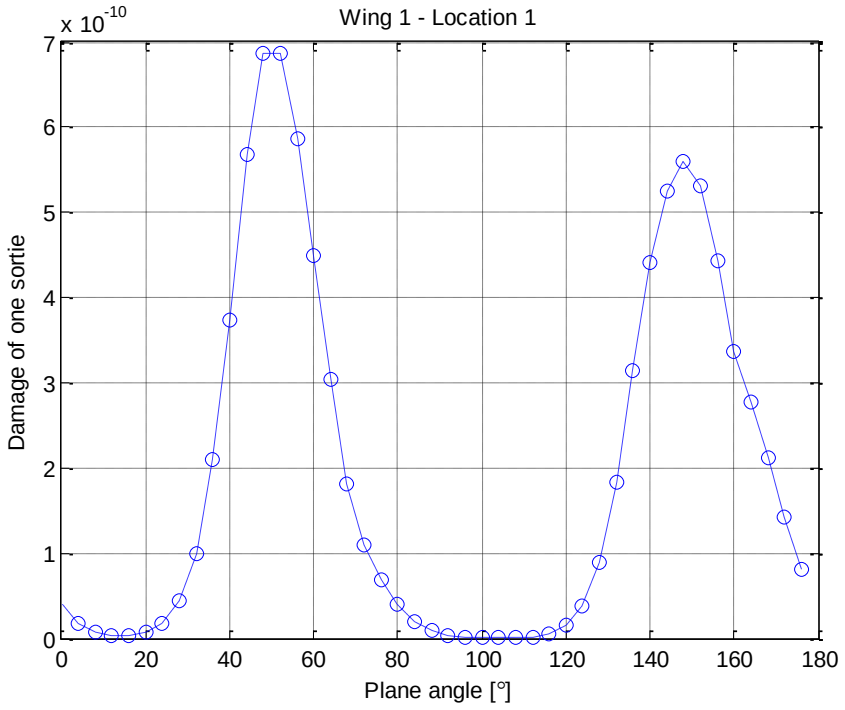

Figure 33. Damage results of different planes at wing 1, location 1

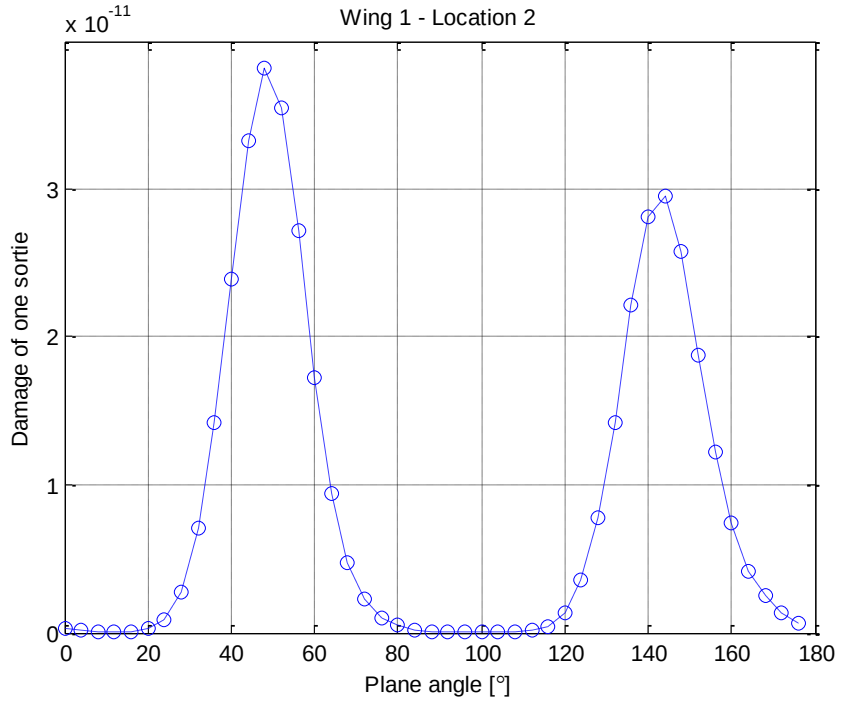

Figure 34. Damage results of different planes at wing 1, location 2

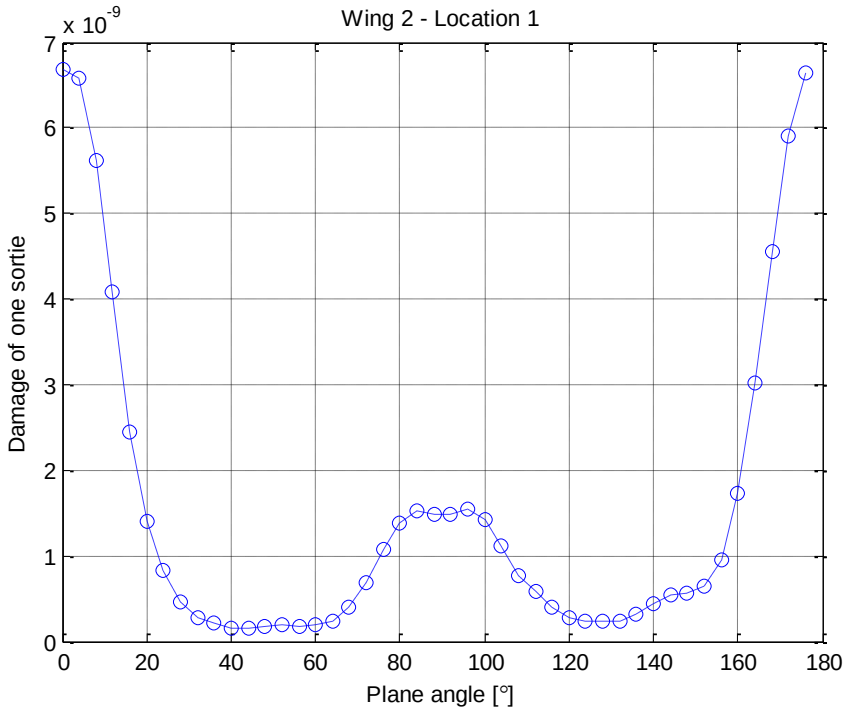

Figure 35. Damage results of different planes at wing 2, location 1

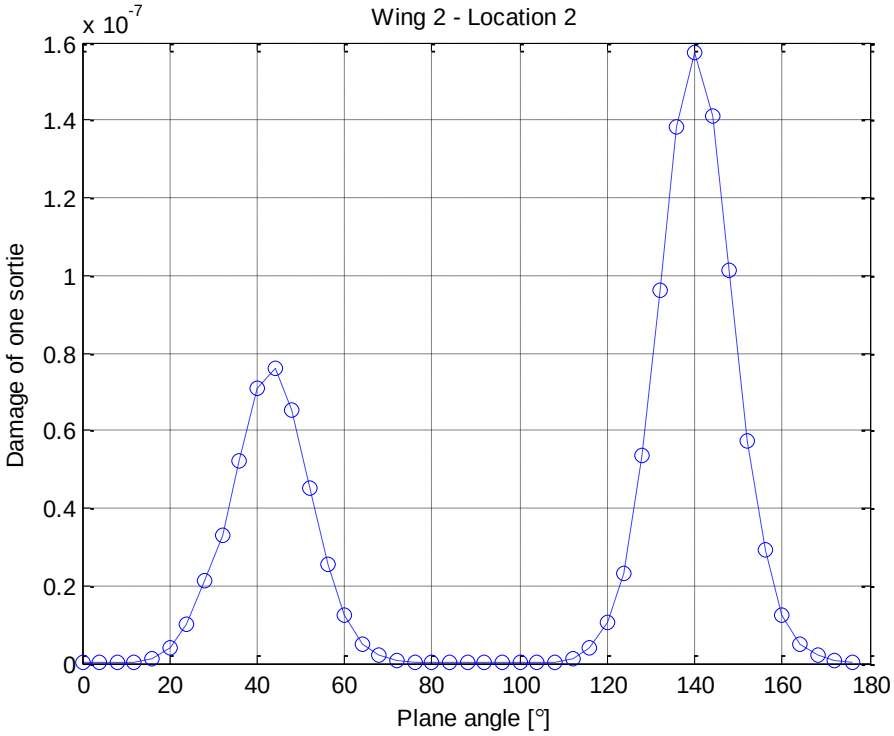

Figure 36. Damage results of different planes at wing 2, location 2

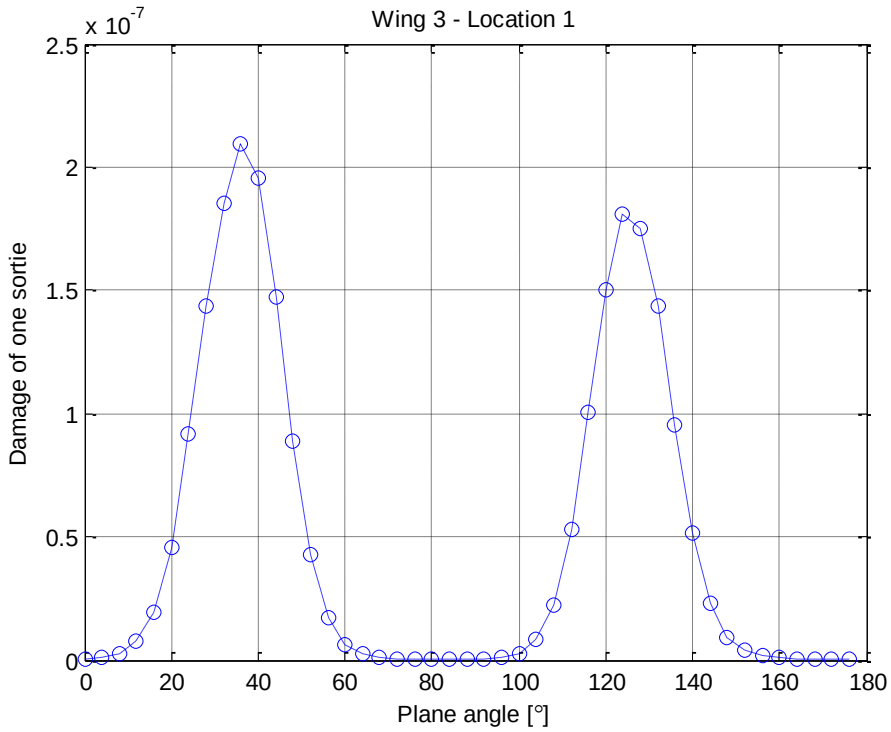

Figure 37. Damage results of different planes at wing 3, location 1

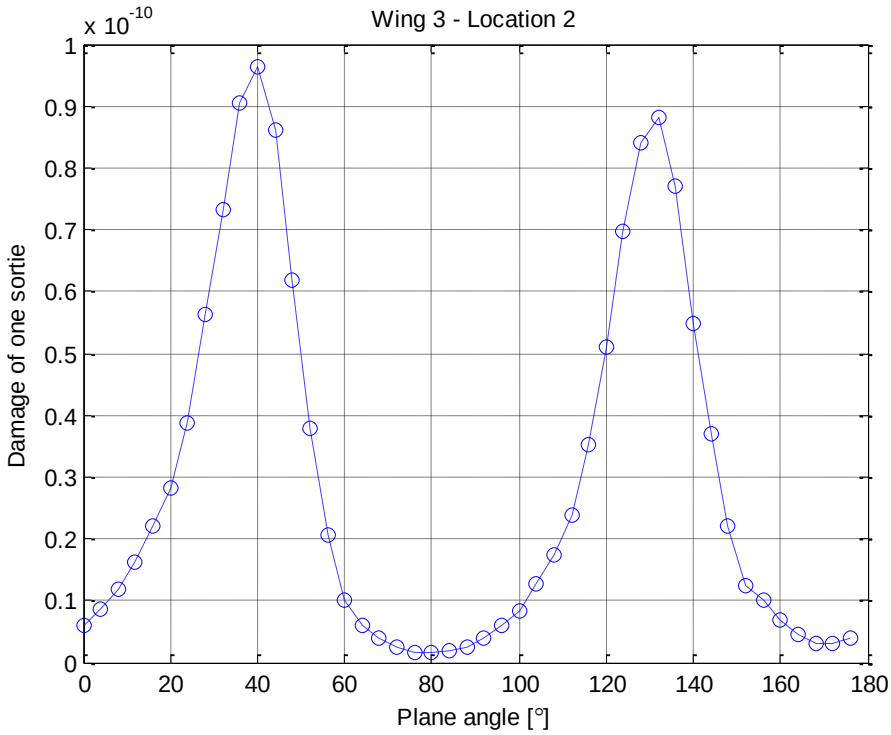

Figure 38. Damage results of different planes at wing 3, location 2

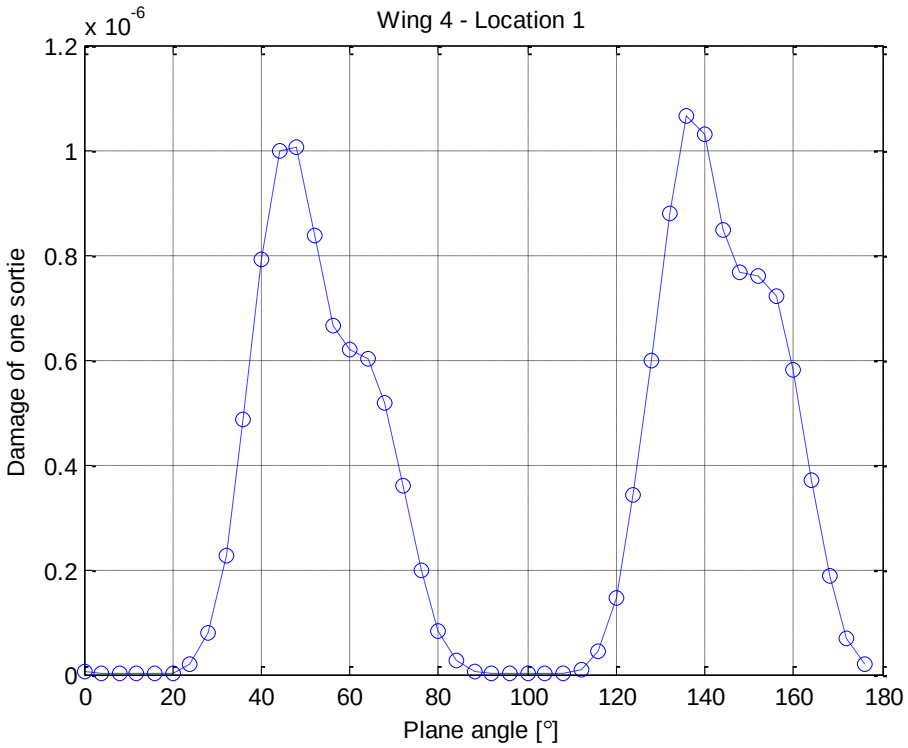

Figure 39. Damage results of different planes at wing 4, location 1

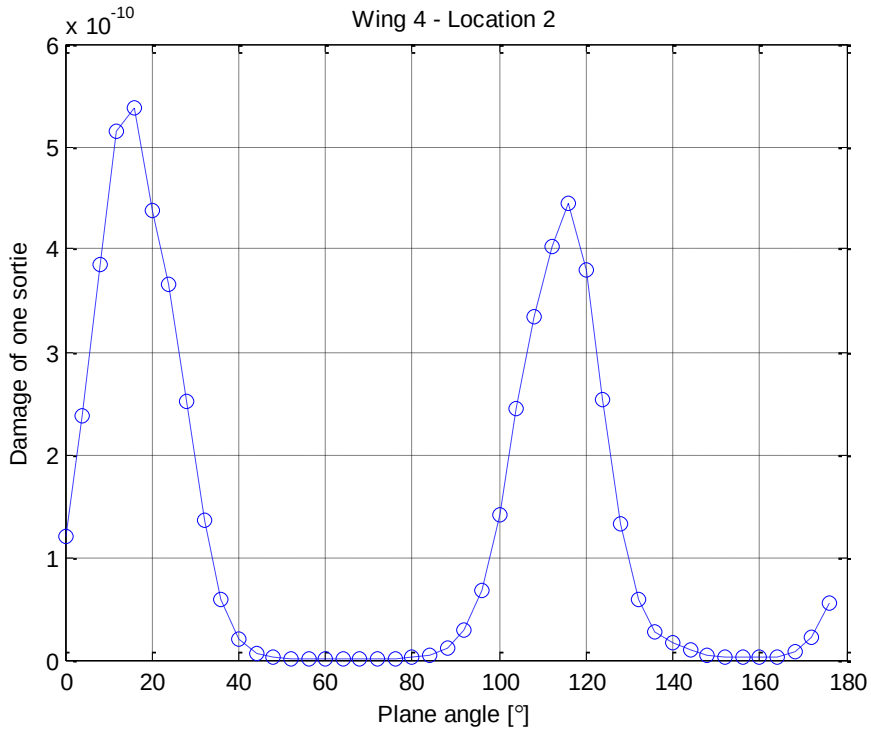

Figure 40. Damage results of different planes at wing 4, location 2

The most critical location at the DMS was found as wing 4, location 1 at 136° angled plane from x axis. The life at this location according to the fatigue damage calculations is 9.3803e+005 ideal average F-16C jet aircraft sorties which is very long duration for failure. This shows the random vibration loads are small and cause high cycle fatigue rather than low cycle fatigue.

3.3 Acceleration Data Preparation

3.3.1 Theory

Acceleration data do not show directly whether a component will fail or not because of the fatigue. Acceleration data are used as an input for fatigue analyses and tests. The theory behind the preparation of the acceleration data for the fatigue analyses and tests are mentioned below.

3.3.1.1 Fatigue Damage Spectrum

The fatigue damage spectrum proposed by Lalanne [24] can be used to compare the severity of different types of vibration environments. In this thesis, the fatigue damge spectrum was used to integrate different types of vibration environments to a single vibration environment while the total damage remained the same.

The fatigue damage spectrum of a vibration signal can be defined as a curve giving the fatigue damage experienced by a linear single degree of freedom system according to the natural frequency of the SDOF system while the SDOF system exposed to the vibratory signal as a base excitation. (Figure 41)

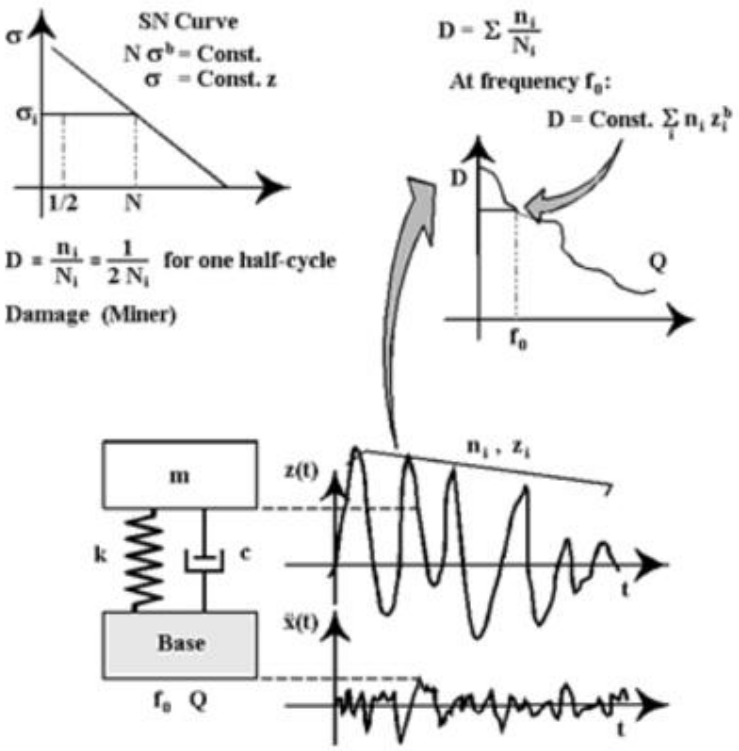

Figure 41. FDS calculation from a time signal [24]

Fatigue damge spectrum can be calculated from an acceleration signal on time domain or from an acceleration spectral density.

Using following assumptions,

- the signal is stationary
- the signal has a Gaussian distribution
- the signal has zero mean
- Basquin's relation ($N\sigma^b = C$) represents the S-N curve
- The Miner's rule (linear accumulation of damage)

derivation steps of the fatigue damage spectrum formula for the time domain signal are defined below:

Firstly, stress of the elastic element will be proportional to the relative displacement because the system is linear. Therefore,

$$\sigma = K \cdot z_p \tag{3.47}$$

Where K is a constant, z_p is the peak value of relative displacement response of the SDOF system $z(t)$ (Figure 41) and σ is the stress in the elastic element.

Then substituting the above equation into the Basquin's relation:

$$N\sigma^b = C \longrightarrow N(K \cdot z_p)^b = C \tag{3.48}$$

Where N is the number of the cycles to failure at stress level σ, C and b are the constants which are related to the material.

Also substituting the equation 3.48 into the Miner's damage accumulation formula, the cumulative damage can be calculated as:

$$D = \sum_{i=1}^{k} d_i = \sum_{i=1}^{k} \frac{n_i}{2N_i} = \sum_{i=1} \frac{n_i \sigma_i^b}{2C} = \frac{K^b}{2C} \sum_{i=1}^{k} n_i z_{p_i}^b \tag{3.49}$$

Where D is the cumulative damage, d_i is the damage and n_i is the number of half cycles at stress level σ_i. k is the class of level z_{pi}.

For a sinusoidal base acceleration $\ddot{x}(t) = \ddot{x}_p sin2\pi ft$ applied to a SDOF system, z_p can be calculated from the below formula.

$$|z_p| = \frac{\ddot{x}_p}{\omega_0^2 \sqrt{\left[1 - \left(\frac{f}{f_0}\right)^2\right]^2 + \left(\frac{f}{Qf_0}\right)^2}} \tag{3.50}$$

Then for a given time T, the cumulative damage will be:

$$D = \frac{K^b}{C} fT \frac{\ddot{x}_p^b}{\omega_0^{2b} \left\{\left[1 - \left(\frac{f}{f_0}\right)^2\right]^2 + \left(\frac{f}{Qf_0}\right)^2\right\}^{b/2}} \tag{3.51}$$

Where f is the frequency of the acceleration input, Q is the quality factor, f_0 is the natural frequency of the SDOF system.

From the above damage equation, the fatigue damage spectrum graph which is the damage response (D) according to the natural frequency (f_0) of the SDOF system can be obtained. As an example, in Figure 42, FDS of a sinusiodal vibration with 1g amplitude, 300 Hz frequency is shown while Q=10, K=1, C=1, T=100 s and b=4.

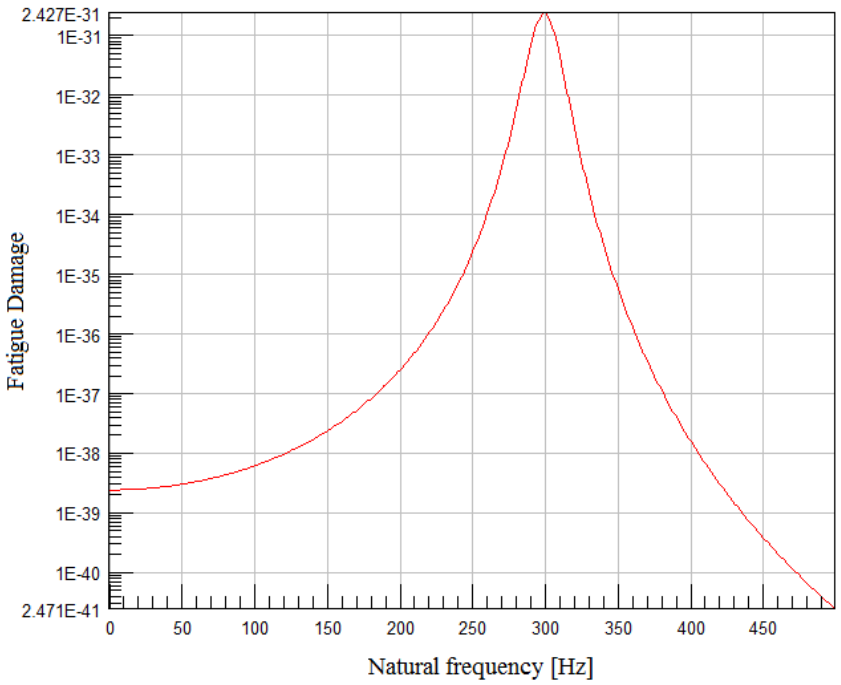

Figure 42. FDS of a sinusoidal vibration

For a random acceleration time history, cycle counting must be done as an extra to calculate the damage spectrum. There are a lot of cycle counting methods such as peak count, range count, range mean count, rainflow count etc. for a time domain signal. However, the frequency domain is widely used to view an acceleration data especially if the acceleration is random. In the frequency domain, a power spectral density, which shows the power distribution of a signal for different frequencies, is usually used to view an acceleration data. Fatigue damage spectrum can also be calculated from the power spectral densities. Firstly, to calculate the fatigue damage

spectrum from a power spectral density, cycles must be counted from the power spectral denisty. There are a lot of methods using the theoretical and experimental research to count cycles from a power spectral denstiy such as Wirsching-Light, the α0.75, Gao-Moan, Dirlik, Zhao-Baker, Tovo-Benasciutti and Petrucci-Zuccarello, Bendat and Rice's Narrowband, Steinberg, Lalanne / Rice methods.

In this thesis, the Lalanne/Rice method [24] which is one of the most accurate one when compared with the time domain data was used for cycle counting from the power spectral densities. Rice assumed the peak probability of a stationary and Gaussian random vibration has Rayleigh distribution. However, Lalanne showed that this assumption is valid only for a narrowband signal. He showed the peak probability density of a stationary and Gaussian random vibration is the weighted sum of the Gaussian law and the Rayleigh law. According to the Lalanne/Rice method, the peak probability density function is:

$$q(z_p) = \frac{\sqrt{1-r^2}}{z_{rms}\sqrt{2\pi}} e^{-\frac{z_p^2}{2(1-r^2)z_{rms}^2}} + \frac{r z_p}{2z_{rms}^2} e^{-\frac{z_p^2}{2z_{rms}^2}} \left[1 + erf\left(\frac{r z_p}{z_{rms}\sqrt{2(1-r^2)}}\right)\right] \tag{3.52}$$

Where irregularity factor, r is:

$$r = \frac{n_0^+}{n_p^+} = \frac{\dot{z}_{rms}^2}{z_{rms}\,\ddot{z}_{rms}} = \frac{\int_0^\infty f^2 G_z(f)df}{\sqrt{\int_0^\infty G_z(f)df \int_0^\infty f^4 G_z(f)df}} \tag{3.53}$$

$$n_0^+ = \frac{1}{2\pi}\frac{\dot{z}_{rms}}{z_{rms}} = \sqrt{\frac{\int_0^\infty f^2 G_z(f)df}{\int_0^\infty G_z(f)df}} \approx f_0 \tag{3.54}$$

$$n_p^+ = \frac{1}{2\pi}\frac{\ddot{z}_{rms}}{\dot{z}_{rms}} = \sqrt{\frac{\int_0^\infty f^4 G_z(f)df}{\int_0^\infty f^2 G_z(f)df}} \tag{3.55}$$

n_0^+ is the mean number of zero-crossings with positive slope per second and n_p^+ is the mean number of maxima per second. z_{rms}, $\dot{z}_{rms}$, $\ddot{z}_{rms}$ is the RMS values of the relative displacement, velocity and acceleration of the SDOF system. $G_z(f)$ is the PSD of the relative response displacement. For a narrowband signal, the irregularity

factor (r) gets closer to 1 and the peak values distribution can be assimilated to the Rayleigh law. Consequently, Rice's Narrowband method and Lalanne/Rice Method give similar solutions. However, for a wideband signal, the irregularity factor (r) gets closer to 0 and the peak values distribution can be assimilated to the Gaussian law and Rice's Narrowband method becomes very conservative for the damage calculation.

In the probability density function $erf()$ is the error function which is defined by:

$$erf(x) = 1 - \frac{2}{\pi}\int_{x}^{\infty} e^{-\lambda^2} d\lambda \tag{3.56}$$

Then, the fatigue damage calculation from a power spectral density is defined as:

$$D = \frac{K^b}{C} n_p^+ T \int_0^{\infty} z_p^b q(z_p) dz_p \tag{3.57}$$

The response relative displacement of a single-degree-of-freedom linear system submitted to white noise can be approximated by:

$$z_{rms} = \sqrt{\frac{G_{\ddot{x}}}{64\pi^3 f_0^3 \xi}} \tag{3.58}$$

Where ξ is the damping factor and $G_{\ddot{x}}$ is the PSD value of the acceleration input (base acceleration).

As an example, in Figure 43, FDS of a random vibration is shown while $Q = 10, K = 1, C = 1, T \sim 10000\ s\ and\ b = 4$.

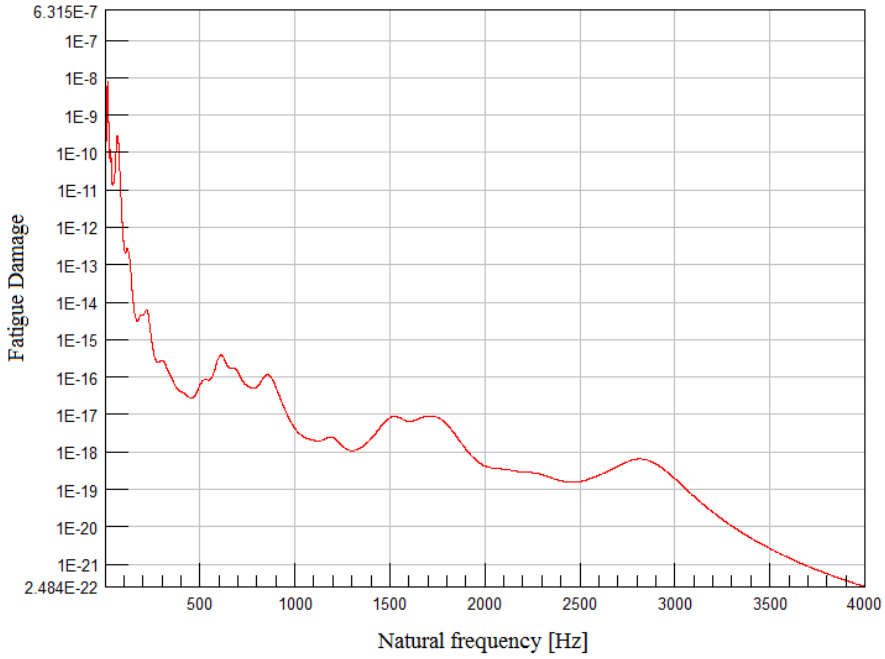

Figure 43. FDS of a random vibration

In this thesis, the fatigue damage spectrum was used to combine the acceleration data obtained for different conditions shown in Table 3. Firstly, the power spectral densities of all the conditions in Table 2 were calculated. Then, the fatigue damage spectrums of these power spectral densities were calculated. In other words, the fatigue damage contributions of all conditions in Table 3 were found. Afterwards, all these fatigue damage were summed up and a single fatigue damage spectrum was found. Finally, from this single fatigue damage spectrum, a PSD was calculated which represents the acceleration PSD for the ideal average F-16C jet aircraft sortie. This PSD was used for the fatigue analysis and vibration test duration reduction.

3.3.1.2 Shock Response Spectrum (SRS)

The shock response spectrum of a vibration is a graphical representation of how a single degree of freedom (SDOF) system responds to that vibration for different natural frequencies of the SDOFs system. Actually, it shows the peak displacement response of an infinite number of SDOFs, each of which has different natural frequencies while the SDOF system is exposed to the vibratory signal as a base

excitation. The SRS which shows the acceleration response of the SDOF system can be obtained from the peak displacement response.

The SRS is calculated from a vibration in time domain. Figure 44 shows the calculation way of the SRS.

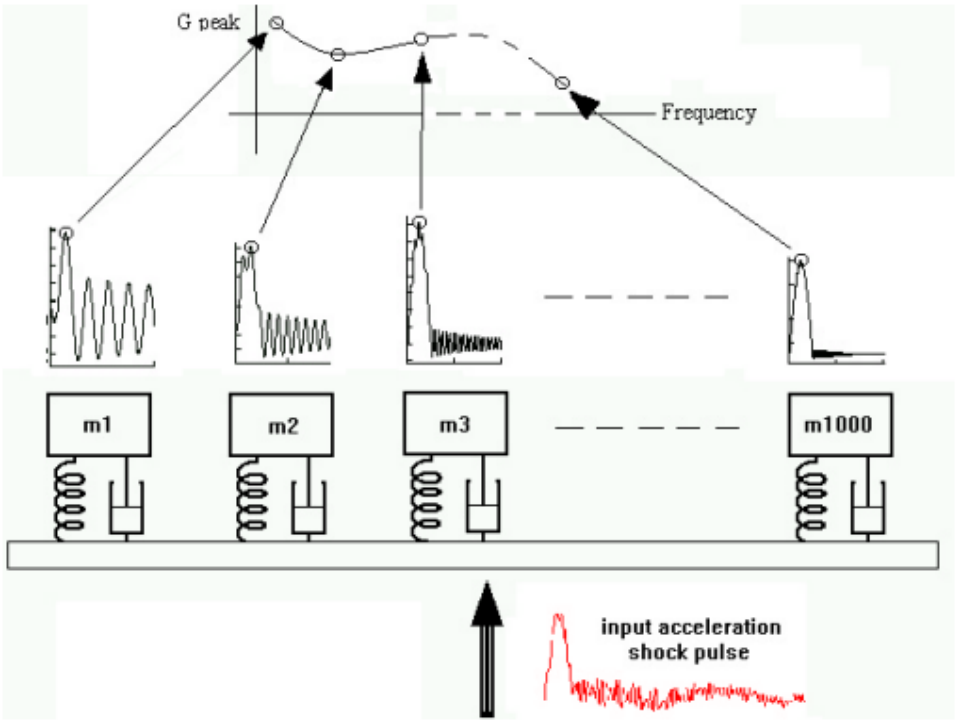

Figure 44. Calculating the Shock Response Spectrum (SRS) [35]

The calculation of the SRS for an acceleration input is shown below:

First, the equation of motion of the SDOF system is:

$$m\ddot{y}(t) + k\big(y(t) - x(t)\big) + c\big(\dot{y}(t) - \dot{x}(t)\big) = 0 \qquad (3.59)$$

Where $x(t)$ is the displacement of the base of the SDOF system and $y(t)$ is the absolute displacement of the mass of the SDOF system as shown in Figure 45. $m, k\ and\ c$ is the mass, stiffness and damping constant of the SDOF system.

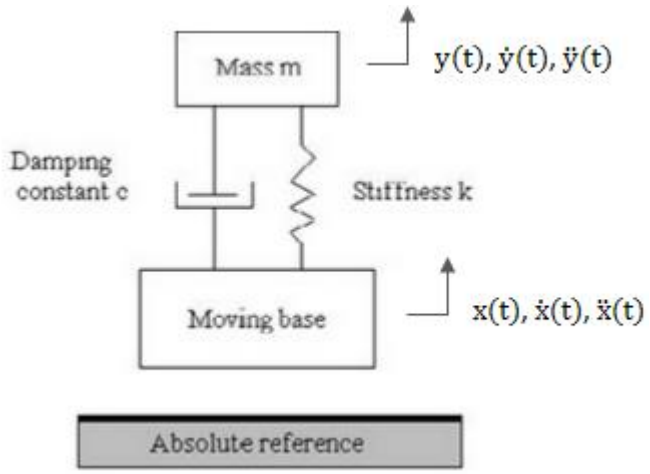

Figure 45. The SDOF system subjested to acceleration [24]

Setting $z(t) = y(t) - x(t)$ and dividing all equation to m, the equation becomes:

$$\ddot{z}(t) + 2\xi\omega_0\dot{z}(t) + \omega_0^2 z(t) = \ddot{x}(t) \tag{3.60}$$

Where ξ is the damping factor and ω_0 is the natural frequency. The closed form solution can be obtained from Duhamel's Integral for equation 3.52.

Then, the relative displacement of the mass of the SDOF sytem:

$$z(t) = \frac{-1}{\omega_0\sqrt{1-\xi^2}} \int_0^t \ddot{x}(\alpha)\, e^{-\xi\omega_0(t-\alpha)}\, sin\, \omega_0 \sqrt{1-\xi^2}(t-\alpha) d\alpha \tag{3.61}$$

And the absolute acceleration of the mass of the SDOF sytem:

$$\ddot{y}(t) = \frac{\omega_0}{\sqrt{1-\xi^2}} \int_0^t \ddot{x}(\alpha)\, e^{-\xi\omega_0(t-\alpha)} \Big[(1-2\xi^2)\, sin\, \omega_0 \sqrt{1-\xi^2}(t-\alpha) + 2\xi\sqrt{1-\xi^2}\, cos\, \omega_0 \sqrt{1-\xi^2}(t-\alpha)\Big] d\alpha \tag{3.62}$$

The shock response spectrum (SRS) is defined as the maximum $|\ddot{y}(t)|$ for each natural frequency of the SDOF system..

In this thesis, The SRS was used to verify the test PSD duration of the acceleration data. For this purpose the SRS was compared with the extreme response spectrum (ERS) which is explained below.

3.3.1.3 Extreme Response Spectrum (ERS)

The extreme response spectrum (ERS) also shows the peak response of an infinite number of SDOFs, each of which has different natural frequencies, while the SDOF system is exposed to the vibratory signal as a base excitation just like the shock response spectrum (SRS). The difference is that, the SRS is computed in the time domain; however, the ERS is computed in the frequency domain.

In case of a single sinusoid, the relative displacement $z(t)$ and maximum displacement z_m of the mass m of the SDOF system is defined by:

$$z(t) = -\frac{\ddot{x}(t)}{\omega_0^2\sqrt{\left[1-\left(\frac{f}{f_0}\right)^2\right]^2+\left(\frac{f}{Qf_0}\right)^2}} \tag{3.63}$$

$$z_m = \pm\frac{\ddot{x}_m}{\omega_0^2\sqrt{\left[1-\left(\frac{f}{f_0}\right)^2\right]^2+\left(\frac{f}{Qf_0}\right)^2}} \tag{3.64}$$

Then ERS becomes:

$$ERS \equiv \omega_0^2 z_m = \frac{\ddot{x}_m}{\sqrt{\left[1-\left(\frac{f}{f_0}\right)^2\right]^2+\left(\frac{f}{Qf_0}\right)^2}} \tag{3.65}$$

For the PSD of a Gaussian stationary random signal, the ERS formula is defined by:

$$ERS \approx \omega_0^2 z_{rms} u_0 \tag{3.66}$$

Where z_{rms} is defined in equation 3.50 and u_0 is the ratio of the peak amplitude of the relative displacement response of the SDOF system, $z(t)$, to the RMS value of this relative displacement. During the calculation of u_0 from the PSD of the vibratory signal, Lalanne again used the Rayleigh law and the Gaussian law together. However, in this thesis, the Extreme Response Spectrum were used to calculate the accelerated vibration test duration and the fatigue tests are conducted with 3σ standard deviation in accordance with the test rigs. Therefore, during calculation of the ERS, the Gaussian distribution with 3σ standard deviation were used instead of the Lalanne method. In 1954, Miles [38] presented an equation to calculate ERS

using a Gaussian approximation to the peak amplitude distribution of the vibration signal. He took the base input amplitude at the natural frequency. From this approach, a general approach is defined which allows the power spectral density to vary with frequency:

$$ERS = \frac{1 + \left(\frac{f}{Qf_0}\right)^2}{\left[1 - \left(\frac{f}{f_0}\right)^2\right]^2 + \left(\frac{f}{Qf_0}\right)^2} G_{\ddot{x}} \tag{3.67}$$

Above equation is valid for 1σ standard deviation. For 3σ standard deviation, above equation must be multiplied by 3.

In this thesis, the Shock Response Spectrum (SRS) and the Extreme Response Spectrum (ERS) were used to calculate the duration of the accelerated fatigue test. Lalanne [24] mentioned about validation of the test duration reduction in his book, "Specification Development". Using the information in this book, the SRS of the life cycle profile, the ERS of the life cycle profile and the ERS of the test profile with reduced duration were compared. Firstly, the test duration was reduced so that the ERS of the test profile is greater than the ERS of the life cycle profile. This means that there is not any life cycle profile event shown in Table 3 has stronger vibrations than the reduced test profile. Secondly, the ERS of the test profile was compared with the SRS. The ERS of the test profile must be smaller than the SRS so that, the test store will not be submitted to instantaneous levels greater than the real environment during vibration tests. In this thesis, the ERS of the test profile whose duration was reduced so that the ERS of the test profile is greater than the ERS of the life cycle profile but smaller than the SRS. In brief, in this thesis, the ERS of the life cycle profile is lower than the the SRS and the test duration was adjusted so that the ERS of the test profile is adjusted between these two spectrum (the ERS of the life cycle profile and the SRS). Beyond the accuracy of the fatigue tests, there are other restraints for the test duration especially financial reasons. The longer the test duration, the more the test costs. Therefore, the test duration of the fatigue tests were reduced and adjusted so that the ERS of the tests is very close to the SRS. As an example, in Figure 46, SRS and ERS of a random vibration are shown for Q=10.

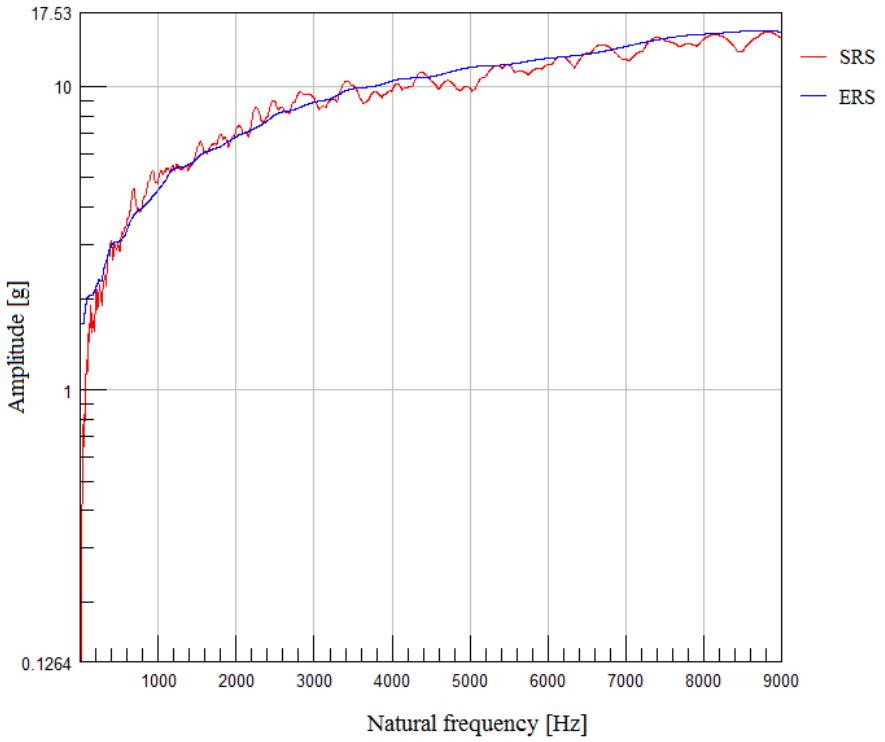

Figure 46. SRS and ERS of a random vibration

3.3.2 Acceleration Data Preparation Steps

Acceleration data steps to prepare data for fatigue analyses and tests are given briefly as follows. Also figures of these steps for accelerometer 2 shown in Figure 9 are shown as an example below the step explanation.

1. Acceleration data collected from the DMS were seperated and picked according to the data on Table 3.

In Figure 47 and Figure 48 acceleration data collected from accelerometer 2 are shown. Figure 47 shows the acceleration data of 18 kft and 0.8 Mach and Figure 48 shows the acceleration data of 30 kft and 0.8 Mach. Just acceleration data of these 2 flight points from Table 3 are shown for simplicity.

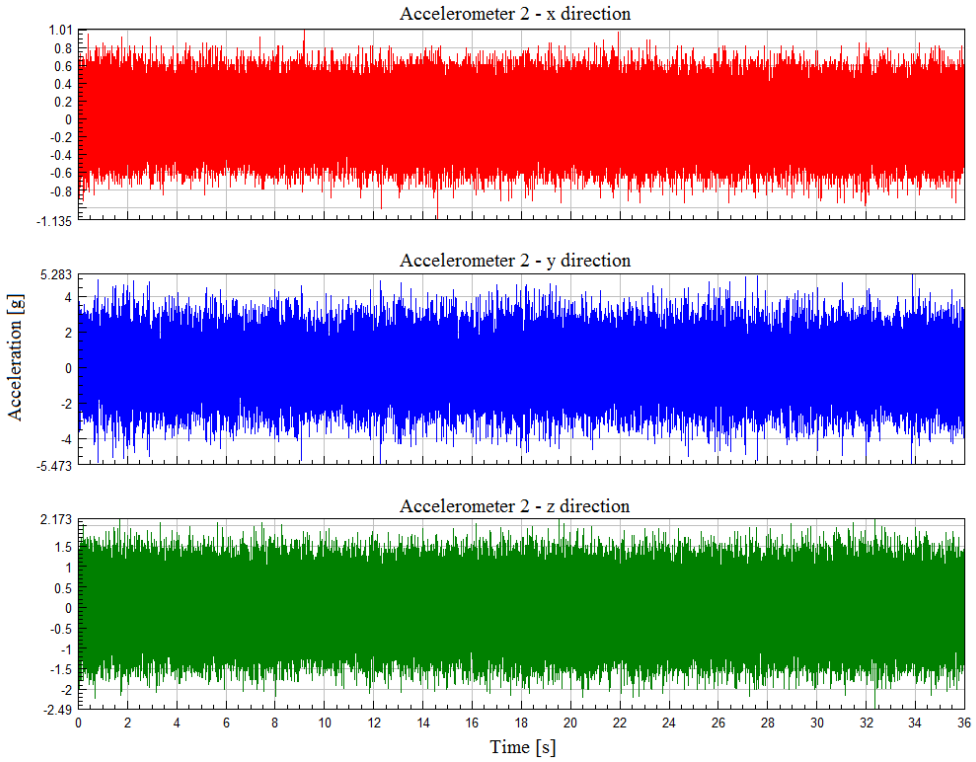

Figure 47. Acceleration data from accelerometer 2 (18 kft – 0.8 M)

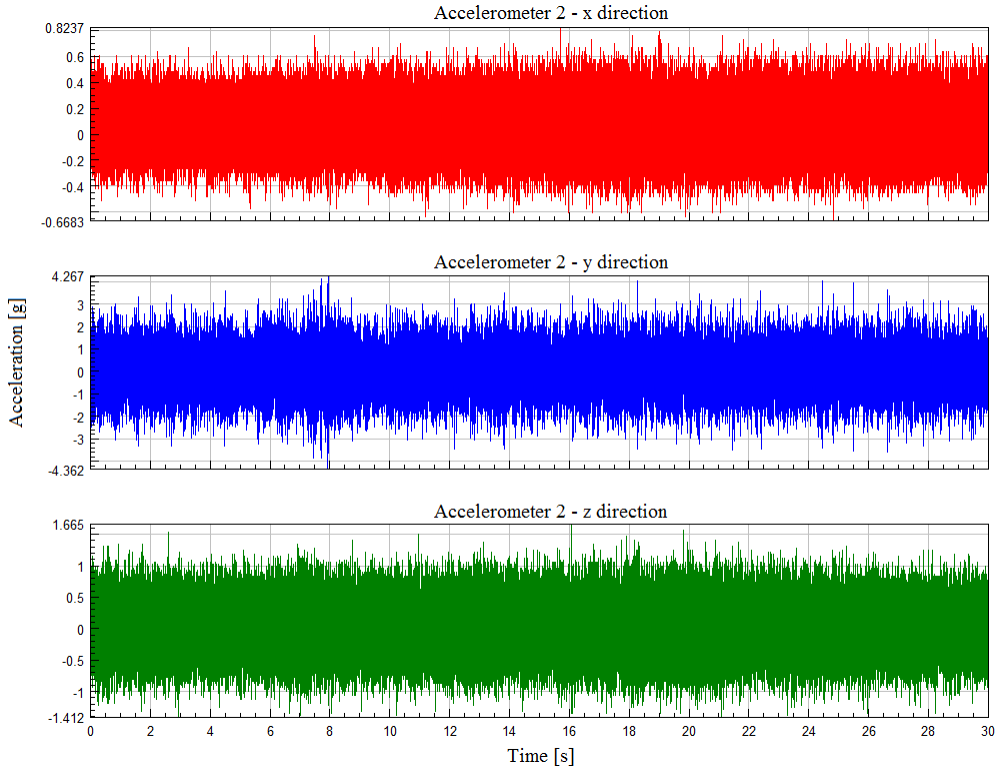

Figure 48. Acceleration data from accelerometer 2 (30 kft – 0.8 M)

2. The acceleration data was checked for stationarity and normality.

Run and trend test are used for stationary check. RMS values of the acceleration data are used to control stationarity. It is seen that, acceleration data are generally within the range of %95 acceptance region.

For example, the acceleration data collected by accelerometer 2 at 18 kft and 0.8 M (Figure 48) were seperated to 18 subregion with 2s duration. Then, RMS values of these subregion were calculated and run and trend tests were applied. From run test, 12, 9 and 10 values were obtained for x, y and z directions respectively. For N=18, the values between 6 and 13 are acceptable for %95 acceptance region. Therefore, 12, 9 and 10 are acceptable values at the %5 level of significance. From trend test, 53, 78 and 44 values were obtained for x, y and z directions respectively. For N=18, the values between 51 and 102 are acceptable for %95 acceptance region. 53 and 78 values are acceptable at the %5 level of significance. However, 44 is acceptable at the %10 level of significance.

For normality check skewness and kurtosis values are controlled. Skewness and kurtosis calculation formula is defined as follows:

$$Skewness = E\left[\frac{(x-\mu)^3}{\sigma^3}\right] \tag{3.68}$$

$$Kurtosis = E\left[\frac{(x-\mu)^4}{\sigma^4}\right] \tag{3.69}$$

For a Gaussian distribution, skewness equals to 0 and kurtosis equals to 3. Skewness and kurtosis values calculated from the collected dara are very similar to the Gaussian distribution values.

For example, skewness values of the data in Figure 48 are 0.0137, -0.0043 and 0.0090 for x, y and z directions respectively. And kurtosis values of the data in Figure 48 are 2.95, 3.03 and 2.96 for x, y and z directions respectively. These skewness and kurtosis values are very close to the skewness and kurtosis values of the Gaussian distribution. Therefore, it can be said, the collected data is very similar to Gaussian distribution. In Figure 49, similarity between the cumulative

distribution function (CDF) of the collected acceleration data and the standard normal CDF is shown. In this figure, the CDF of the acceleration data (y axis) from accelerometer 2 and the standard normal CDF is compared.

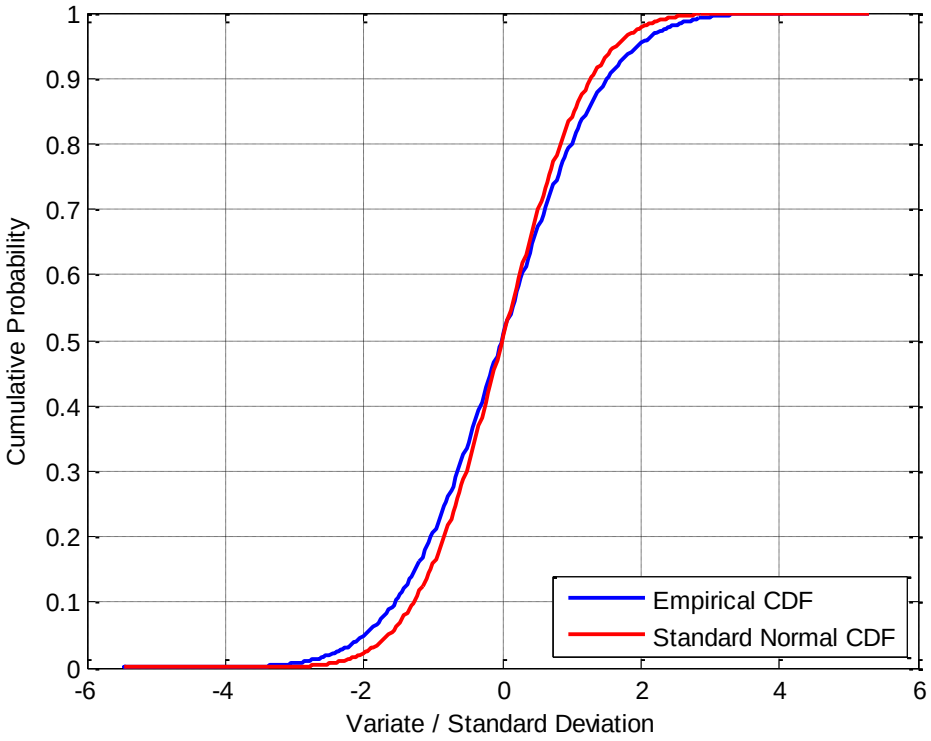

Figure 49. Comparison of cumulative distribution function (CDF) of acceleration data (y axis) from accelerometer 2 (30 kft – 0.8 M) and the standard normal CDF

3. Mean of the selected data was removed and filtered with 2 Hz high pass filter as shown in Figure 50.

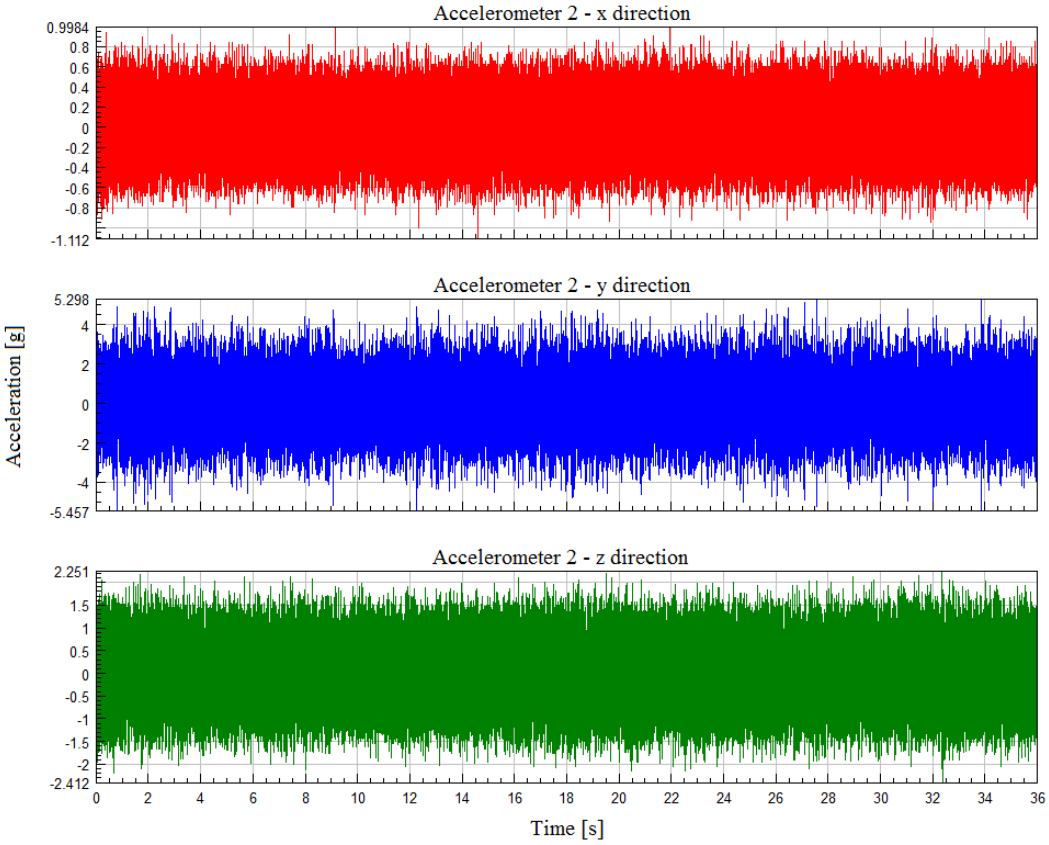

Figure 50. Filtered acceleration data from accelerometer 2 (18 kft – 0.8 M)

4. The power spectral densities (PSD) of all the selected data were calculated seperately as shown in Figure 51 and Figure 52.

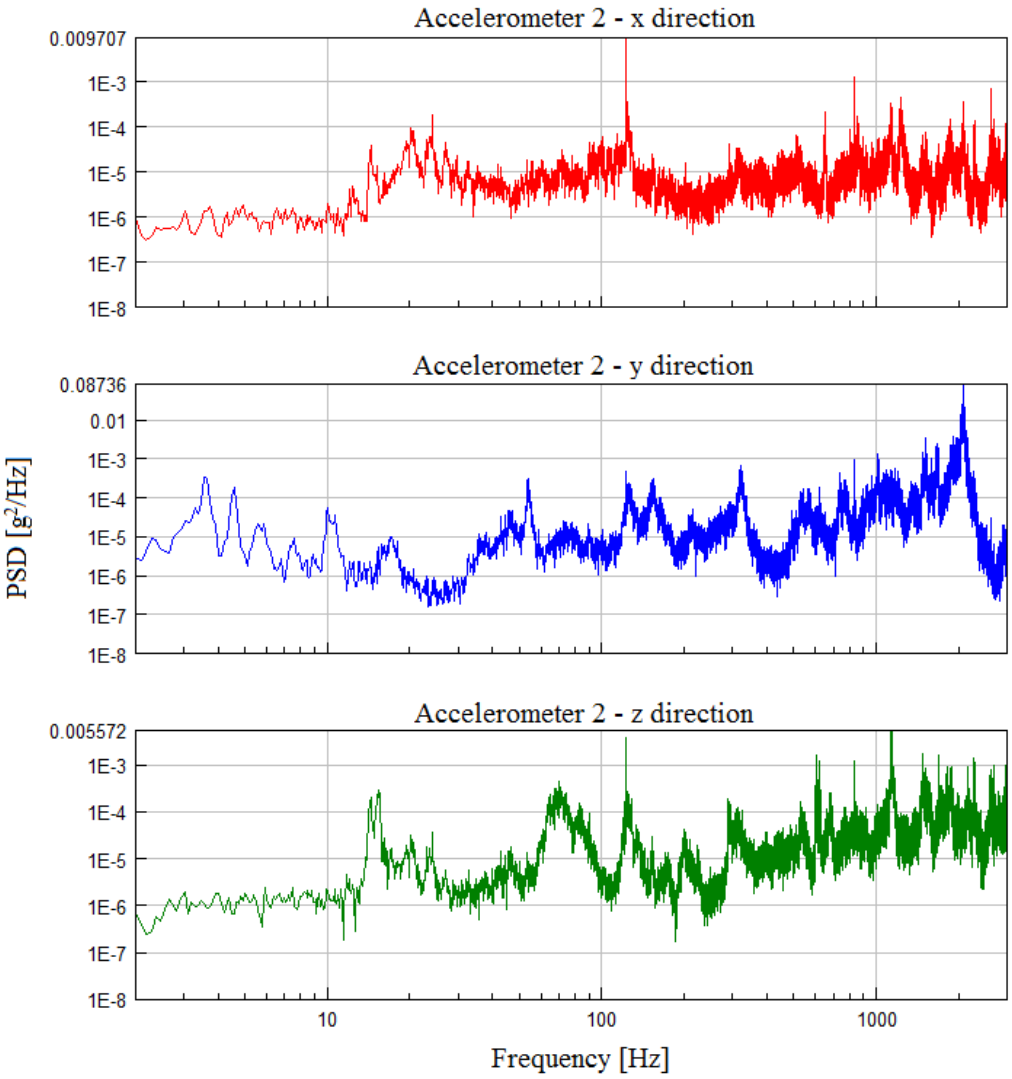

Figure 51. PSD of the acceleration data from accelerometer 2 (18 kft – 0.8 M)

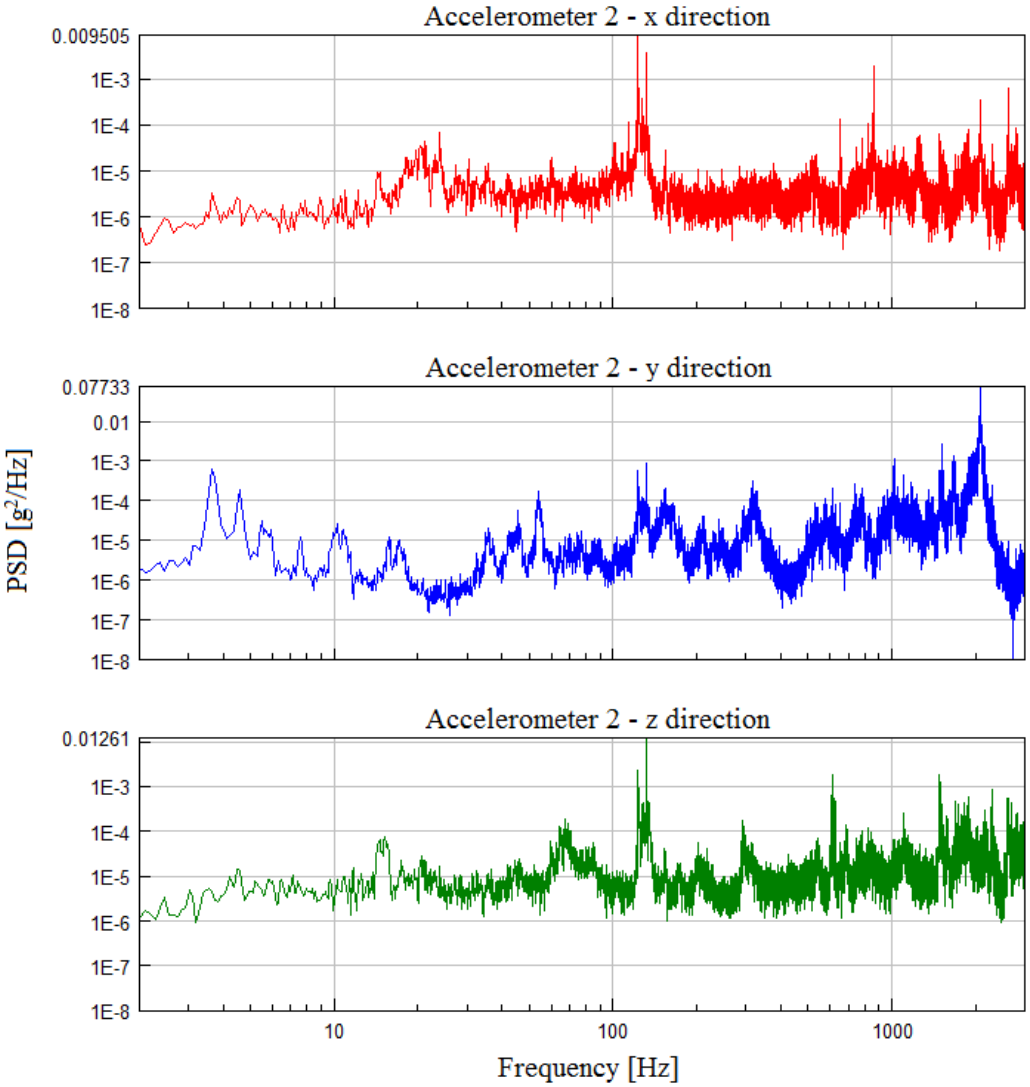

Figure 52. PSD of the acceleration data from accelerometer 2 (30 kft – 0.8 M)

5. The fatigue damage spectrums (FDS) of the PSDs were calculated as shown in Figure 53 and Figure 54.

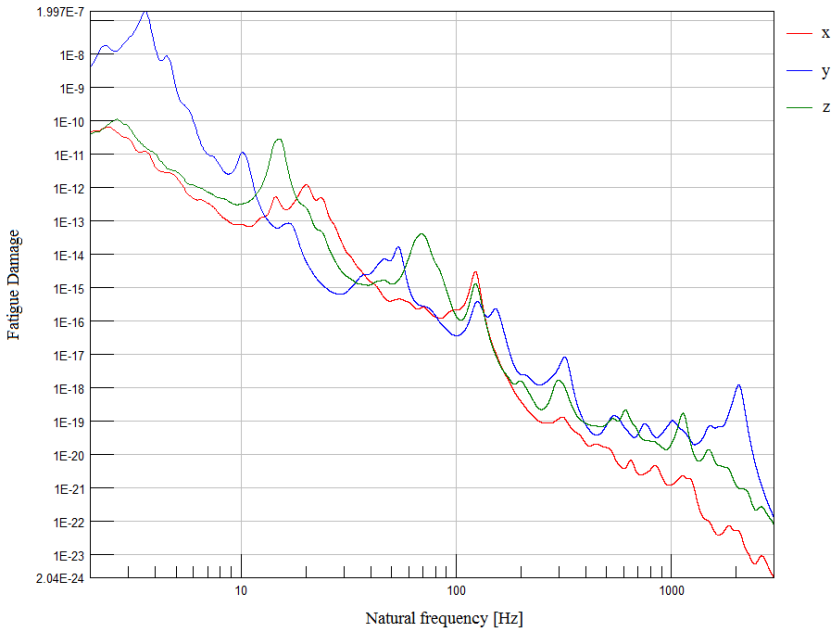

Figure 53. FDS of the acceleration data from accelerometer 2 (18 kft – 0.8 M)

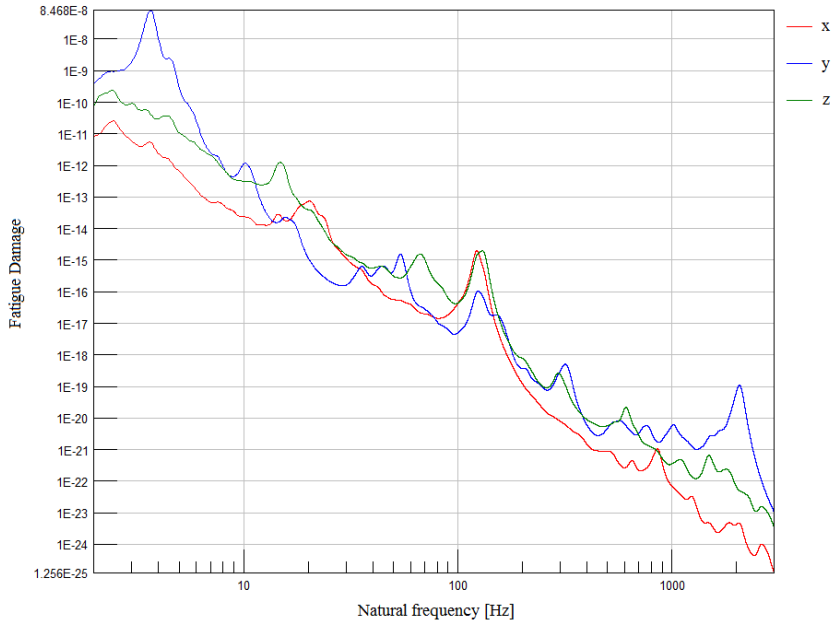

Figure 54. FDS of the acceleration data from accelerometer 2 (30 kft – 0.8 M)

6. The FDSs were summed up. Figure 55 shows the cumulative FDS of the acceleration data which were obtained from accelerometer 2.

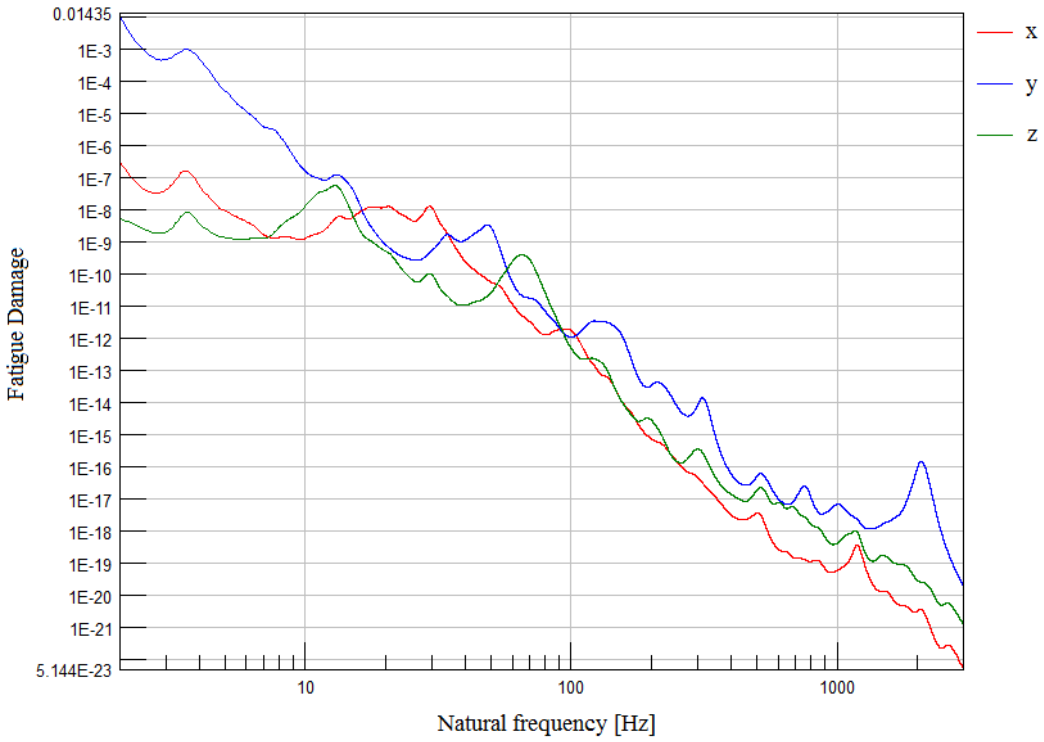

Figure 55. Cumulative FDS of the acceleration data from accelerometer 2

7. A unique PSD which represents the ideal average F-16 jet aircraft sortie was calculated from the FDS as shown in Figure 56.

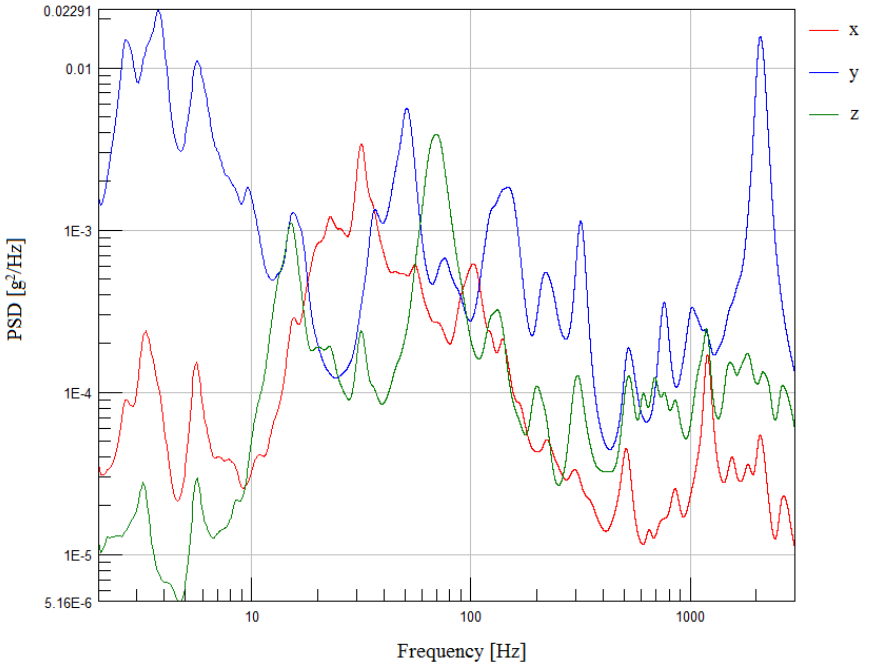

Figure 56. PSD of the acceleration data from accelerometer 2

8. PSD envelope is composed from the real environment PSDs to use in analyses and tests as shown in from Figure 57 to Figure 59 .

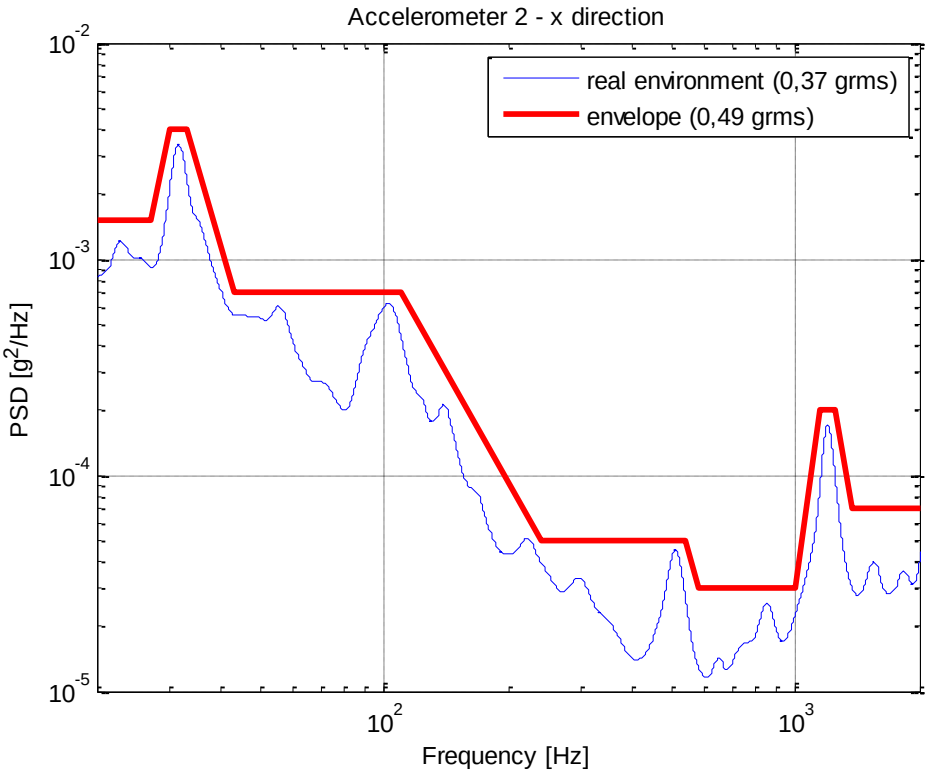

Figure 57. PSD envelope for the acceleration data from accelerometer 2 (x direction)

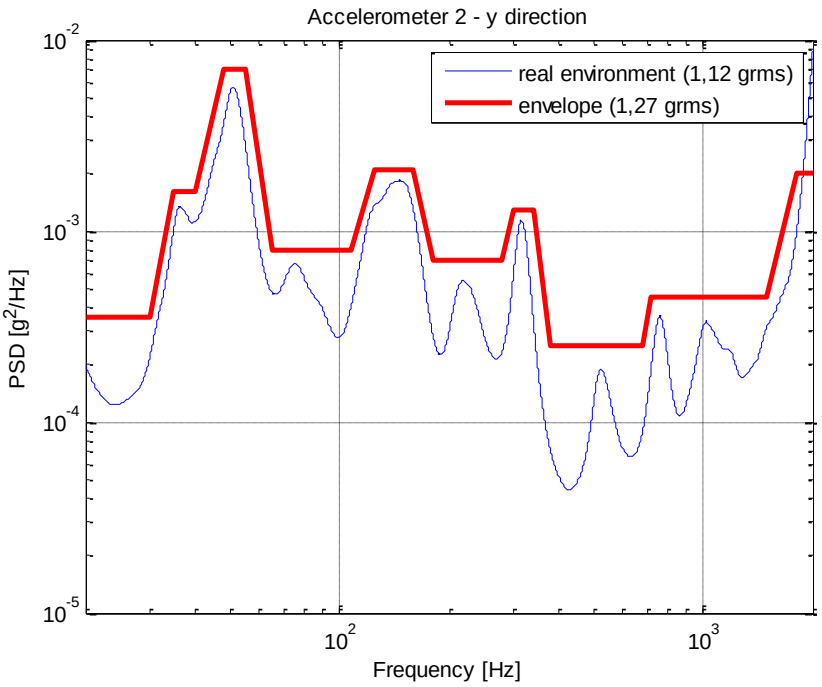

Figure 58. PSD envelope for the acceleration data from accelerometer 2 (y direction)

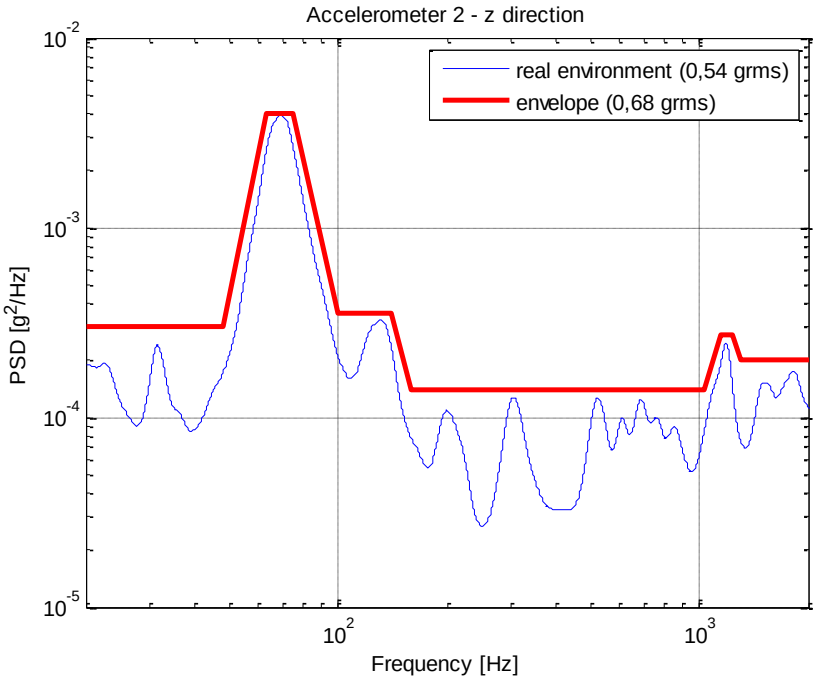

Figure 59. PSD envelope for the acceleration data from accelerometer 2 (z direction)

9. Vibration test duration was determined according to the SRS and ERS.

The total captive carriage duration was assumed as 1000 hours. The Miner-Palmgren hypothesis wass used for test duration reduction. This hypothesis which uses a fatigue-based power law relationship to relate exposure time and amplitude is the most commonly used method for calculating a reduction in test. The hypothesis is:

$$\frac{t_2}{t_1} = \left(\frac{W(f)_1}{W(f)_2}\right)^{m/2} \tag{3.70}$$

Where t_1 and t_2 are the equivalent test time and in-service time, $W(f)_1$ and $W(f)_2$ are the PSD value at test condition and in-service condition, respectively. m is the value based on the S-N curve. In calculations, m was taken as 4.

ERSs were determined for different test durations (5 hours, 10 hours and 20 hours) and compared with the SRS. These are shown between Figure 60 and Figure 62.

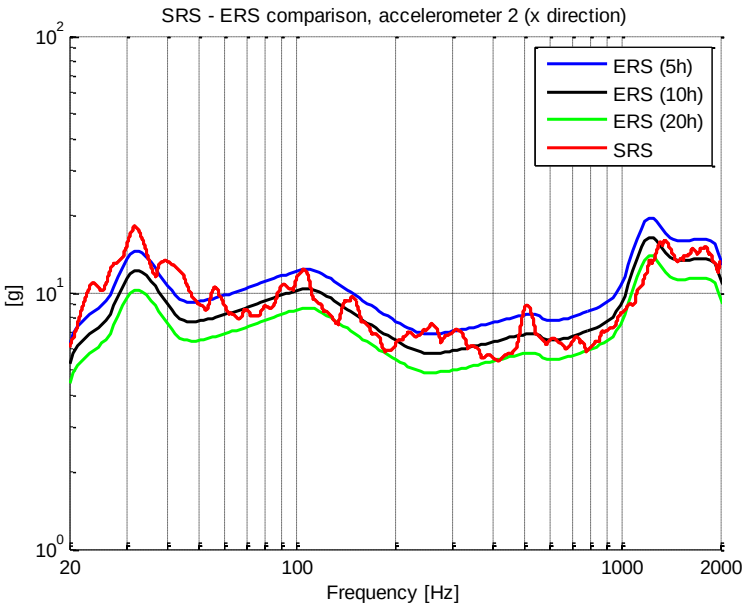

Figure 60. SRS and ERS comparion of the acceleration data from accelerometer 2 (x direction)

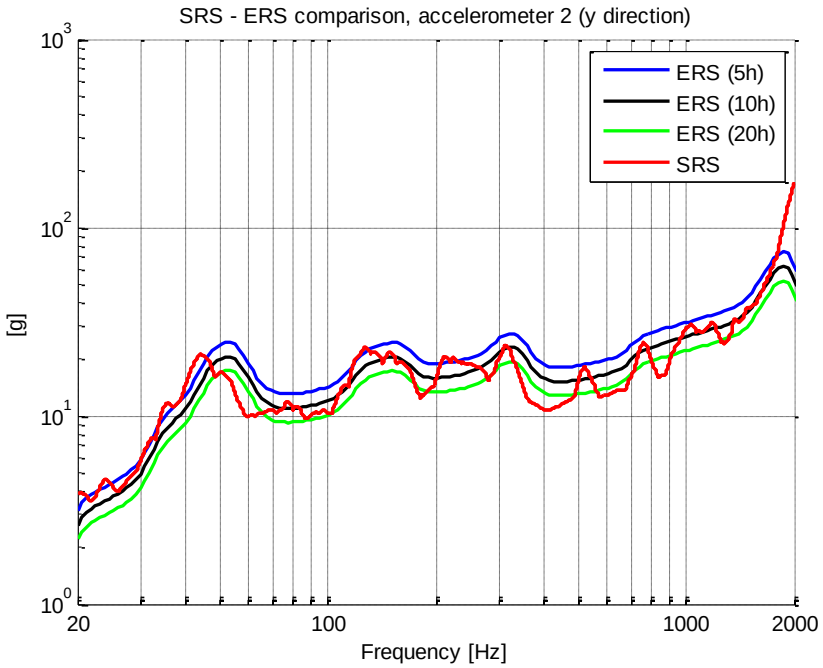

Figure 61. SRS and ERS comparion of the acceleration data from accelerometer 2 (y direction)

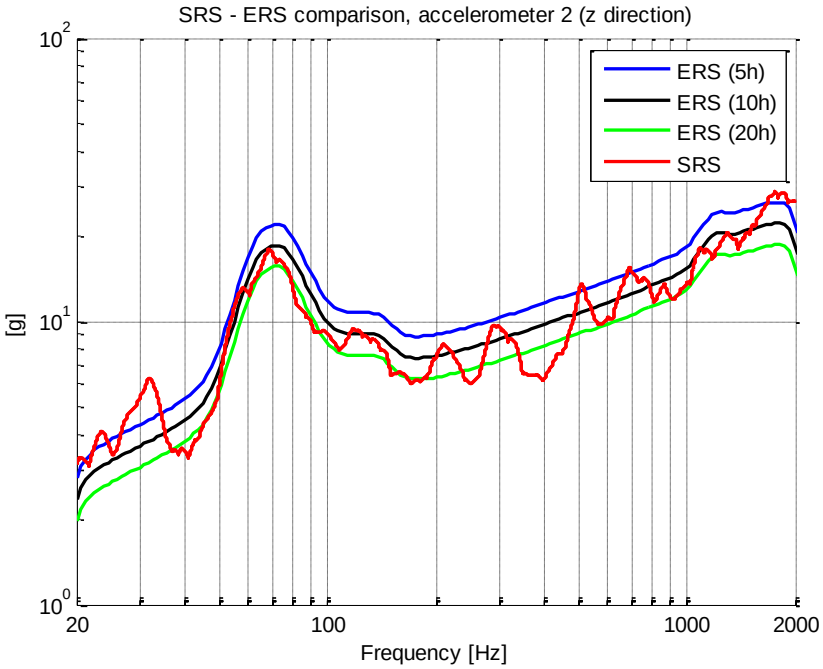

Figure 62. SRS and ERS comparion of the acceleration data from accelerometer 2 (z direction)

From above figures, the ERS of the 10 hours vibration test is very close to the SRS. However, the ERS of 5 hours vibration tests is generally higher than the SRS. Therefore, 10 hours seeems to be the optimum test duration for accuracy and cost of the test.

3.3.3 Generated PSDs

PSD envelopes of real environment and 10 hours test specification for accelerometer 2 are given in Figure 63 and Figure 64, respectively.

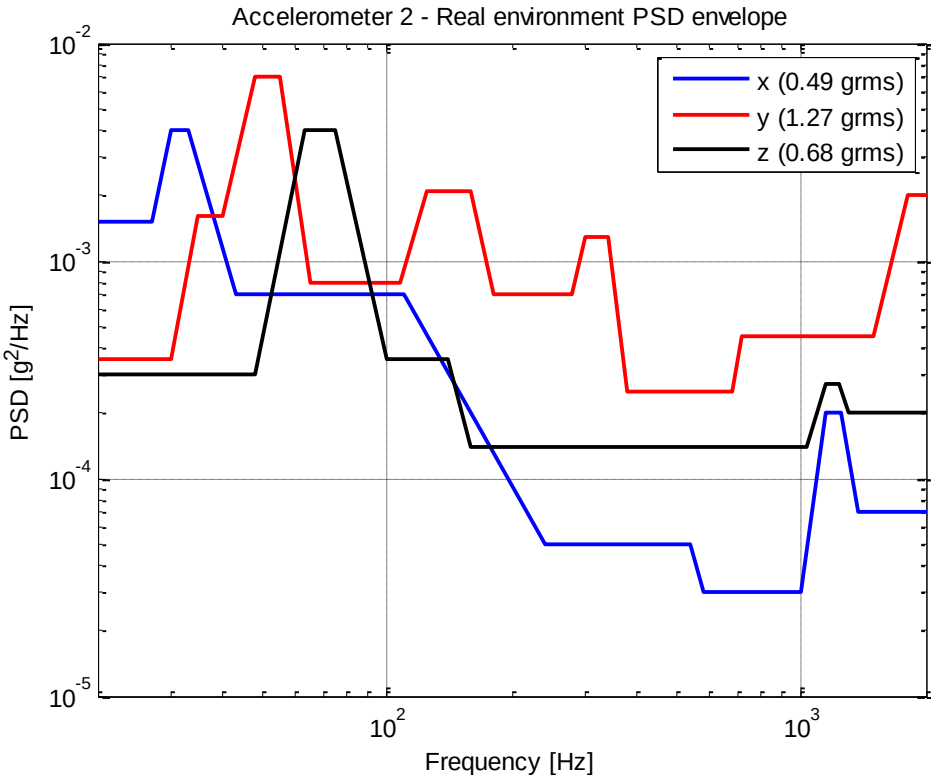

Figure 63. Real environment PSD envelope of accelerometer 2

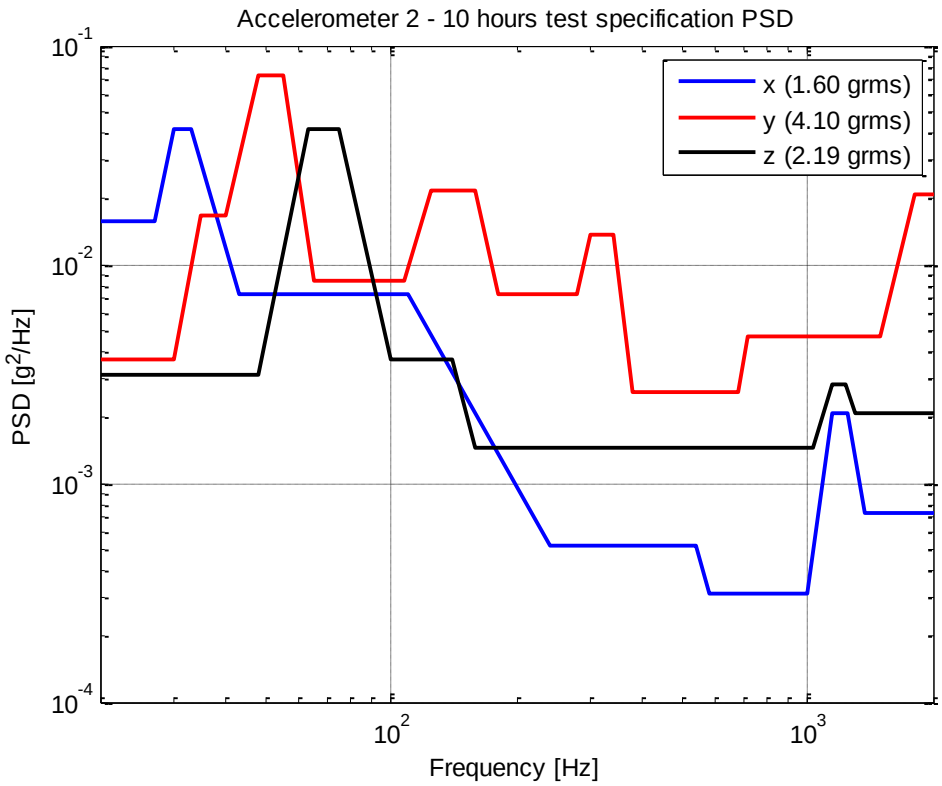

Figure 64. 10 hours test specification PSD of accelerometer 2

3.3.4 Vibration Fatgiue Analysis

Vibration fatigue analysis is a frequency based fatigue analysis because PSD loads are used instead of time loads during analysis. Hereby, the structural frequency responses are taken into account during fatigue calculations. Cycles are counted from stress PSDs instead of load time signals. After finding cycles, rest of the analysis is similar to time domain fatigue analysis. However in this thesis, firstly, stress PSDs for unit acceleration load were obtained by frequency respone function (FRF) analysis for vibration fatigue analysis. Then, acceleration PSDs obtain from flights are used to obtain stress PSDs during flghts. In Figure 65, vibration fatigue analysis steps are summarized.

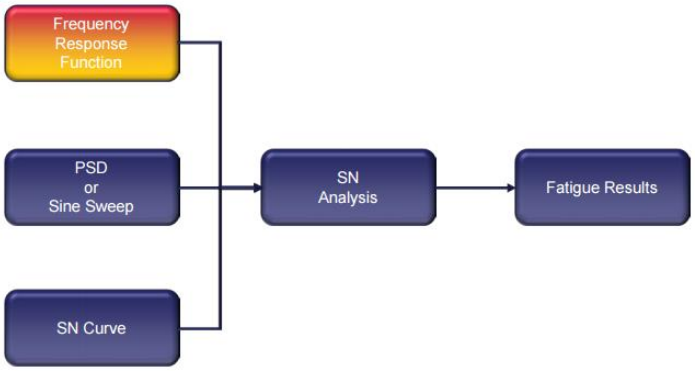

Figure 65. Vibration fatigue steps [36]

As an example, fatigue analysis was done using PSD obtained from accelerometer 2 in this thesis. Accelerometer 2 location is right beside the front hanger of the DMS. For fatigue analysis, front part of the DMS was used and PSD obtained from accelerometer 2 was given as a base vibration. Model was also fixed from the base. The finite element model used for fatigue analysis is shown in Figure 66. The model was meshed with solid TET10 meshes and RBE2 and RBE3 MPC elements were used instead of bolts to attach solid bodies and point masses, respectively.

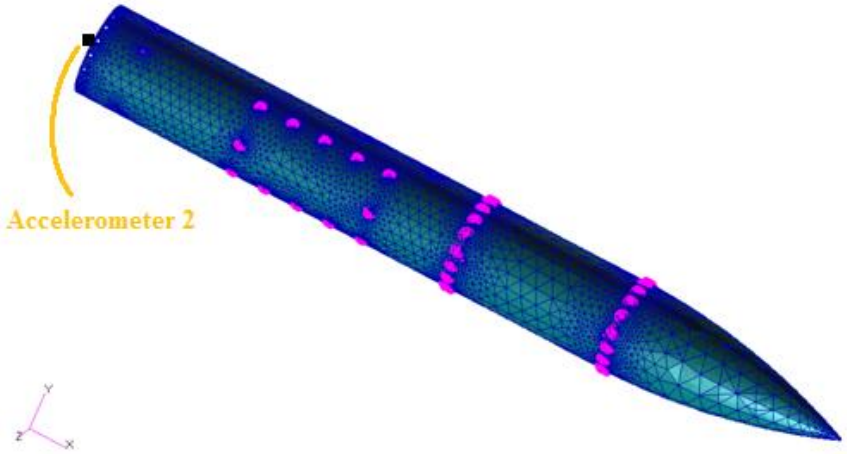

Figure 66. Finite element model for fatgiue analysis

To make fatigue analysis, firstly stress PSDs of the model for every direction were obtained by FRF analysis choosing the unit load input location as accelerometer 2 location. FRF gives the relation between the input and output as follows:

$$H(f) = \frac{\sigma(f)}{\ddot{x}(f)} \tag{3.71}$$

Where $H(f)$ is the FRF, $\sigma(f)$ is the stress (output) and $\ddot{x}(f)$ is the base acceleration (input).

After finding FRF, stress PSD can be found as follows:

$$PSD_{\sigma} = H(f) \times H^{*}(f) \times PSD_{\ddot{x}} \tag{3.72}$$

Where $H^{*}(f)$ is the conjugate of the $H(f)$. $PSD_{\ddot{x}}$ corresponds to the PSDs in Figure 63 for this case.

Von Mises RMS stress results of the model obtained from the PSD_{σ} are shown in Figure 67 - Figure 76. These results were obtained for every axis seperately because of software limitations. Therefore, multiaxial load effects were not taken into account. However, from figures, it can be seen that high stress locations are different for each axes vibration. Also, magnitude of the von Mises RMS stresses are very different for each axis. Therefore, the results of uniaxial fatigue analysis would not be too different from the results of multiaxial stresses.

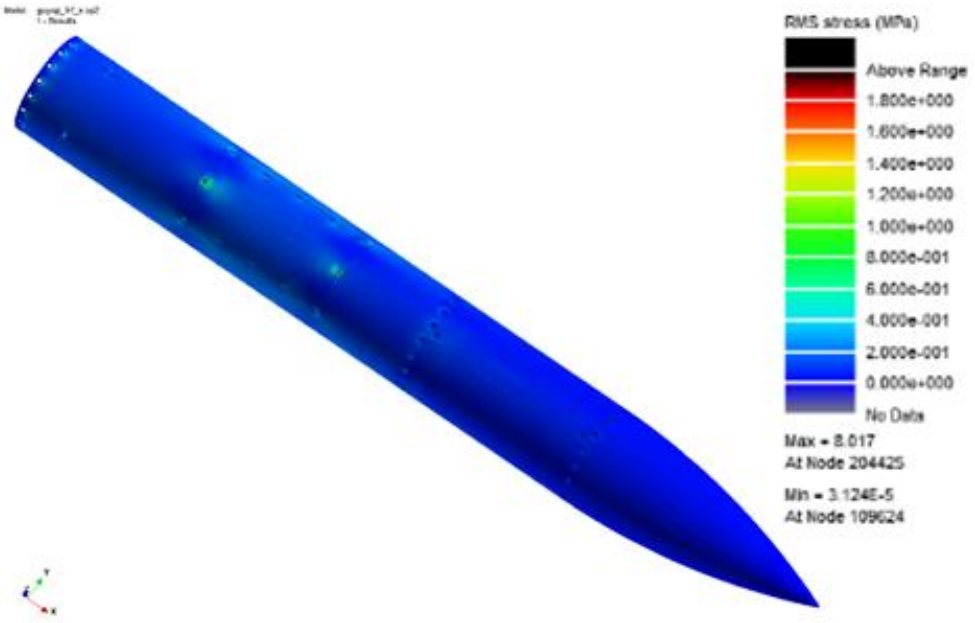

Figure 67. von Mises RMS stress – x direction

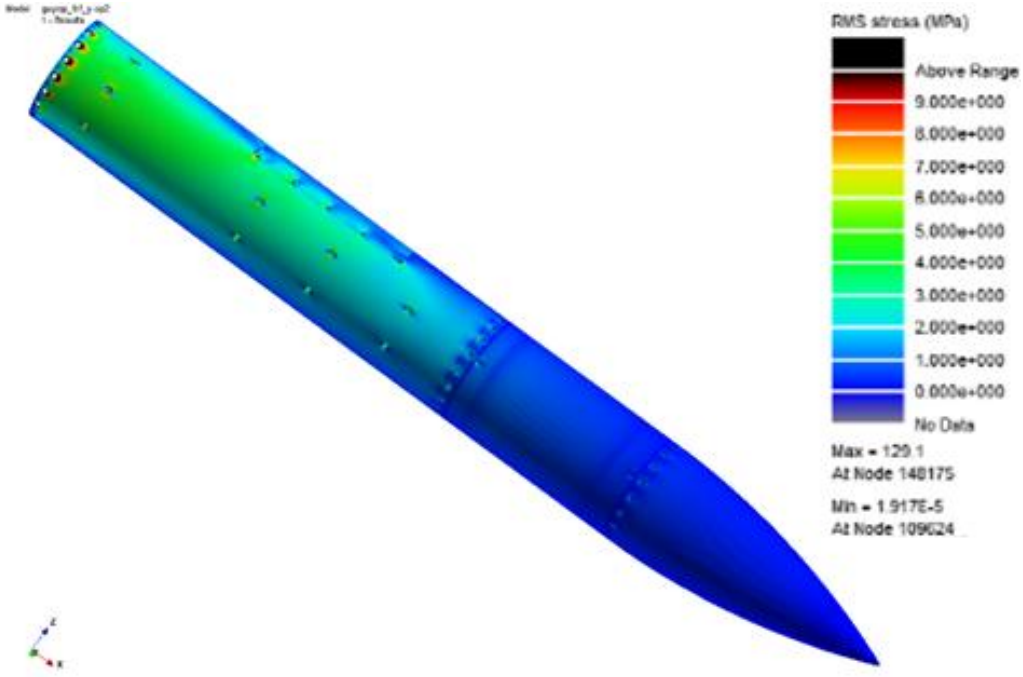

Figure 68. von Mises RMS stress – y direction

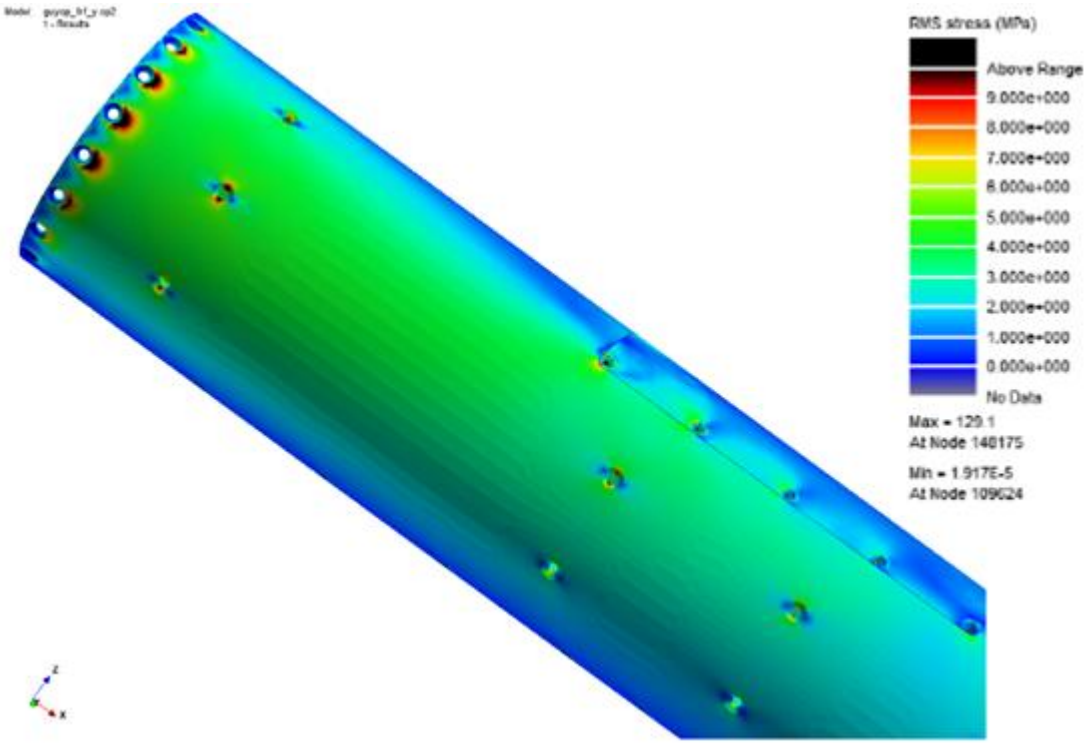

Figure 69. von Mises RMS stress – y direction

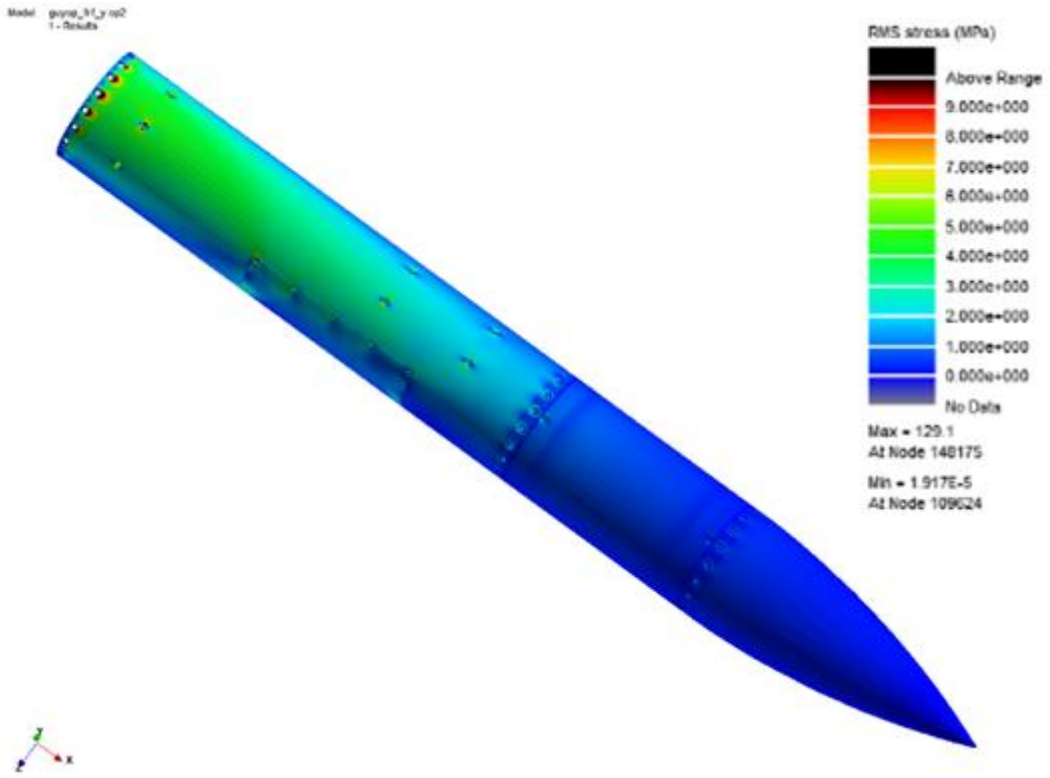

Figure 70. von Mises RMS stress – y direction

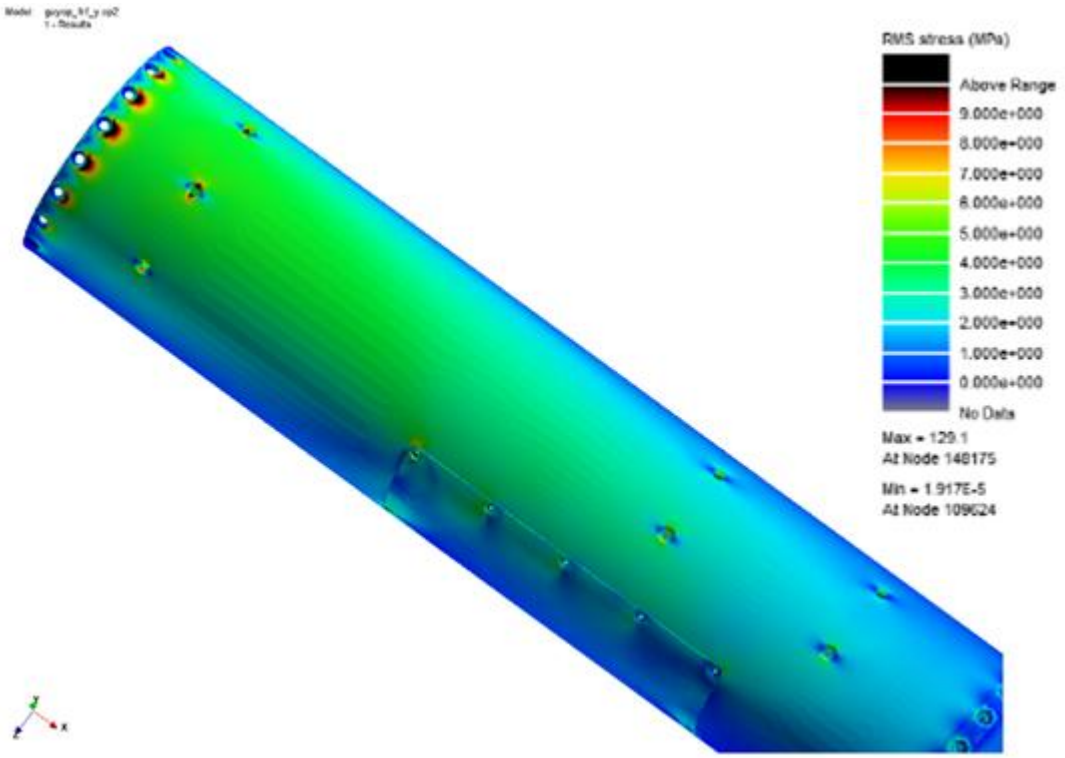

Figure 71. von Mises RMS stress – y direction

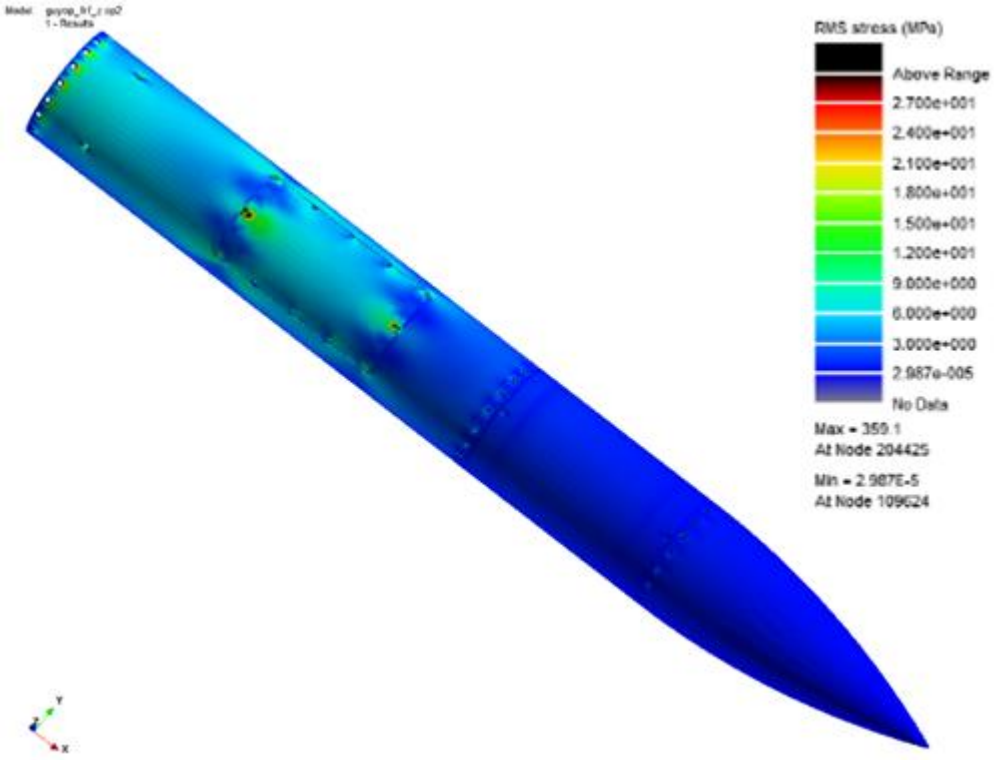

Figure 72. von Mises RMS stress – z direction

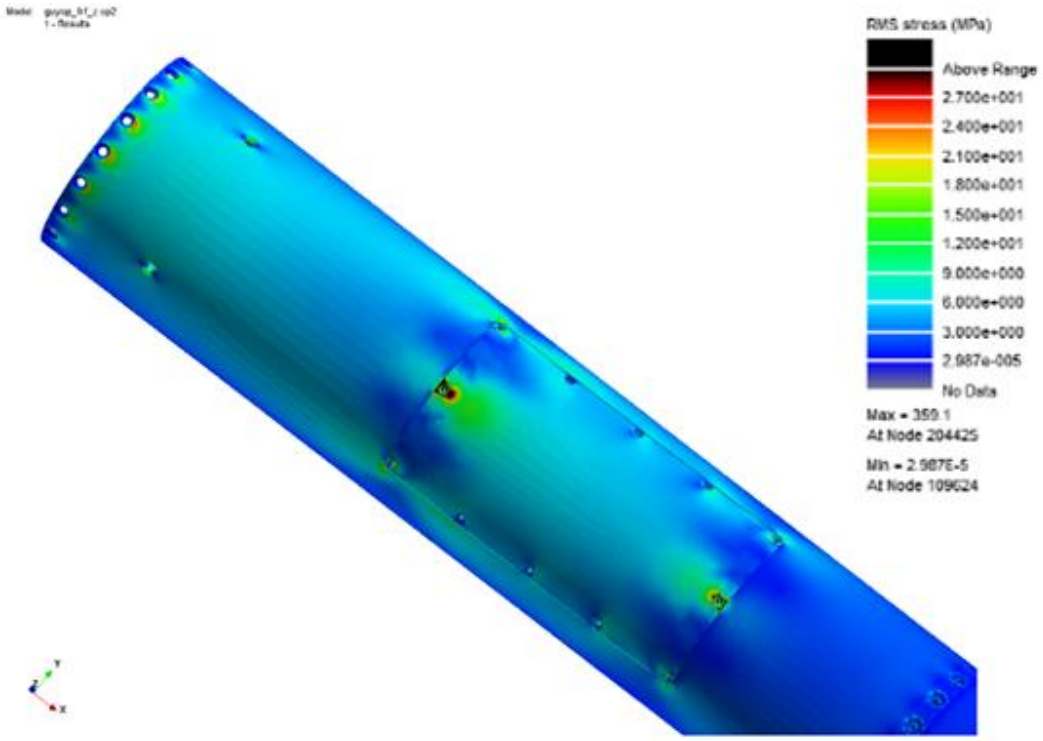

Figure 73. von Mises RMS stress – z direction

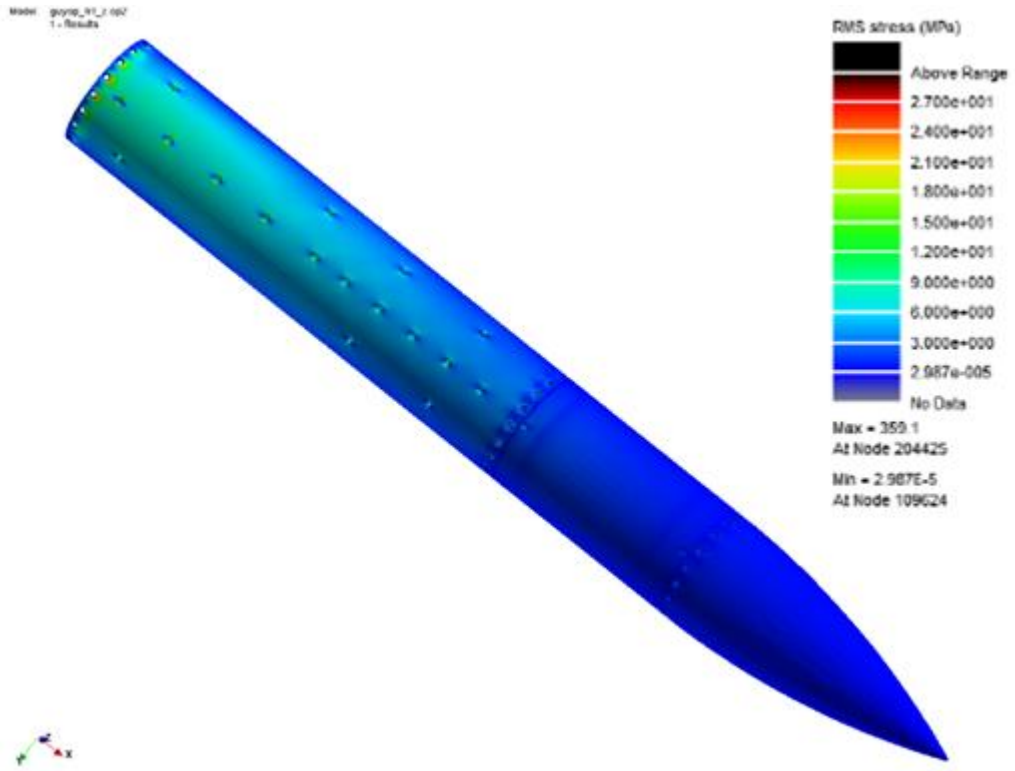

Figure 74. von Mises RMS stress – z direction

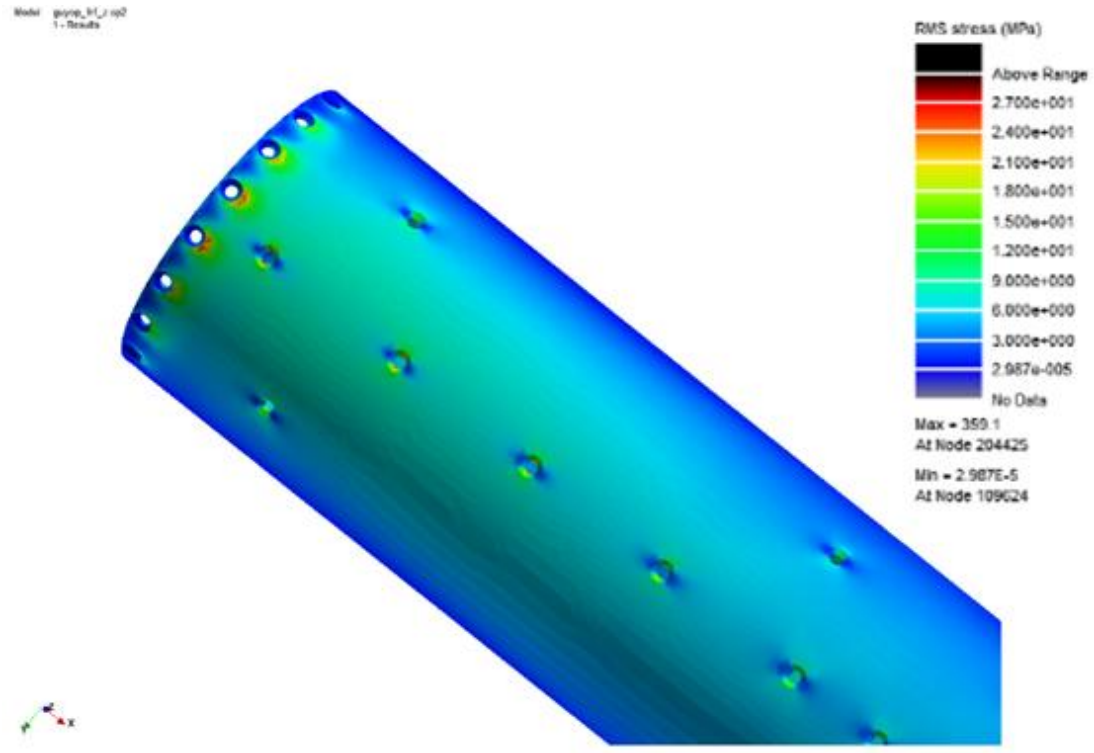

Figure 75. von Mises RMS stress – z direction

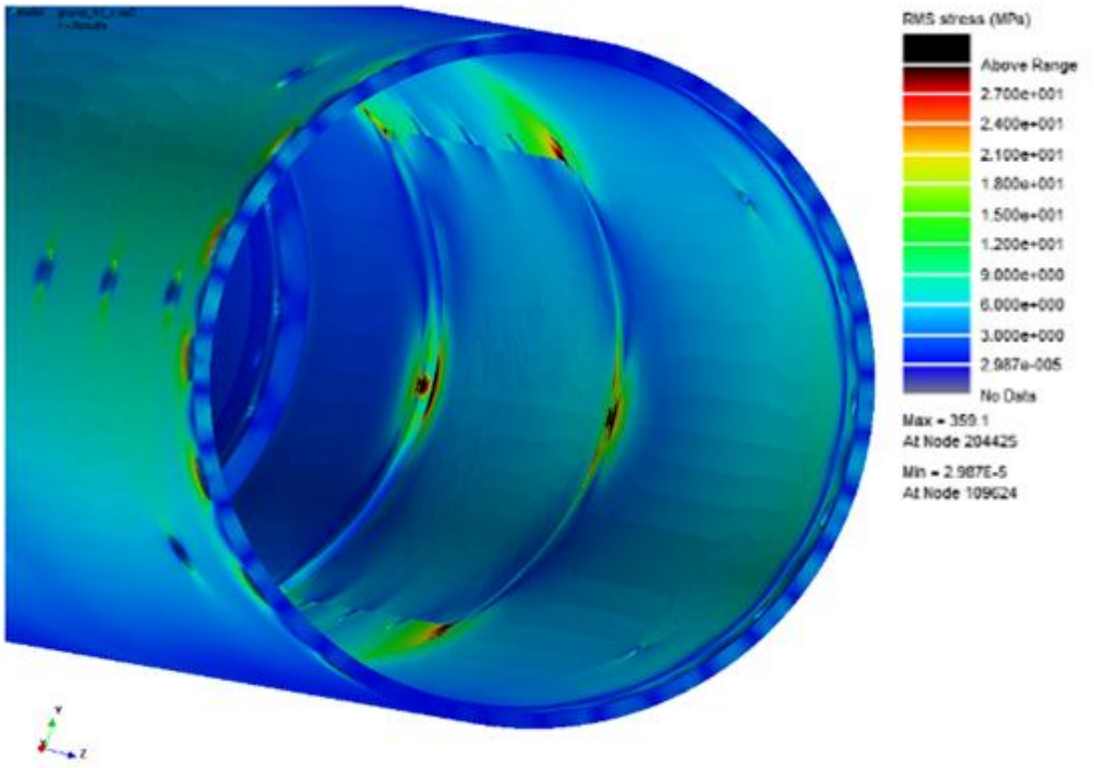

Figure 76. von Mises RMS stress – z direction

The von Mises RMS stress figures show that stresses are not very high on the model. Especially stresses calculated for x direction vibration is very low because of high rigidity, high natural frequencies and low acceleration PSD input. Stress calculated for z direction vibration is higher than the stress calculated for y direction vibration although structural behaviors of the model for y and z directions are similar. It is because of the gap in the middle of the cylinder shell and low thickness of the gap hatch and shell in this location.

After obtaining the stress PSDs for each axis, they are cycle counted by Lalanne method which is explained in equation 3.52. In this situation, stress probabilty density function was found instead of peak probability of the displacement as follows:

$$N(S) = \frac{\sqrt{1-r^2}}{\sigma_{rms}\sqrt{2\pi}} e^{-\frac{\Delta S^2}{2(1-r^2)\sigma_{rms}^2}} + \frac{r \cdot \Delta S}{2\sigma_{rms}}\left[1 + erf\left(\frac{r \cdot \Delta S}{\sigma_{rms}\sqrt{2(1-r^2)}}\right)\right] \tag{3.73}$$

Where $N(S)$ is the number of stress cycles, ΔS is the stress range, σ_{rms} is the RMS value of the stress, r and erf function are defined in equation 3.53 and 3.56 respectively.

After cycle counting, S-N curve of the material was used to calculate life. The material of the model is 4140 steel 36-42 HRC and S-N curve of this material is shown in Figure 77.

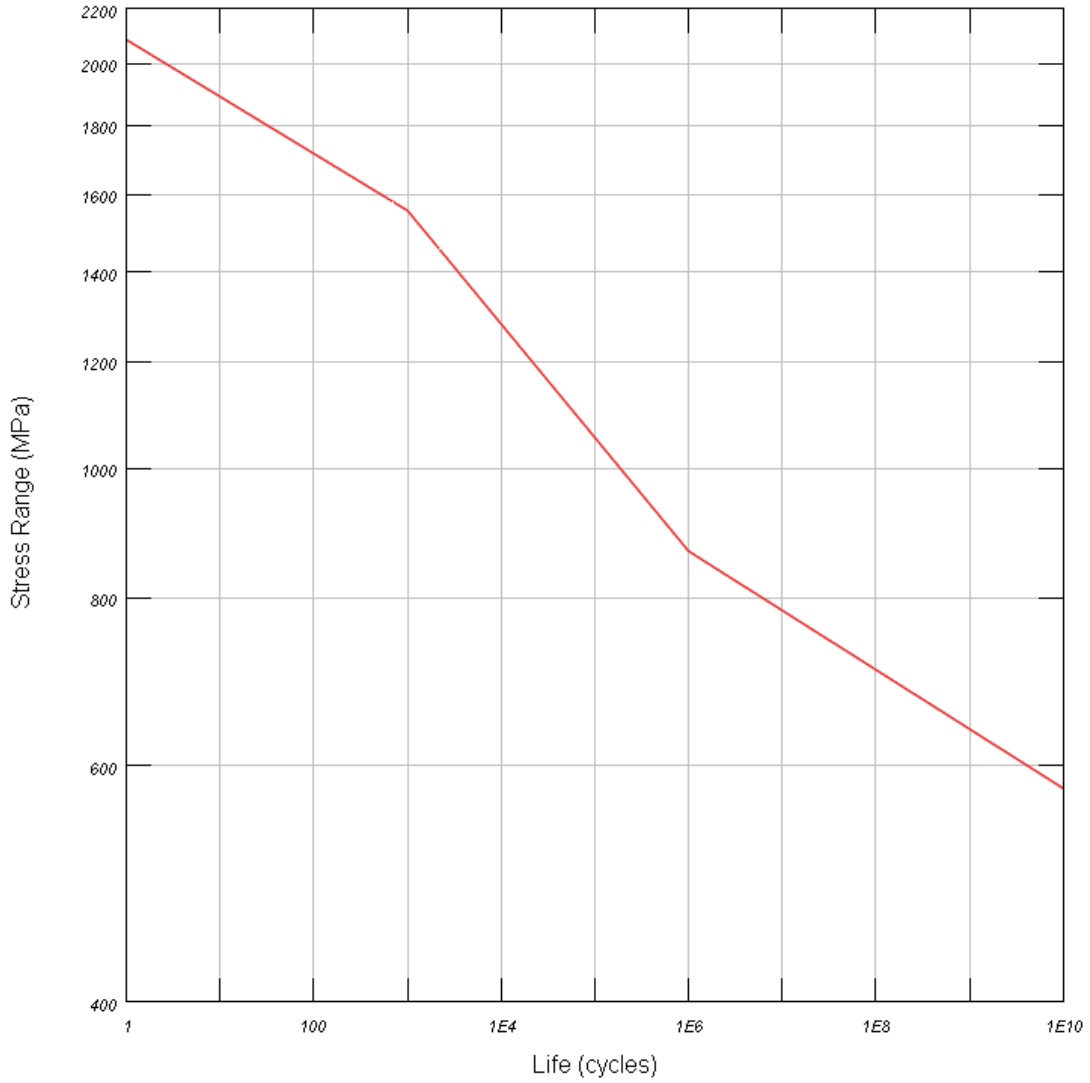

Figure 77. SN curve of 4140 steel [37]

Life results are shown in Figure 78 - Figure 87. Life results are given in seconds because instead of cycles, probability density function was used for fatigue analysis. Life range is limited above 1e20 seconds because of better understanding.

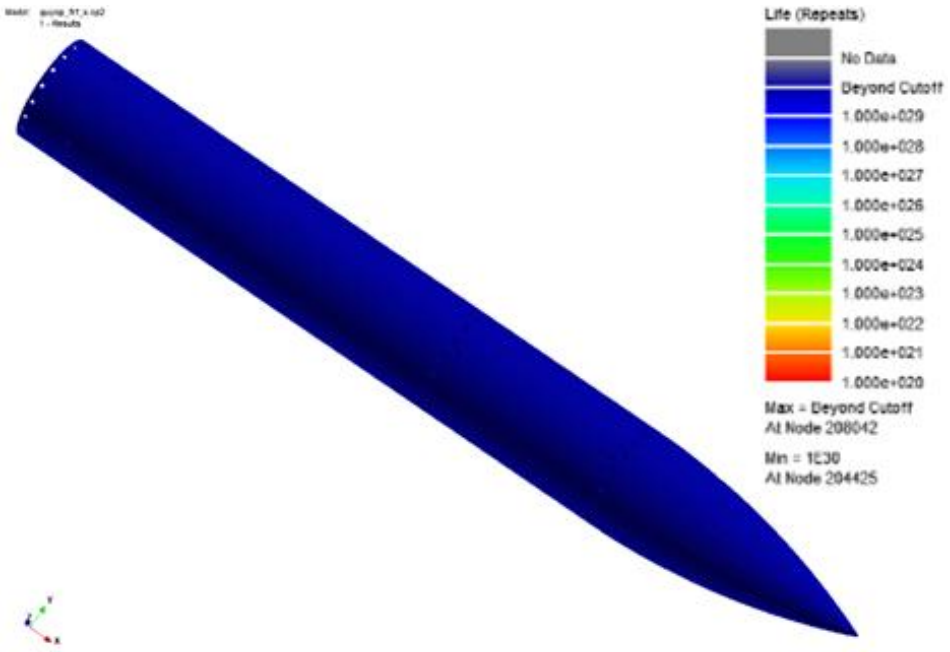

Figure 78. Life – x direction

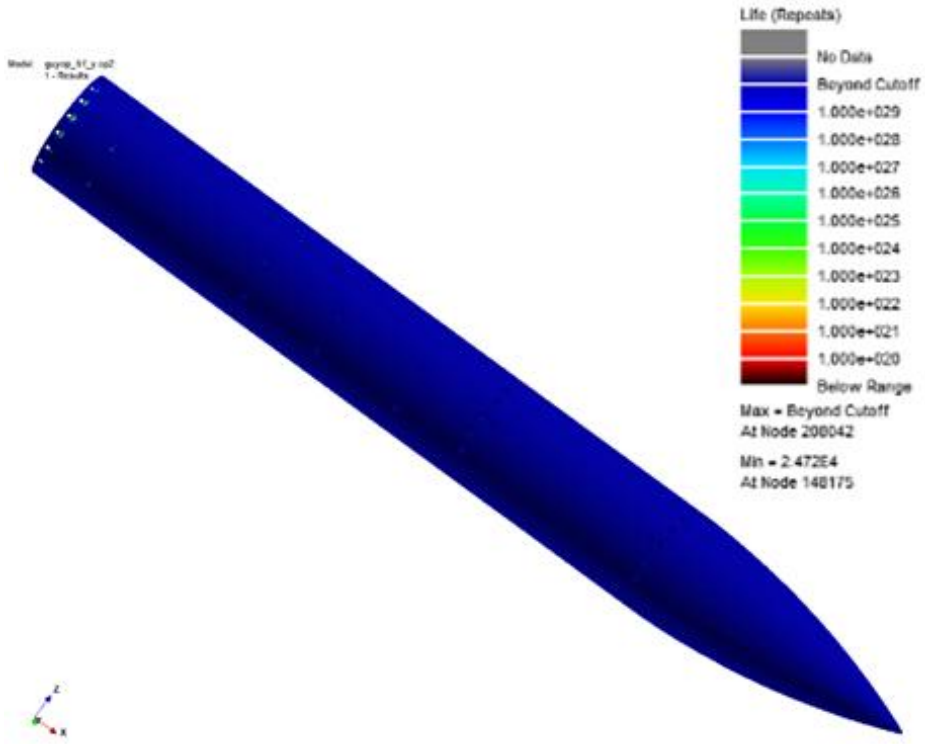

Figure 79. Life – y direction

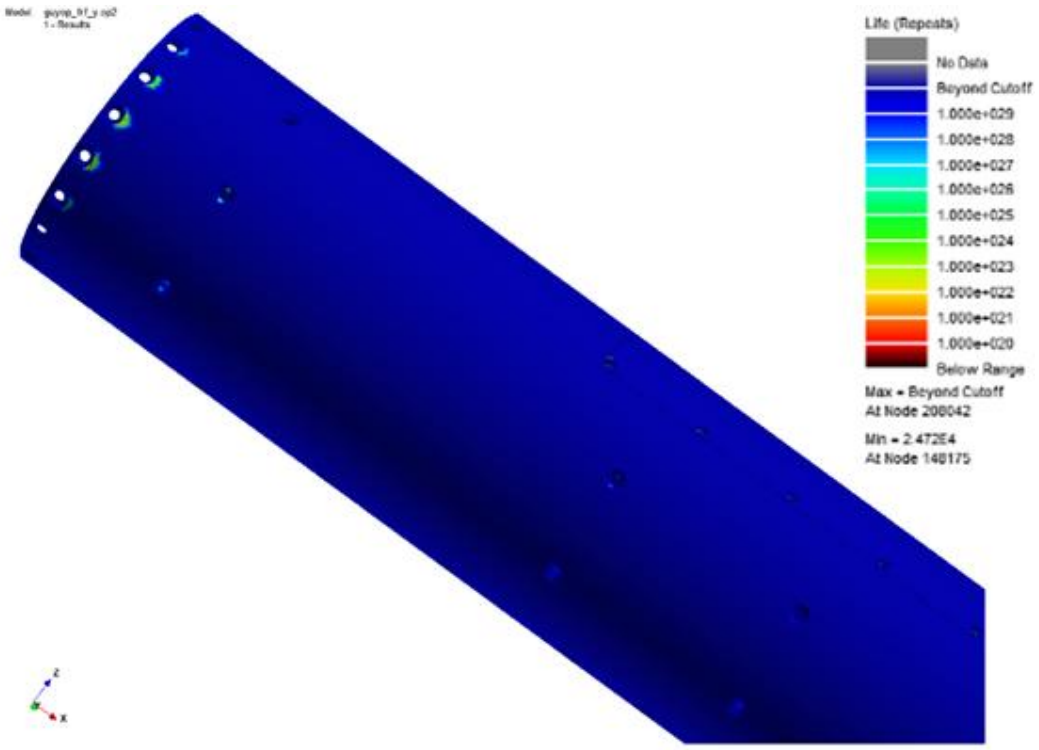

Figure 80. Life – y direction

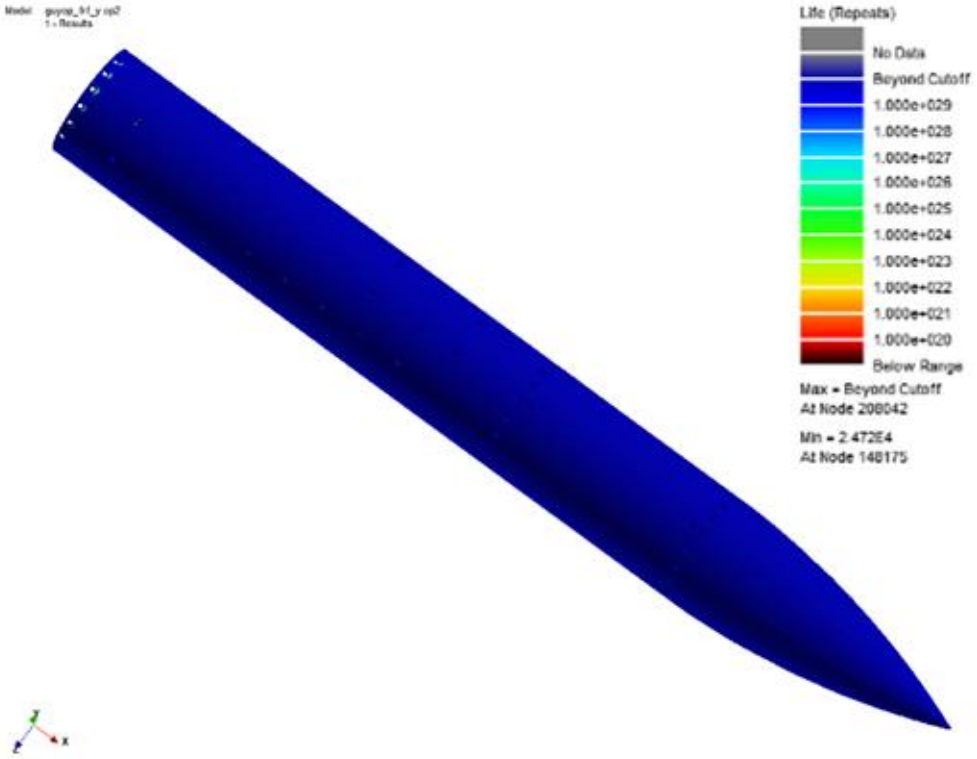

Figure 81. Life – y direction

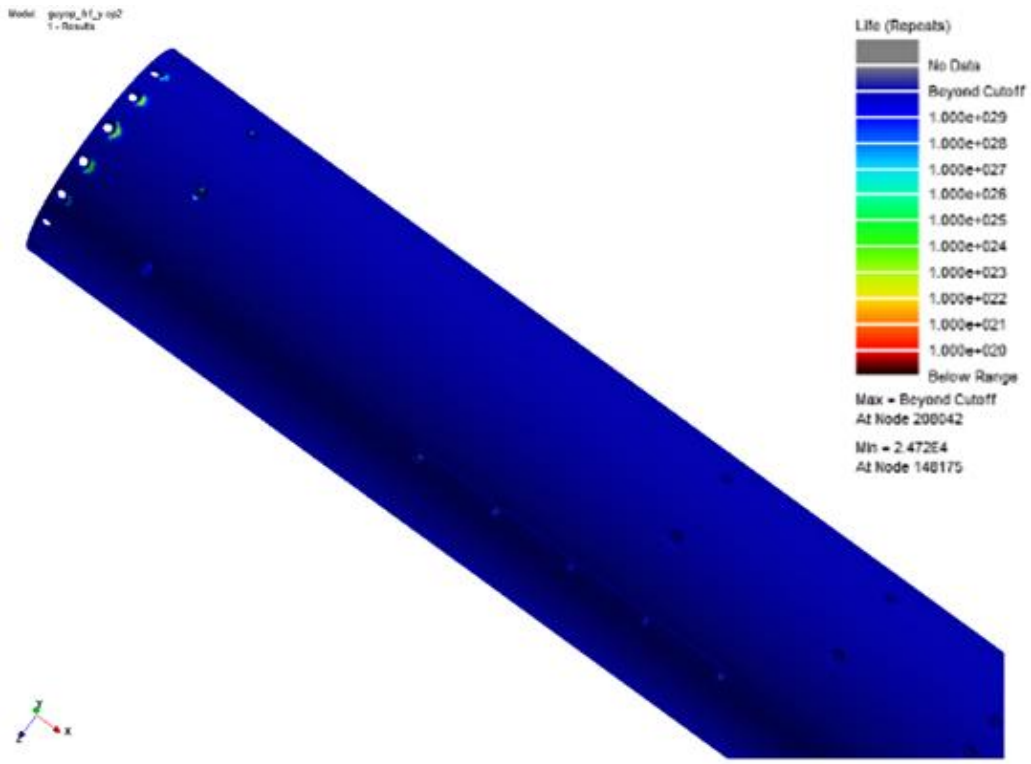

Figure 82. Life – y direction

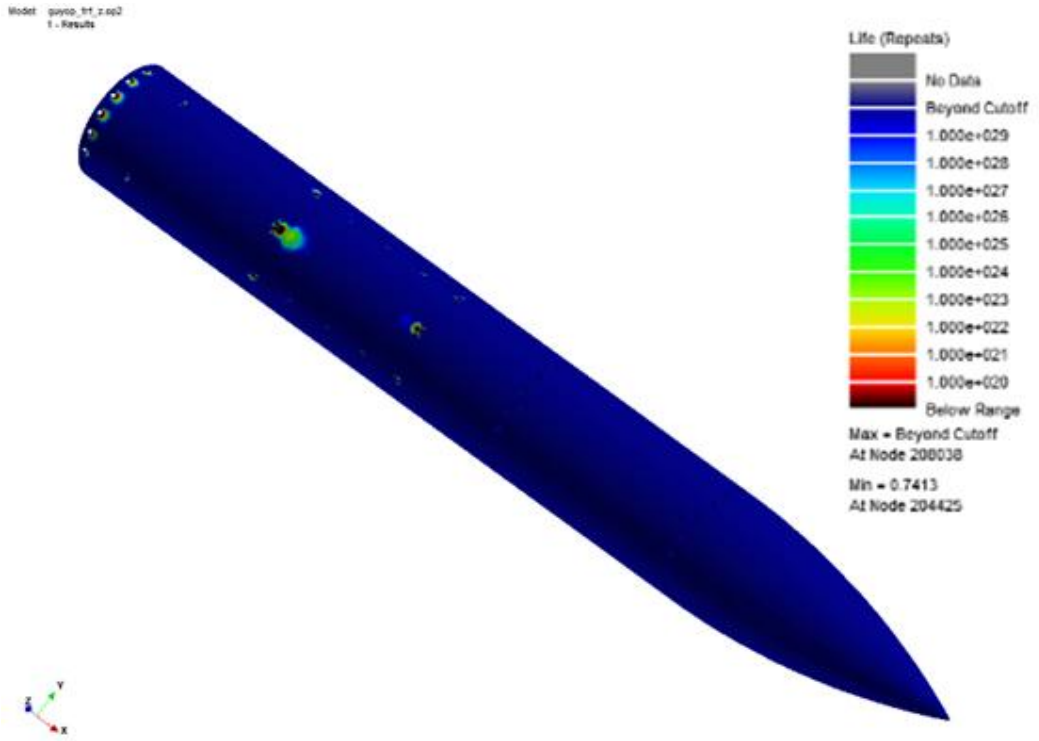

Figure 83. Life – z direction

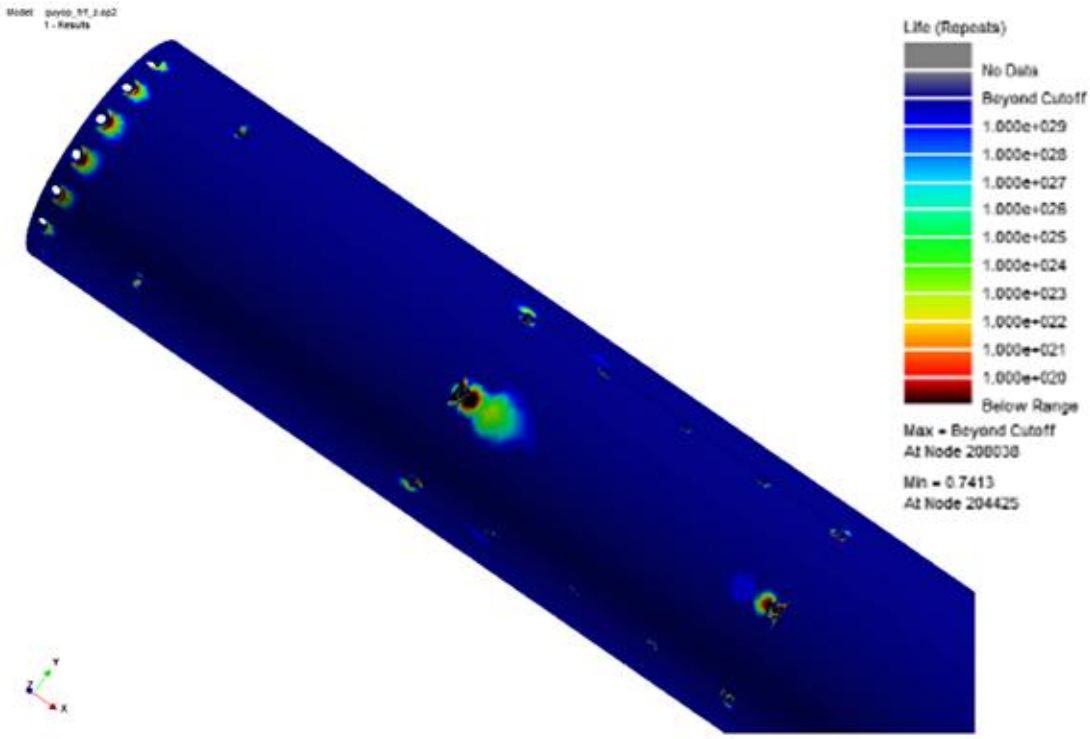

Figure 84. Life – z direction

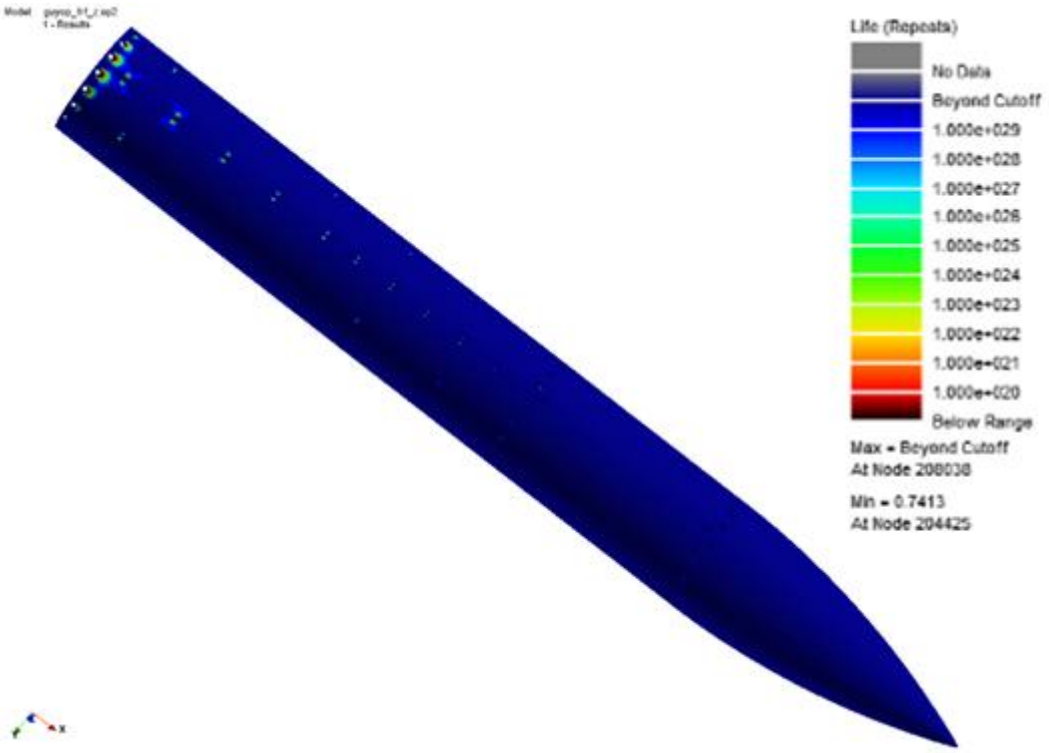

Figure 85. Life – z direction

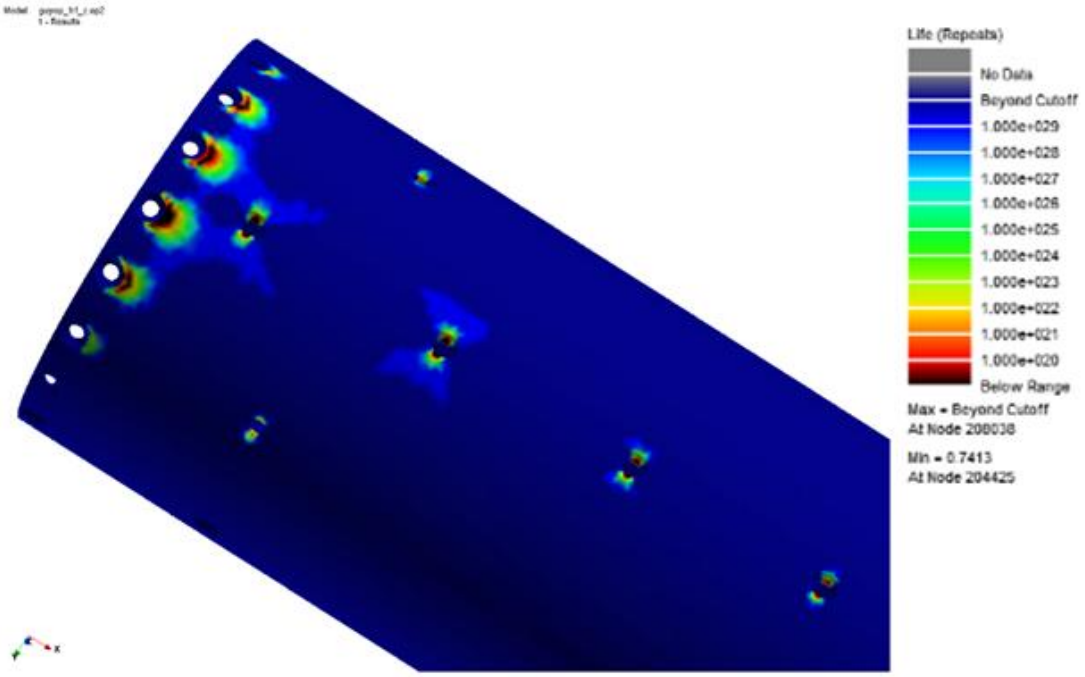

Figure 86. Life – z direction

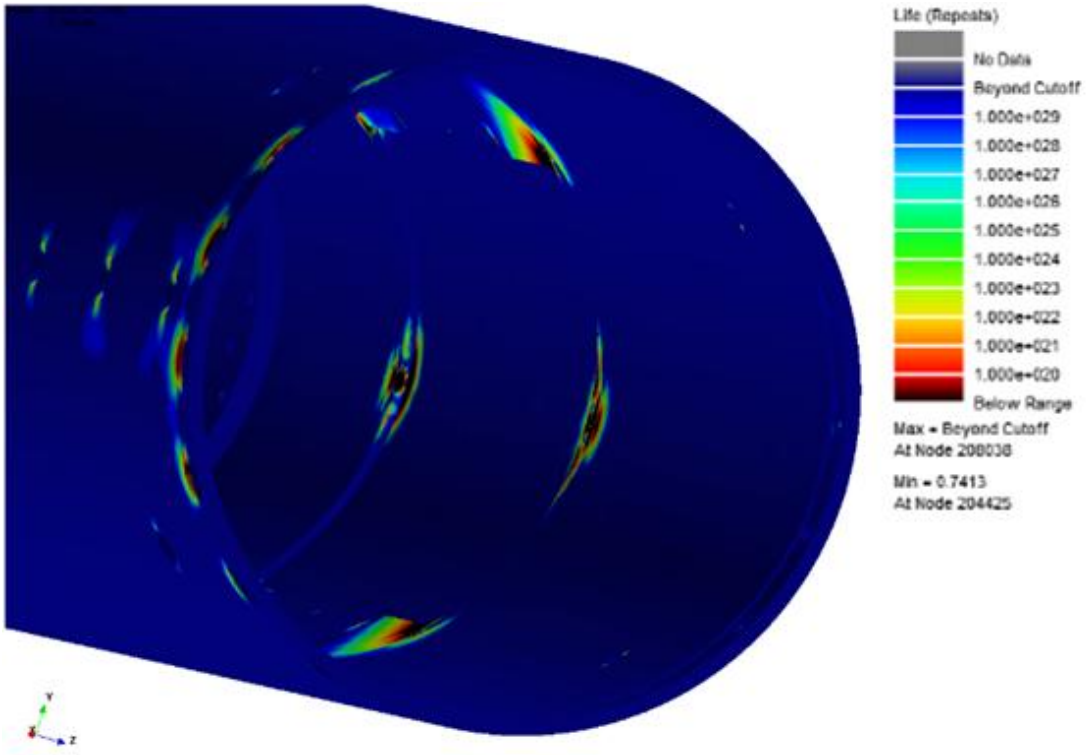

Figure 87. Life – z direction

Life results in Figure 78 - Figure 87 show that the components are durable for long flight durations. Not too much locations have lower life than 1e20 seconds. The most critical vibration direction seems to be the z direction because of the gap in the middle of the cylinder shell and low thickness of the gap hatch and shell in this location. Results also show that multiaxial fatigue analysis would not change the results too much because z direction is much more dominant than the other 2 axis.

CHAPTER 4

DISCUSSION & CONCLUSION

4.1. Conclusion

As a result of this study, fatigue behaviour of an external store under fixed wing aircraft platforms during random vibration is investigated. For this purpose, a data measurement store (DMS) was produced. Strain and acceleration data from the DMS was collected during 5 different sorties. An ideal average sortie for F-16C jet aircraft shown in Table 3 was generated for fatigue calculations.

Strain gages were placed to the most critical locations on the DMS. After investigating, separating the strain data according to the ideal average sortie for F-16C jet aircraft, it is seen that the shaft of the aft wings of the DMS are the most critical components. Strain data for the shaft of the 4 aft wings were used for multiaxial nonproportional fatigue calculations. Fatemi-Socie method was used for fatigue prediction. The life found for every shaft of the aft wings was very long because of the geometric and material properties of the component.

Acceleration data were used for PSD calculation for an ideal average sortie for F-16C jet aircraft. FDS was used for merging acceleration data for different flight conditions in Table 3. SRS and ERS of acceleration data were compared to find the vibration test duration. Lastly, a sample vibration fatigue analysis were made using FRF of the component and Lalanne PSD cycle conting method. However, the life of the component was very long because of the geometric and material properties of the component.

4.2. Future Work

After that, vibration and fatigue tests are going to be done for accuracy of the results. Then using the fatigue results, it is expected to optimize the DMS components by modifying geometric or material properties. Maybe, a new data measurement store can be produced after optimization to check the optimization effects.

Also, especially using the LEFM method, store inspection terms and periods will be determined.

Besides, influence of other events like aging to the fatigue will be investigated.

REFERENCES

[1] TÜBİTAK-SAGE. http://www.sage.tubitak.gov.tr/en/urunler/stand-missile-som. [Accessed: 18 August 2015].

[2] "Aircraft Accident Report: Aloha Airlines, Flight 243", 28 April 1988. http://www.aloha.net/~icarus/. [Accessed: 18 August 2015].

[3] "MIL-STD-810G, Department of Defense Test Method Standard for Environmental Engineering Considerations and Laboratory Tests", United States Department of Defense, 2008.

[4] H. F. Moore and J. B. Kommers, "The Fatigue of Metals", McGraw-Hill, New York, 1927.

[5] S. P. Timoshenko, "History of Strength of Materials", McGraw-Hill, New York, 1953.

[6] W. J. Rankine, "On the Causes of the Unexpected Breakage of the Journals of Railway Axles; and on the Mean of Preventing such Accidents by Observing the Law of Continuity in Their Construction", Proc. Inst. Civil Engrs, 2, 105, 1843.

[7] C. Lalanne, "Fatigue Damage", London: ISTE Ltd, 2009.

[8] O. H. Basquin, "The Exponential Law of Endurance Tests", Proceedings ASTM, 10, pp. 625-630, 1910.

[9] N. P. Inglis, "Stresses in a Plate Due to the Presence of Cracks and Sharp Corners", The Metallurgist, pp. 23-27, February 1927.

[10] A. A. Griffith, "The Theory of Rupture", Proc. 1st Int. Congress Appl. Mech., pp. 55-63, 1925.

[11] A. Palmgren, "Die Lebensdauer von Kugellagern", VDI Zeitschrift, pp. 339-341, 1924.

[12] M. A. Miner, "Cumulative Damage in Fatigue", Journal of Applied Mechanics, Trans. ASME, vol 67, no. A159-A164, pp. 60-62, 1945.

[13] H. M. Westergaard, "Bearing Pressures and Cracks", Journal of Applied Mechanics, 6, A49-A54, 1939.

[14] G. R. Irwin, "Analysis of Stressses and Strains Near the End of a Crack Traversing a Plate", Journal of Applied Mechanics, 24(3), 361-364, 1957.

[15] P. Paris and F. Erdogan, "A Critical Analysis of Crack Propogation Laws", Journal of Basic Engineering, 85, 528-534, 1963.

[16] W. Elber, "The Significance of Fatigue Crack Closure, Damage Tolerance in Aircraft Structures", ASTM STP 486, 230-242, 1971.

[17] J. F. Dreher, "Aircraft Equipment Random Vibration Test Criteria Based on Vibrations Induced by Turbulent Airflow Across Aircraft External Surfaces", United States Air Force Flight Dynamics Laboratory, Ohio, 1982.

[18] K. Eldred, W. Roberts and R. White, "Structural Vibrations in Space Vehicles", Northrop Corporation Norair Division and Western Electro Acoustic Laboratory, California, 1961.

[19] R. H. Lyon, "Random Noise and Vibration in Space Vehicles", The Shock and Vibration Information Center, United States Department of Defense, Washington, 1967.

[20] J. S. Bendat, L. D. Enochson and A. G. Piersol, "Tests for Randomness, Stationarity, Normality and Comparison of Spectra", Measurement Analysis Corporation, California, 1965.

[21] C. J. Padera, "Control Surface Having Flexure Areas for Force Measurements". United States of America Patent 3460383, 12 August 1969.

[22] T. Dirlik, "Application of Computers In Fatigue Analysis", Ph.D. Thesis, University of Warwick, 1985.

[23] A. Halfpenny, "A Frequency Domain Approach for Fatigue Life Estimation from Finite Element Analysis", Damage Assessment of Structures, Dublin, 1999.

[24] C. Lalanne, "Specification Development", London: ISTE Ltd, 2009.

[25] A. Halfpenny and F. KIHM, "Environmental Accelerated Testing. Use of Virtual Test to Extend Physical Approach", nCode, Sheffield, 2008.

[26] K. C. Topham, "Fatigue Damage Due to Vibration Testing", Master Thesis, The University of Arizona, 1991.

[27] "Constant Amplitude Stress-Life Technical Background", https://www.efatigue.com/constantamplitude/background/stresslife.html. [Accessed: 18 August 2015].

[28] "An energy-based fatigue life model for proportional and nonproportional loading conditions", https://uwaterloo.ca/fatigue-stress-analysis-lab/research-areas/energy-based-fatigue-life-model-proportional-and. [Accessed: 18 August 2015].

[29] http://www.owlnet.rice.edu/~msci301/Fuchs%20fig4_8.jpg. [Accessed: 18

August 2015].

[30] J. W. Cardinal, J. H. Feiger and P. C. McKeighan, "Fatigue Crack Growth Equations for TC-128B Tank Car Steel", Southwest Research Institute, San Antonio, 2006.

[31] C. Boller and M. Buderath, "Fatigue in Aerostructures — Where Structural Health Monitoring can Contribute to a Complex Subject", The Royal Society, München, 2006.

[32] "Multiaxial Stress-Life Technical Background", https://www.efatigue.com/multiaxial/background/stresslife.html. [Accessed: 18 August 2015].

[33] M. A. Meggiolaro and J. T. Castro, "Evaluation of multiaxial stress-strain models and fatigue life prediction methods under proportional loading" Brazilian Society of Mechanical Sciences and Engineering, Brazil, 2009.

[34] E. A. Zimmermann, M. E. Launey and R. O. Ritchie, "Mixed-Mode Fracture of Human Cortical Bone", http://www2.lbl.gov/ritchie/Programs/BIO/MixedModeFracture.htm. [Accessed: 18 August 2015].

[35] http://www.signalysis.com/pdf/srs.pdf. [Accessed: 25 September 2015].

[36] J. Mentley, "Vibration Fatigue", nCode Products User Group Meeting, 2013.

[37] SN Curve of 4140 Steel, nCode Material Database.

[38] J.W. Miles, "On Structural Fatigue under Random Loading", Journal of the Aeronautical Sciences, 21, 753-776, 1954.

[39] J.F. Tavernelli and L.F. Coffin, “Experimental Support for Generalized Equation Predicting Low Cycle Fatigue” and S.S. Manson, Discussion. Trans ASME, Journal of Basic Engineering, 84, 4, 533–537, 1962.

[40] G. Sines, "Behavior of Metals Under Complex Static and Alternating Stresses", *Metal Fatigue*, McGraw Hill, 145-169, 1959.

[41] W. N. Findley, "A Theory for the Effect of Mean Stress on Fatigue of Metals Under Combined Torsion and Axial Load or Bending," *Journal of Engineering for Industry*, 301-306, November 1959.

[42] K. Dang-Van, "Macro-Micro Approach in High-Cycle Multiaxial Fatigue", *Advances in Multiaxial Fatigue*, ASTM STP 1191, D.L. McDowell and R. Ellis, Eds., American Society for Testing and Materials, Philadelphia, 120-130, 1993.

[43] M.W. Brown and Miller, K.J., "A Theory for Fatigue Under Multiaxial Stress-Strain Conditions", *Proceedings of the Institute of Mechanical Engineers*, 187, 745-756, 1973.

[44] A. Fatemi and D.F. Socie, "A Critical Plane Approach to Multiaxial Fatigue Damage Including Out-of-Phase Loading", *Fatigue and Fracture of Engineering Materials and Structures*, 11, 3, 149-166, 1988.

[45] R.N. Smith, P. Watson and T.H. Topper, "A Stress-Strain Parameter for the Fatigue of Metals", *Journal of Materials*, 5, 4, 767-778, 1970.

[46] K. Tanaka, “Fatigue Propagation from a Crack Inclined to the Cyclic Tensile Axis”, *Engng Fract Mech*, 6, 493–507, 1974.

[47] L. Reis, B. Li and M. de Freitas “Analytical and Experimental Studies on Fatigue Crack Path under Complex Multiaxial Loading”, *Fracture of Engineering Materials and Structures*, 29, 4, 281-289, 2006.

[48] M. Behrooz, R. Ghajar and H. Moztarzadeh, "Critical Plane and Fatigue Damage Analysis of a High-Speed Microgenerator Shaft", *Proc. 9th Int. Conf. Mech. Design Production*, 1206-14, 2007.

[49] Z. Gao, T. Zhao, X. Wang and Y. Jiang, "Multiaxial Fatigue of 16MnR Steel," *ASME Journal of Pressure Vessel Technology*, 131, 2, 2009.

[50] M. Mršnik, J. Slavič and M. Boltežar, "Multiaxial Fatigue Criteria for Random Stress Response – Theoretical and Experimental Comparison", *Procedia Engineering*, 101, 459-466, 2015.